

EISSN 1305-3612

# DIR

## Diagnostic and Interventional Radiology

**TSR**  
1924  
TURKISH SOCIETY  
OF RADIOLOGY

[dirjournal.org](http://dirjournal.org)

VOLUME 30  
ISSUE 5  
SEPTEMBER 2024

**Editor in Chief**


Mehmet Ruhi Onur, MD

Department of Radiology, Hacettepe University Faculty of Medicine, Ankara, Türkiye

ORCID ID: 0000-0003-1732-7862


**Section Editors and Scientific Editorial Board**

**Abdominal Imaging**

İlkay S. İdilman, MD 

Department of Radiology, Hacettepe University Faculty of Medicine, Ankara, Türkiye

ORCID ID: 0000-0002-1913-2404

Sonay Aydın, MD 

Department of Radiology, Erzincan Binali Yıldırım University Faculty of Medicine, Erzincan, Türkiye

ORCID ID: 0000-0002-3812-6333


**Artificial Intelligence and Informatics**

Burak Koçak, MD 

Department of Radiology, University of Health Sciences, Başakşehir Çam and Sakura City Hospital, İstanbul, Türkiye

ORCID ID: 0000-0002-7307-396X


**Breast Imaging**

Füsun Taşkın, MD 

Department of Radiology, Acıbadem University Faculty of Medicine, İstanbul, Türkiye

ORCID ID: 0000-0001-7985-3660


**Chest and Cardiovascular Imaging**

Furkan Ufuk, MD 

Department of Radiology, The University of Chicago, Chicago, USA

ORCID ID: 0000-0002-8614-5387


**Hybrid Imaging and Nuclear Medicine**

Evrin Bengi Türkbey, MD 

Radiology and Imaging Sciences, Clinical Center, National Institutes of Health Bethesda, Maryland, United States


ORCID ID: 0000-0002-5216-3528

**Interventional Radiology**

Barbaros Çil, MD, FCIRES 


Department of Radiology, Koç University School of Medicine, İstanbul, Türkiye

ORCID ID: 0000-0003-1079-0088

Bahri Üstünsöz, MD 

Department of Radiology, LSUHSC (Louisiana State University Health Science Center) School of Medicine, New Orleans, United States


ORCID ID: 0000-0003-4308-6708

James Milburn, MD 

Department of Radiology, Ochsner Medical System, New Orleans, Louisiana, USA

ORCID ID: 0000-0003-3403-2628


**Musculoskeletal Imaging**

Zeynep Maraş Özdemir, MD 

Department of Radiology, İnönü University Faculty of Medicine, Malatya, Türkiye

ORCID ID: 0000-0003-1085-8978

**Neuroradiology**

Gülgün Yılmaz Ovalı, MD 

Department of Radiology, Celal Bayar University Faculty of Medicine, Manisa, Türkiye


ORCID ID: 0000-0001-8433-5622

Erkan Gökçe, MD 

Department of Radiology, Tokat Gaziosmanpaşa University Faculty of Medicine, Tokat, Türkiye


ORCID ID: 0000-0003-3947-2972

**Pediatric Radiology**

Meltem Ceyhan Bilgici, MD 

Department of Radiology, 19 Mayıs University Faculty of Medicine, Samsun, Türkiye

ORCID ID: 0000-0002-0133-0234

Evrin Özmen, MD 

Department of Radiology, Koç University Hospital, İstanbul, Türkiye

ORCID ID: 0000-0003-3100-4197


**Publication Coordinator**

Şükrü Mehmet Ertürk, MD 

Department of Radiology, İstanbul University, İstanbul Faculty of Medicine, İstanbul, Türkiye

ORCID ID: 0000-0003-4086-675X

**Biostatistical Consultant**

İlker Ercan, PhD 

Department of Biostatistics, Uludağ University School of Medicine, Bursa, Türkiye

ORCID ID: 0000-0002-2382-290X

**Publication Services**

Galenos Publishing, İstanbul, Türkiye

**Past Editors**

**Editors in Chief**

Mustafa Seçil, MD (2016-2023)

Nevzat Karabulut, MD (2011-2016)

Üstün Aydingöz, MD (2010-2011)

Okan Akhan, MD (2001-2010)

Ferhun Balkancı, MD (1999-2001)

Aytekin Besim, MD (1994-1999)\*

\* Dr. Aytekin Besim actually served as the General Coordinator. His work in this capacity, however, was in effect that of an Editor in Chief.

**Editors**

Ayşenur Cila, MD (2001-2002)

Suat Kemal Aytaç, MD (1997-2001)

Erhan Ilgıt, MD (1994-2001)

Okan Akhan, MD (1994-2001)

Ferhun Balkancı, MD (1994-2000)

Serdar Akyar, MD (1994-1997)

**Section Editors**

Section Editorship was established in 2002 at the tenure of Dr Okan Akhan, Editor in Chief.

**Abdominal Imaging**

Bengi Gürses, MD (2020-2023)

Mehmet Ruhi Onur, MD (2016-2023)

Bariş Türkbey, MD (2014-2020)

Mustafa N. Özmen, MD (2012-2018)

Murat Acar, MD (2015-2016)

Mustafa Seçil, MD (2011-2016)

Ahmet Tuncay Turgut, MD (2011)

Deniz Akata, MD (2007-2011)

Ayşe Erden, MD (2002-2011)

Okan Akhan, MD (2002-2010)

Hakan Özdemir, MD (2002-2010)

**Artificial Intelligence and Informatics**

Barış Türkbey, MD (2020-2023)

**Breast Imaging**

Mustafa Erkin Arıbal, MD (2016-2023)

Sibel Kul (2015-2018)

Ayşenur Oktay, MD (2009-2014)

Ayşegül Özdemir, MD (2004-2009)

**Cardiovascular Imaging**

Uğur Bozlar, MD (2016-2023)

Muşturay Karçaaltıncaba, MD (2007-2010)

Mecit Kantarcı (2010-2016)

**Chest Imaging**

Nevzat Karabulut, MD (2010-2014)

Çetin Atasoy, MD (2007-2010)

Macit Arıyürek, MD (2002-2007)

Figen Demirkazık, MD, (2014-2018)

**General Radiology**

Ersin Öztürk, MD (2014-2017)

Utku Şenol, MD (2010-2013)

Oğuz Dicle, MD (2007-2010)

**Interventional Radiology**

Cüneyt Aytekin, MD (2016-2023)

Bora Peynircioğlu, MD (2012-2015)

Levent Oğuzkurt, MD (2011-2014)

Fatih Boyvat, MD (2007-2010)

İsmail Oran, MD (2015-2019)

**Musculoskeletal Imaging**

Hatice Tuba Sanal, MD (2016-2023)

Fatih Kantarcı, MD (2014-2016)

Ayşenur Oktay, MD (2011-2013)

Üstün Aydıngöz, MD (2002-2011)

Berna Dirim Mete (2016-2017)

**Neuroradiology and Head & Neck Imaging**

Kubilay Aydın, MD (2016-2023)

Nafı Aygün, MD (2016-2023)

Kader Karlı Oğuz, MD (2011-2015)

Süleyman Men, MD (2007-2013)

Muhteşem Ağıldere, MD (2002-2011)

**Nuclear Medicine**

A. Cahid Civelek, MD (2016-2023)

Oktay Sarı, MD (2015)

Akın Yıldız, MD (2011-2014)

**Pediatric Radiology**

Korgün Koral, MD (2016-2023)

Murat Kocaoğlu, MD (2016-2023)

Ensar Yekeler, MD (2014-2016)

Suat Fitöz, MD (2007-2013)

Diagnostic and Interventional Radiology (Diagn Interv Radiol) is a bimonthly periodical of the Turkish Society of Radiology and the content of the journal is available at <https://www.dirjournal.org/>. It is peer-reviewed and adheres to the highest ethical and editorial standards. The editors of the journal endorse the Editorial Policy Statements Approved by the Council of Science Editors Board of Directors (<https://cse.memberclicks.net/>). The journal is in compliance with the Recommendations for the Conduct, Reporting, Editing and Publication of Scholarly Work in Medical Journals published by the International Committee of Medical Journal Editors (updated May 2022, [www.icmje.org](http://www.icmje.org)).

First ten volumes of Diagnostic and Interventional Radiology have been published in Turkish under the name of Tanısal ve Girişimsel Radyoloji (Index Medicus® abbreviation: Tani Girişim Radyol), the current title's exact Turkish translation.

Diagnostic and Interventional Radiology is an open access publication, and the journal's publication model is based on Budapest Open Access Initiative (BOAI) declaration. All published content is available online, free of charge at <https://www.dirjournal.org/>. Authors retain the copyright of their published work in Diagnostic and Interventional Radiology. The journal's content is licensed under a Creative Commons Attribution-NonCommercial (CC BY-NC) 4.0 International License which permits third parties to share and adapt the content for non-commercial purposes by giving the appropriate credit to the original work.

Please refer to the journal's webpage (<https://dirjournal.org/>) for "Aims and Scope", "Instructions to Authors" and "Instructions to Reviewers".

The editorial and publication processes of the journal are shaped in accordance with the guidelines of the ICMJE, WAME, CSE, COPE, EASE, and NISO.

Diagnostic and Interventional Radiology is indexed in **SCI-Expanded, Pubmed/Medline, Pubmed Central, TUBITAK ULAKBIM TR Index, DOAJ, HINARI, EMBASE, CINAHL, Scopus, Gale and CNKI.**

The journal is published online.

**Owner:** Can Çevikol on behalf of Turkish Society of Radiology

**Responsible Manager:** Mehmet Ruhi Onur

**Contact Information**

Diagnostic and Interventional Radiology Turkish Society of Radiology

Hoşdere Cad., Güzelkent Sok., Çankaya Evleri, F/2, 06540

Ankara, Türkiye

**E-mail:** [info@dirjournal.org](mailto:info@dirjournal.org)

**Phone:** +90 (312) 442 36 53 **Fax:** +90 (312) 442 36 54

**Publisher Contact**

**Address:** Molla Gürani Mah. Kaçamak Sk.

No: 21/1 34093 İstanbul, Türkiye

**Phone:** +90 (530) 177 30 97

**E-mail:** [info@galenos.com.tr](mailto:info@galenos.com.tr)/[yayin@galenos.com.tr](mailto:yayin@galenos.com.tr)

**Web:** [www.galenos.com.tr](http://www.galenos.com.tr) **Publisher Certificate Number:** 14521

**Online Publication Date:** September 2024

**EISSN** 1305-3612

International scientific journal published bimonthly.



## Contents

### ABDOMINAL IMAGING

**275 Technical Note.** Post-contrast abdominal magnetic resonance imaging of critically ill patients using compressed sensing free-breathing golden radial angle imaging. *Anup S. Shetty, Mark J. Hoegger, Koushik K. Das*

**279 Original Article.** Association of body composition and systemic inflammation for patients with locally advanced cervical cancer following concurrent chemoradiotherapy. *Juan Li, Cuili Niu, Ling Zhang, Yanmin Mu, Xiuyin Gui*

### ARTIFICIAL INTELLIGENCE AND INFORMATICS

**291 Original Article.** Meta-research on reporting guidelines for artificial intelligence: are authors and reviewers encouraged enough in radiology, nuclear medicine, and medical imaging journals? *Burak Koçak, Ali Keleş, Fadime Köse*

**299 Original Article.** Application of deep learning and radiomics in the prediction of hematoma expansion in intracerebral hemorrhage: a fully automated hybrid approach. *Mengtian Lu, Yaqi Wang, Jiaqiang Tian, Haifeng Feng*

### GENERAL RADIOLOGY

**313 Invited Review.** Burnout and the role of mentorship for radiology trainees and early career radiologists. *Richard J Fagan, Dane Eskildsen, Tara Catanzano, Rachel Stanietzky, Serageldin Kamel, Mohamed Eltaher, Khaled M. Elsayes*

### INTERVENTIONAL RADIOLOGY

**318 Original Article.** Percutaneous nephrostomy in infants: a 20-year single-center experience. *Onur Taydaş, Emre Ünal, Devrim Akıncı, Mehmet Şeker, Osman Melih Topçuoğlu, Okan Akhan, Türkmen Turan Çiftçi*

**325 Technical Note.** Use of gelatin sponge to seal the biliary tract after percutaneous transhepatic biliary drainage in patients with liver transplants. *Ali Özgen*

### PEDIATRIC RADIOLOGY

**328 Original Article.** Cortical and subcortical structural changes in pediatric patients with infratentorial tumors. *Barış Genç, Kerim Aslan, Derya Bako, Semra Delibalta, Meltem Necibe Ceyhan Bilgici*



# Post-contrast abdominal magnetic resonance imaging of critically ill patients using compressed sensing free-breathing golden radial angle imaging

Anup S. Shetty<sup>1</sup>  
 Mark J. Hoegger<sup>1</sup>  
 Koushik K. Das<sup>2</sup>

<sup>1</sup>Washington University School of Medicine,  
Mallinckrodt Institute of Radiology, St. Louis, United States

<sup>2</sup>Washington University School of Medicine,  
Department of Internal Medicine, Division of  
Gastroenterology, St. Louis, United States

## ABSTRACT

Obtaining diagnostic-quality magnetic resonance imaging (MRI) of the abdomen in critically ill patients can be difficult due to challenges with breath-holding and the inability to follow technologist instructions. Protocols that harness advances in commercially available MRI techniques provide a potential solution, particularly using the golden radial angle sparse parallel (GRASP) technique for dynamic post-contrast T1-weighted imaging. The GRASP technique uses a combination of free-breathing, a stack-of-stars radial acquisition, and compressed sensing reconstruction acquired over several minutes to produce motion-free images at time points defined by the user; these include the non-contrast, arterial, venous, and delayed images, which are typical of abdominal MRI protocols. The three cases discussed herein illustrate the use of this technique in providing both exquisite image quality and diagnostic value in the care of critically ill patients with hepatopancreaticobiliary diseases. Our work aims to raise awareness of this technique and its utility in imaging patients who cannot hold their breath for dynamic T1-weighted post-contrast imaging.

## KEYWORDS

Aneurysm, biliary tract, free-breathing, intensive care unit, MRI, pancreatitis

Abdominal magnetic resonance imaging (MRI) of critically ill patients is often challenging. Altered mental status and respiratory failure requiring mechanical ventilation strongly increase the likelihood of motion artifacts and non-diagnostic imaging, often related to the inability to follow commands for adequate breath-holding.

Technical advances in commercially available MRI techniques offer a potential solution for obtaining diagnostic dynamic contrast-enhanced T1-weighted images in critically ill patients. The golden radial angle sparse parallel (GRASP) technique is ideally suited for imaging these patients.<sup>1-3</sup> In a study of non-cooperative patients undergoing liver MRI, 65.6%–80.5% of studies using GRASP for free-breathing imaging produced acceptable image quality, compared with 31.1% of patients using breath-holding imaging.<sup>2</sup>

The GRASP technique combines a 3D radial stack-of-stars *k*-space trajectory and compressed sensing for the free-breath acquisition of contrast-enhanced T1-weighted 3D MRI. Imaging takes place over several minutes, during which time data are continuously acquired in a semi-random, undersampled fashion. A sparsity transformation alters the *k*-space data such that most of the information is contained within only a few data points. A non-linear iterative reconstruction method is then used to reconstruct denoised images. The retrospectively self-gated reconstruction of radially acquired *k*-space data reduces motion artifact, and the use of the compressed sensing technique allows for high-quality reconstructions despite data undersampling. The golden angle offset of radially acquired spokes gives the user flexibility in defining the temporal resolution of reconstructed time points. In patients with renal failure and suspected bleeding, avoiding the additional iodinated contrast load from computed

Corresponding author: Anup S. Shetty

E-mail: anup.shetty@wustl.edu

Received 02 January 2024; revision requested 05 February 2024; last revision received 23 February 2024; accepted 27 February 2024.



Epub: 05.04.2024

Publication date: 09.09.2024

DOI: 10.4274/dir.2024.232646

You may cite this article as: Shetty AS, Hoegger MJ, Das KK. Post-contrast abdominal magnetic resonance imaging of critically ill patients using compressed sensing free-breathing golden radial angle imaging. *Diagn Interv Radiol.* 2024;30(5):275-278.

tomography (CT) angiography makes MRI an attractive alternative. Combining this technique with other motion-resistant sequences to create an MRI protocol tailored to the breathing patient provides a comprehensive abdominal evaluation.

This paper describes this technique as part of a moving patient protocol used in critically ill patients to obtain diagnostic-quality MRI free of respiratory motion artifact.

## Technique

We employed the GRASP dynamic MRI sequence as part of a “moving patient” protocol, either selected by the radiologist prospectively at the time of protocolling a case when motion is anticipated or used by the technologist when motion or inability to actively participate in the exam is discovered at the time of performing the MRI. In addition to GRASP, this protocol also used respiratory-navigated free-breathing single-shot T2-weighted fast-spin echo, free-breathing radial stack-of-stars 3D gradient echo chemical shift, respiratory-navigated free-breathing radial T2 fat-suppressed fast-spin echo, free-breathing diffusion-weighted imaging ( $B$  values of 50, 400, and 800  $s/mm^2$ ), and free-breathing compressed-sensing 3D heavily T2-weighted magnetic resonance cholangiopancreatography (MRCP) sequences (Table 1).

The implementation of the GRASP sequence acquired data over 3 minutes of free-breathing, with the reconstruction of a non-contrast phase, three arterial phases, a portal venous phase (approximately 60–70 seconds post-injection), and a 3-minute delay. Automated subtraction images using the non-contrast phase as a mask were generated for each post-contrast time point.

### Main points

- Critically ill patients are frequently unable to hold their breath for abdominal magnetic resonance imaging (MRI), potentially limiting the diagnostic value of breath-hold post-contrast dynamic imaging.
- Compressed sensing golden radial angle sparse parallel MRI offers the ability to obtain diagnostic-quality dynamic post-contrast imaging in such patients.
- This technique ideally supplements comprehensive abdominal MRI protocols but requires awareness on the part of the radiologist/technologist for appropriate incorporation, and specialized MRI scanner hardware to perform computationally intensive reconstructions for image acquisition.

The sequence output also included a “static” sequence, which used every spoke from the minutes-long radial acquisition to reconstruct higher signal-to-noise non-dynamic images.

No informed consent was required for the use of this commercially available MRI technique.

## Case 1

Patient 1 was a 76-year-old man with stage 4 chronic kidney disease who underwent orthotopic liver transplantation 14 years prior for alcoholic cirrhosis. He initially presented for excision of his squamous cell skin cancer but was found with elevations in liver chemistries [aspartate aminotransferase 137 U/L (normal 10–50 U/L), alanine aminotransferase 340 U/L (normal 7–55 U/L), alkaline phosphatase 335 U/L (normal 40–130 U/L), total bilirubin 1.2 mg/dL (normal 0.1–1.2 mg/dL)]. Staging positron emission tomography with 2-deoxy-2-[fluorine-18] fluoro-D-glucose integrated with CT (not shown) identified incidental biliary dilation and choledocholithiasis associated with the transplanted liver. MRI/MRCP confirmed extensive common bile duct and common hepatic duct stones of up to 5.8 cm diameter, involving the confluence of the right and left ducts and extending 2.6 cm into the right posterior duct (Figure 1a, b). Endoscopic retrograde cholangiopancreatography was performed (Figure 1c); however, due to the extensive nature of the stone and intrahepatic extension, clearance could not be achieved, and a plastic biliary pigtail stent was placed into the right hepatic duct.

The patient returned 14 weeks later with hematemesis, endoscopic findings of hemobilia, and hemorrhagic shock requiring mechanical ventilation, vasopressor support, and blood transfusion. Imaging was required to guide clinical management but was limited by the patient’s poor renal function [estimated glomerular filtration rate (eGFR) of 17 mL/min/1.73  $m^2$ ] and a desire to avoid iodinated contrast. Imaging was also limited by an inability to follow instructions for the exam due to shock and intubation. Hemobilia was thought to be related to a potential pseudoaneurysm, which can be associated with endoscopic procedural manipulation and biliary stone disease, although rare.<sup>4,6</sup>

Given the patient’s clinical status and inability to hold his breath for conventional liver MRI, contrast-enhanced MRI was performed with gadoterate meglumine (Dotarem, Guerbet, Princeton, NJ) using the GRASP

technique. Dynamic enhancement showed a 4 mm right hepatic artery pseudoaneurysm (Figure 1d, Video 1), caused by a combination of extensive choledocholithiasis and chronic biliary stenting, as the source of hemobilia. This was subsequently identified with cone-beam CT at catheter angiography and treated with coil embolization, resulting in the cessation of bleeding. The patient’s hospital course was complicated by bacteremia and cholangitis. He ultimately expired 6 months later.

## Case 2

Patient 2 was a 35-year-old man who sustained a gunshot wound to the abdomen requiring emergent operative intervention for a bleeding liver laceration and subsequent management in the intensive care unit (ICU) with mechanical ventilation. The bullet fragment was retained within the T12 spinal canal, resulting in paraplegia. A bile leak protocol MRCP with the hepatobiliary contrast agent gadoxetate disodium (Eovist, Bayer, Whippany, NJ) was requested to assess for bile leak and vascular injury. A thorough safety review determined that the bullet was likely ferromagnetic,<sup>7</sup> but given the suspected injury, the patient’s documented paraplegia, and the potential need for hemihepatectomy, the benefits were deemed to outweigh the risks, and the decision was made to proceed with MRI. Gadoxetate was administered in the ICU before the patient was transported to the MRI department to minimize his duration outside of the ICU. Dynamic contrast-enhanced MRI was performed after administration of gadoterate meglumine using the GRASP technique, revealing a ballistic injury causing a bile leak from the right posterior duct and thrombosis of the posterior division of the right portal vein (Figure 2). The patient was ultimately managed with biliary stenting and did not require further operative intervention. The patient was discharged 2 weeks later.

## Case 3

Patient 3 was a 21-year-old female university student hospitalized with severe acute pancreatitis. She developed new hypoxia requiring supplemental oxygen, fever, and hyponatremia, necessitating transfer to the ICU. The patient underwent MRI at 2 a.m. for evaluation of potential pancreatitis-related complications. The patient could not comply with breath-hold instructions during the exam, which prompted the MRI technologist to use the “moving patient” protocol.

**Table 1.** "Moving patient" abdominal magnetic resonance imaging protocol

Sequence name	Slice thickness (mm)	Matrix (pixels)	TR (ms)	TE (ms)	NSA	Notes
T2W single-shot FSE coronal	6	320 × 320	1,000	100	1	Free-breathing respiratory-navigated
T1W 3D spoiled GRE Dixon axial	3	260 × 320	6.68	2.39, 4.77	1	Free-breathing radial acquisition; acquire in-phase and opposed-phase, reconstruct fat-only and water-only Dixon
T2W single-shot FSE axial	4	320 × 320	1,000	100	1	Free-breathing respiratory-navigated
T2W FSE fat-suppressed axial	6	260 × 320	3,000	93	1	Free-breathing respiratory-navigated radial acquisition
DWI single-shot axial	6	256 × 268	9,500	56	2, 4, 10	Free-breathing; obtain <i>B</i> values of 50, 400, 800; reconstruct ADC map
T1W 3D spoiled GRE axial GRASP	3	260 × 320	4.3	2.35	1	Compressed sensing free-breathing 3-minute radial acquisition; reconstruct non-contrast, 3 arterial phases, portal venous phase, 3-minute delay, and subtractions for each post-contrast phase
Coronal 3D MRCP	1	288 × 384	5,520	701	2	Compressed sensing free-breathing respiratory-navigated

TR, repetition time; TE, echo time; NSA, number of signal averages; T1W, T1-weighted; T2W, T2-weighted; 3D, three-dimensional; GRE, gradient-recalled echo; FSE, fast spin echo; DWI, diffusion-weighted imaging; GRASP, golden radial angle sparse parallel; MRCP, magnetic resonance cholangiopancreatography; ADC, apparent diffusion coefficient.

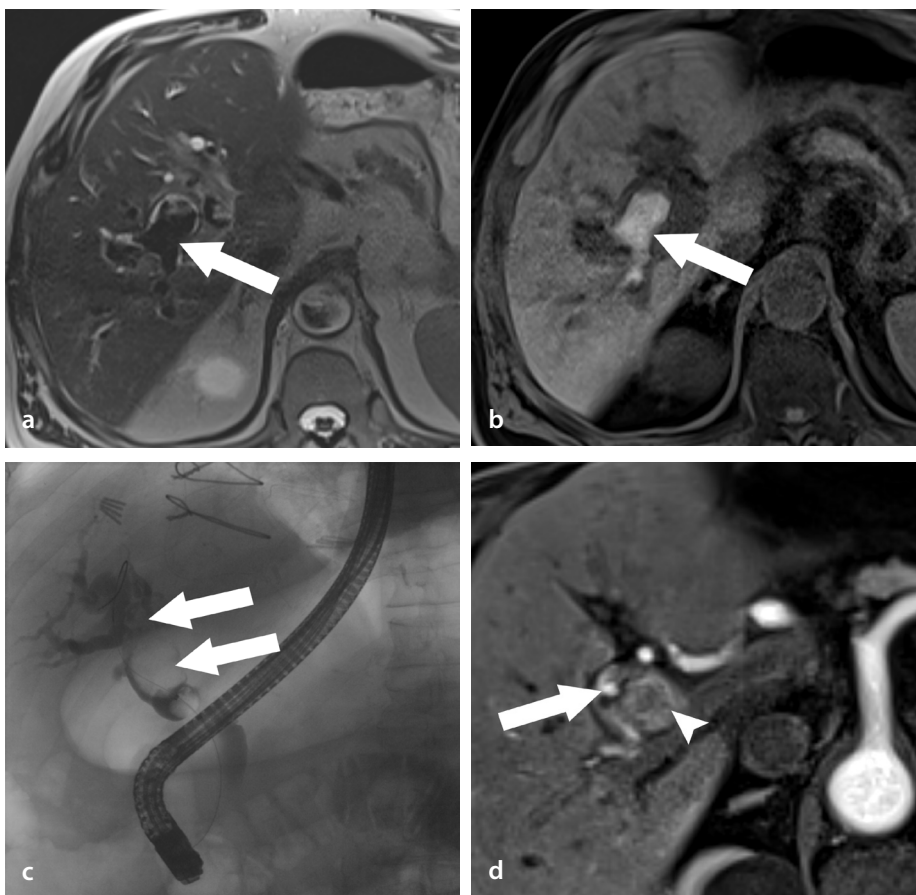


**Figure 1.** Seventy six-year-old man with right hepatic artery pseudoaneurysm related to choledocholithiasis and biliary stent placement. (a) Axial T2 single-shot fast-spin echo magnetic resonance imaging (MRI) shows a large volume of choledocholithiasis (arrow) filling the right hepatic duct. (b) Axial T1-weighted fat-suppressed 3D spoiled gradient echo MRI shows the extent of T1 hyperintense stone burden within the right hepatic ductal system (arrow). (c) Endoscopic retrograde cholangiopancreatography performed after the MRI shows a large volume of stone disease (arrows), which could not be adequately cleared and was managed with the placement of a plastic stent into the right hepatic duct. (d) T1-weighted fat-suppressed 3D gradient echo arterial phase MRI obtained during free-breathing using a compressed-sensing golden radial angle sparse parallel technique shows a right hepatic artery pseudoaneurysm (arrow) adjacent to a large T1 hyperintense right hepatic duct stone (arrowhead). Despite the patient freely breathing, there is no motion artifact, enabling detection of the subtle abnormality.

GRASP MRI revealed non-enhancement of the distal body and proximal tail of the pancreas, indicating acute necrosis (Figure 3). The patient subsequently developed walled-off necrosis secondary to a disconnected duct in the pancreatic tail that was managed with cystogastrostomy drainage.

## Discussion

The aforementioned cases illustrate the value of the GRASP technique for problem-solving in complex clinical situations that can arise in hospitalized patients.<sup>2</sup>

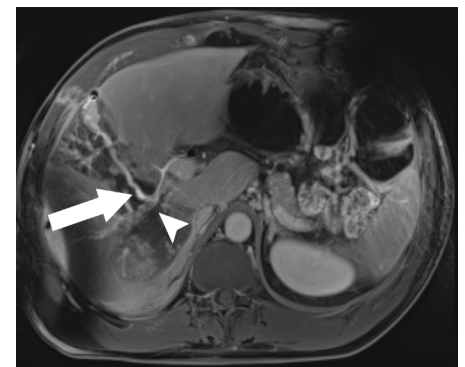


**Figure 2.** Thirty five-year-old man with ballistic liver injuries from a gunshot wound. Axial T1-weighted fat-suppressed 3D gradient echo arterial phase magnetic resonance imaging obtained during free-breathing using a compressed-sensing golden radial angle sparse parallel technique shows a large bile leak from the right hepatic duct (arrow) and traumatic occlusion of the posterior division of the right portal vein (arrowhead) in close proximity. Despite the patient freely breathing, there is no motion artifact, enabling clear delineation of these abnormalities.

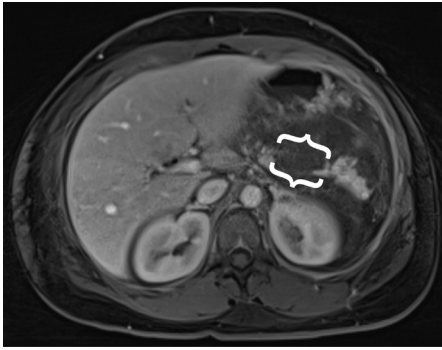


**Figure 3.** Twenty one-year-old woman with severe pancreatitis. Axial T1-weighted fat-suppressed 3D gradient echo arterial phase magnetic resonance imaging obtained during free-breathing using a compressed-sensing golden radial angle sparse parallel technique shows non-enhancement of the distal pancreatic body and proximal tail, consistent with necrotizing pancreatitis (brackets). Despite the patient freely breathing, there is no motion artifact, enabling clear delineation of the margin of necrosis.

For patient 1, a CT angiography would normally be the first-line diagnostic imaging test for a patient with this clinical scenario; however, the patient's chronic kidney disease and the expected need for additional iodinated contrast for catheter angiography led to MRI, which secured the diagnosis. Although patients with chronic kidney disease are at increased risk of nephrogenic systemic fibrosis (NSF), this patient had an eGFR  $>15$  mL/min/ $1.73$  m<sup>2</sup>, meeting institutional criteria for administration of a macrocyclic ionic extracellular gadolinium contrast agent (gadoterate meglumine in this example), with benefits outweighing the low risk of NSF.<sup>8</sup> Breath-holding and timing normally pose a challenge in the MRI of critically ill ventilated patients. Arterial phase-timing and lack of respiratory motion are critical for distinguishing a dynamic contrast-enhanced hepatic pseudoaneurysm from adjacent tissues with similar enhancement. If a longer, non-dynamic, free-breathing radial acquisition had been performed without the compressed sensing technique, the high temporal resolution would not have been achievable.

The potential streak artifact on CT from the adjoining, indwelling biliary stent was also avoided with MRI.

Patient 2 presented a complex challenge as he required mechanical ventilation and carried the additional risk of a ferromagnetic bullet near the spine. A moving patient protocol using GRASP MRI is ideally suited for imaging such a patient and maximizing the likelihood of obtaining diagnostic-quality imaging, a key factor to consider when weighing the risk of MRI causing further injury, as GRASP may prevent the need for re-imaging.

Patient 3 proved the value of GRASP MRI in imaging critically ill patients when the technologist is faced with a dyspneic patient. The rate of non-diagnostic abdominal MRI performed overnight can be reduced by the judicious application of moving patient protocols utilizing the GRASP technique, as in this case.

Although GRASP has been available for several years, the radiologist and/or technologist must know that this technique exists and can be used either routinely or for problem-solving, as we did in the provided cases. The GRASP technique also requires a high-end computing platform to perform complex imaging reconstruction. GRASP packages are available as an additional expense at the time of scanner purchase or as an upgrade. Limitations of the GRASP technique include radial "streak" artifacts and the inability to currently match the overall image quality of a good breath-hold standard acquisition, which is why we do not use this technique on every examination. In our anecdotal experience as a high-volume center for quaternary hepatopancreaticobiliary clinical referrals, we observe that this technique is underutilized in patients who present for second-opinion MRI consultation with outside imaging.

In conclusion, a moving-patient abdominal MRI protocol utilizing the GRASP tech-

nique for dynamic post-contrast imaging can provide value in the imaging and management of critically ill patients.

### Conflict of interest disclosure

The authors declared no conflicts of interest.

### References

- Shetty AS, Fraum TJ, Ludwig DR, et al. Body MRI: imaging protocols, techniques, and lessons learned. *Radiographics*. 2022;42(7):2054-2074. [\[CrossRef\]](#)
- Young Park J, Min Lee S, Sub Lee J, Chang W, Hee Yoon J. Free-breathing dynamic T1WI using compressed sensing-golden angle radial sparse parallel imaging for liver MRI in patients with limited breath-holding capability. *Eur J Radio*. 2022;152:110342. [\[CrossRef\]](#)
- Nepal P, Bagga B, Feng L, Chandarana H. Respiratory motion management in abdominal MRI: radiology in training. *Radiology*. 2023;306(1):47-53. [\[CrossRef\]](#)
- Yu YH, Sohn JH, Kim TY, et al. Hepatic artery pseudoaneurysm caused by acute idiopathic pancreatitis. *World J Gastroenterol*. 2012;18(18):2291-2294. [\[CrossRef\]](#)
- Austin AS, Lobo DN, Hinwood D, Iftikhar SY, Norton B. Intra-hepatic false aneurysm: a rare complication of ERCP. *Eur J Gastroenterol Hepatol*. 1999;11(10):1171-1173. [\[CrossRef\]](#)
- Gaduputi V, Tariq H, Dev A. Visceral arterial aneurysms complicating endoscopic retrograde cholangiopancreatography. *Case Rep Gastrointest Med*. 2013;2013:515201. [\[CrossRef\]](#)
- Fountain AJ, Corey A, Malko JA, Strozier D, Allen JW. Imaging appearance of ballistic wounds predicts bullet composition: implications for MRI safety. *AJR Am J Roentgenol*. 2021;216(2):542-551. [\[CrossRef\]](#)
- Weinreb JC, Rodby RA, Yee J, et al. Use of intravenous gadolinium-based contrast media in patients with kidney disease: consensus statements from the American College of Radiology and the National Kidney Foundation. *Radiology*. 2021;298(1):28-35. [\[CrossRef\]](#)

Video 1 link: <https://youtu.be/1pW7nzD11U8>

**Video 1.** Seventy six-year-old man with right hepatic artery pseudoaneurysm related to choledocholithiasis and biliary stent placement. T1-weighted fat-suppressed 3D gradient echo arterial phase magnetic resonance imaging obtained during free-breathing using a compressed-sensing golden radial angle sparse parallel technique shows a pseudoaneurysm (arrowhead) arising from the right hepatic artery (arrow) adjacent to a large T1 hyperintense right hepatic duct stone. Despite the patient freely breathing, there is no motion artifact, enabling detection of the subtle abnormality.





# Association of body composition and systemic inflammation for patients with locally advanced cervical cancer following concurrent chemoradiotherapy

Juan Li  
 Cuili Niu  
 Ling Zhang  
 Yanmin Mu  
 Xiuyin Gui

Xingtai Third Hospital, Clinic of Gynecology,  
Xingtai, China

## PURPOSE

Systemic inflammation and body composition are associated with survival outcomes of cancer patients. This study aimed to examine the combined prognostic value of systemic inflammatory markers and body composition parameters in patients with locally advanced cervical cancer (LACC).

## METHODS

Patients who underwent concurrent chemoradiotherapy (CCRT) for LACC at a tertiary referral teaching hospital between January 2010 and January 2018 were enrolled. A predictive model was established based on systemic immune-inflammation index (SII) and computer tomography-derived visceral fat-to-muscle ratio (vFMR). Overall survival (OS) and progression-free survival (PFS) were assessed using the Kaplan–Meier method and Cox regression models. The model performance was assessed using discrimination, calibration, and clinical usefulness.

## RESULTS

In total, 212 patients were enrolled. The SII and vFMR were closely related, and both independently predicted survival ( $P < 0.05$ ). A predictive model was established based on the above biomarkers and included three subgroups: high-risk [both high SII ( $>828$ ) and high vFMR ( $>1.1$ )], middle-risk (either high SII or high vFMR), and low-risk (neither high SII nor high vFMR). The 3-year OS (PFS) rates for low-, middle-, and high-risk patients were 90.5% (86.0%), 73.9% (58.4%), and 46.8% (36.1%), respectively ( $P < 0.05$ ). This model demonstrated satisfactory predictive accuracy (area under the curve values for predicting 3-year OS and PFS were 0.704 and 0.718, respectively), good fit (Hosmer–Lemeshow tests:  $P > 0.05$ ), and clinical usefulness.

## CONCLUSION

Systemic inflammatory markers combined with body composition parameters could independently predict the prognosis of patients with LACC, highlighting the utilization of commonly collected indicators in decision-making processes.

## CLINICAL SIGNIFICANCE

The SII and vFMR, as well as their composite indices, were promising prognostic factors in patients with LACC who received definitive CCRT. Future studies are needed to explore novel therapies to improve the outcomes in high-risk patients.

## KEYWORDS

Cervical cancer, concurrent chemoradiotherapy, systemic inflammation, body composition, prognosis

Corresponding author: Juan Li

E-mail: lj2759434@126.com

Received 05 March 2024; revision requested 26 March 2024; accepted 11 April 2024.



Epub: 03.06.2024

Publication date: 09.09.2024

DOI: 10.4274/dir.2024.242751

You may cite this article as: Li J, Niu C, Zhang L, Mu Y, Gui X. Association of body composition and systemic inflammation for patients with locally advanced cervical cancer following concurrent chemoradiotherapy. *Diagn Interv Radiol.* 2024;30(5):279-290.

Cervical cancer is the fourth most frequently diagnosed malignancy in women, causing an estimated 342,000 deaths worldwide in 2020.<sup>1</sup> Patients with early stage disease generally have a favorable prognosis, whereas those with locally advanced disease experience a high risk of treatment failure.<sup>2</sup> Concurrent chemoradiotherapy (CCRT) remains the cornerstone of treatment for patients with locally advanced cervical cancer (LACC). However, even with the same tumor stage and similar treatments, there is significant heterogeneity in prognosis.<sup>3</sup> Great efforts have been made to improve survival, and the identification of factors affecting patient prognosis is crucial for ensuring proper treatment.

Cumulative evidence has demonstrated that systemic inflammation and sarcopenia are closely associated with poor prognosis in various malignant tumors.<sup>4-6</sup> Activation of the systemic inflammatory response plays a vital role in tumorigenesis, progression, and metastasis.<sup>7</sup> Pretreatment blood biomarkers [e.g., systemic immune-inflammation index (SII)] are commonly used to predict the prognosis of patients with cervical cancer.<sup>8</sup> Sarcopenia is characterized by the progressive loss of skeletal muscle mass and is associated with poor outcomes in patients with LACC.<sup>9-11</sup> A deeper understanding of systemic inflammation and sarcopenia, as well as their interplay, may facilitate more accurate prognostic stratification.

Visceral obesity has been associated with a poor prognosis in several gynecologic malignancies, including cervical cancer.<sup>12,13</sup> Visceral fat-to-muscle ratio (vFMR), which is based on body composition, has been reported to be associated with the prognosis of patients with ovarian cancer.<sup>14</sup> In this study, we examine the prognostic signifi-

cance of vFMR and its association with the SII in patients with LACC.

## Methods

### Patients and treatment

This retrospective study identified 234 patients with biopsy-confirmed LACC [IB2-IVA disease according to the 2009 International Federation of Gynecology and Obstetrics (FIGO) staging criteria] who underwent definitive radiotherapy (RT) or CCRT with curative intent at Xingtai Third Hospital between January 2010 and January 2018. Among them, 22 patients were excluded from the analysis because of concurrent malignant tumors of other organs (n = 2), incomplete clinical data (n = 5), absence of abdominal enhanced computed tomography (CT) images obtained before treatment (n = 13), or inflammatory conditions before treatment (e.g., acute infections) (n = 2). A total of 212 patients were included in the final analysis (Figure 1). This study was conducted in accordance with the Declaration of Helsinki and approved by the Ethics Committee of Xingtai Third Hospital (approval number: 2023Y0668, date: 12/8/2023). Informed consent was not required due to the retrospective and observational nature of this study.

All patients underwent external beam radiotherapy (EBRT) of the pelvis and brachytherapy. The clinical target volume (CTV) covered the gross tumor, uterus, cervix, parametrium, upper half of the vagina, uterosacral ligaments, and pelvic lymph

node region. The para-aortic region was also covered in the CTV when there was evidence of para-aortic lymph node involvement or enough of a risk of microscopic disease (e.g., common iliac node involvement).<sup>15</sup> Intensity-modulated RT was used for external irradiation, which was planned using the RT treatment planning system (Varian Eclipse software; Varian Medical Systems Inc., Palo Alto, CA, USA). The EBRT was administered with a fraction of 1.8 Gy for a total dose of 45–50.4 Gy. Intracavitary brachytherapy was prescribed to point A with a fraction of 6 Gy for a total dose of 30–36 Gy. Cisplatin-based chemotherapy was administered concurrently with RT (40 mg/m<sup>2</sup> intravenously weekly). After treatment, all patients were followed up every 3 months for the first 2 years and every 6 months for the next 3 years. The final follow-up evaluation was conducted in January 2021.

### Definitions

The primary outcomes of this study included overall survival (OS) and progression-free survival (PFS), with the former defined as the time interval from the date of diagnosis to death from any cause or last follow-up, and the latter as the interval from the date of diagnosis to the date of disease progression or recurrence.

Laboratory parameters were obtained within 1 week prior to treatment. The SII was calculated as neutrophil count × platelet count/lymphocyte count.<sup>16</sup> Pre-treatment CT images were used for body composition

### Main points

- Both the systemic immune-inflammation index (SII) and computed tomography-derived visceral fat-to-muscle ratio (vFMR) were independent prognostic factors in patients with locally advanced cervical cancer who underwent concurrent chemoradiotherapy.
- The SII and vFMR were closely related; a higher SII was significantly associated with a higher vFMR and vice versa.
- The composite indices of SII and vFMR enabled accurate prognostic stratification and could serve as a complement to the International Federation of Gynecology and Obstetrics staging.

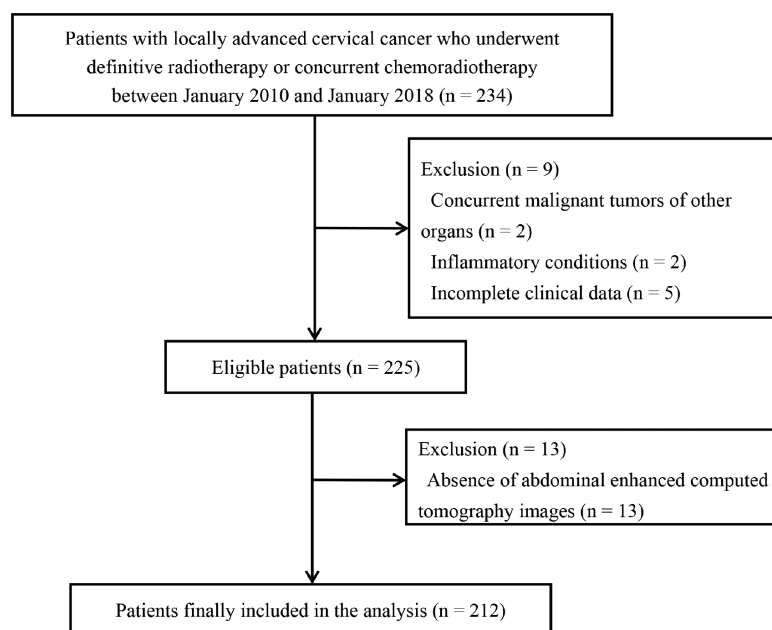


Figure 1. Diagram of study population.

measurements. A single CT slice of the third lumbar vertebra was selected to quantify the fat and muscle compartments. These images were analyzed by an experienced radiologist who was blinded to patient information using the sliceOmatic software (TomoVision). According to the standard density thresholds, skeletal muscle area was identified with a radiation density ranging from -29 to 150 Hounsfield units (HU), and visceral adipose area was identified with a radiation density ranging from -150 to -50 HU (Supplementary Figure 1). Both of the areas (in centimeters squared) were converted into indexes (skeletal muscle index and visceral adipose index) after dividing by height in meters squared. The vFMR was calculated by dividing the visceral adipose area by the skeletal muscle area.<sup>14</sup>

### Statistical analysis

Data were described as frequencies (percentages) for categorical variables and means [standard deviation (SD)] or medians [interquartile range (IQR)] for continuous variables. The Shapiro–Wilk test was used to verify the normality of variable distribution. Inter-group differences were evaluated using the chi-square test or t-test. The optimal cut-off values of the SII and vFMR for OS were determined by selecting the minimum *P* value with the maximum chi-square value in all possible subdivisions of the populations using X-tile software.<sup>17</sup> Spearman's coefficient was calculated to evaluate the correlation between SII and vFMR. Moreover, OS and PFS were evaluated using the Kaplan–Meier method, and differences were compared using the log-rank test. Multivariate Cox regression models were used to identify the independent risk factors for OS and PFS. Variables with a *P* value of <0.1 in the univariate analysis were included in the multivariate analysis. Receiver operating characteristic curves were used to evaluate the predictive accuracy by calculating the area under the curve (AUC). The Hosmer–Lemeshow test was used to evaluate the goodness of fit, and a *P* value of >0.05 was considered a good fit. Decision curve analysis was used to evaluate clinical usefulness by calculating the net benefit of prediction models at different threshold levels.<sup>18</sup> This allowed for the comparison of net benefits between different models to select the optimal model.

Statistical significance was set at two-tailed *P* < 0.05. All statistical analyses were performed using R software, version 4.1.2 (R Foundation for Statistical Computing, Vienna, Austria).

## Results

### Clinicopathological characteristics

The clinicopathological characteristics of the study cohort (*n* = 212) are summarized in Table 1. The mean (SD) age of the patients was 58.8 (10.6) years, and the mean (SD) body mass index was 23.1 (3.1) kg/m<sup>2</sup>. Most of the patients (85.8%) underwent CCRT.

### Overall survival and progression-free survival

The median (IQR) follow-up duration was 47 (40–63) months. The 3-year OS and PFS rates for all the patients were 82.1% and 73.6%, respectively. The optimal cutoff values of SII and vFMR were calculated to be 828 and 1.1, respectively (Supplementary Figure 2). A higher SII (>828) was significantly associated with poorer OS [88.3% vs.

62.1%; hazard ratio (HR): 3.399, 95% confidence interval (CI): 1.924–6.003, *P* < 0.001] and PFS (80.8% vs. 49.3%; HR: 3.347, 95% CI: 2.005–5.587, *P* < 0.001). Patients with a higher vFMR (>1.1) also exhibited significantly poorer OS (86.2% vs. 65.4%; HR: 3.443, 95% CI: 1.944–6.095, *P* < 0.001) and PFS (80.4% vs. 48.3%; HR: 3.398, 95% CI: 2.025–5.701, *P* < 0.001). Factors significantly associated with survival also included histology, FIGO stage, pelvic lymph node, squamous cell carcinoma antigen level, and CCRT (*P* < 0.05). In the multivariate analysis, SII and vFMR were both independent risk factors for OS and PFS (*P* < 0.05) (Table 2).

### Correlation between systemic immune-inflammation and visceral fat-to-muscle ratio

There was a significant linear association between the SII and vFMR (Spearman *r* = 0.198, *P* = 0.004) (Figure 2). A higher SII was

**Table 1.** Clinicopathological variables

Characteristics	Overall (n = 212)
<b>Age, mean ± SD, yrs</b>	58.8 ± 10.6
<b>BMI, mean ± SD, kg/m<sup>2</sup></b>	23.1 ± 3.1
<b>ECOG performance status, n (%)</b>	
0	139 (65.6)
1	73 (34.4)
<b>Histology, n (%)</b>	
Squamous cell carcinoma	193 (91.0)
Adenocarcinoma	19 (9.0)
<b>FIGO stage, n (%)</b>	
IB-II	158 (74.5)
III-IVA	54 (25.5)
<b>Pelvic lymph node, n (%)</b>	
Negative	106 (50.0)
Positive	106 (50.0)
<b>SCC-Ag level, n (%)</b>	
<10 ng/mL	146 (68.9)
>10 ng/mL	66 (31.1)
<b>Concurrent chemotherapy, n (%)</b>	
No	30 (14.2)
Yes	182 (85.8)
<b>SII level, median (IQR)</b>	518.5 (358.2–835.1)
<b>SMI, median (IQR), cm<sup>2</sup>/m<sup>2</sup></b>	46.7 (39.1–54.0)
<b>VAI, median (IQR), cm<sup>2</sup>/m<sup>2</sup></b>	32.7 (13.4–53.9)
<b>vFMR level, median (IQR)</b>	0.68 (0.34–1.10)

BMI, body mass index; ECOG, Eastern Cooperative Oncology Group; FIGO, International Federation of Gynecology and Obstetrics; SCC-Ag, squamous cell carcinoma antigen; SII, systemic immune-inflammation index; SMI, skeletal muscle index; VAI, visceral adipose index; vFMR, visceral fat-to-muscle ratio; SD, standard deviation; IQR, interquartile range.

significantly associated with a higher vFMR (35.2% vs. 17.7%,  $P = 0.008$ ); however, there were no significant associations between SII and other clinicopathological characteristics ( $P > 0.05$ ) (Supplementary Table 1). Patients with a higher vFMR were more likely to be older (mean: 63.5 vs. 57.4 years,  $P < 0.001$ ), and have a more advanced FIGO stage (36.2% vs. 22.4%,  $P = 0.056$ ), pelvic lymph node involvement (61.7% vs. 46.7%,  $P = 0.069$ ), and a higher SII score (40.4% vs. 21.2%,  $P = 0.008$ ) (Supplementary Table 2).

### Establishment of the systemic immune-inflammation and fat-to-muscle ratio score

The SII and vFMR were combined and four subgroups were generated. Patients with a higher SII and vFMR exhibited the worst survival, whereas those with a lower SII and vFMR survived the longest ( $P < 0.001$ ). The OS and PFS of patients with a higher SII and lower vFMR were similar to those of patients

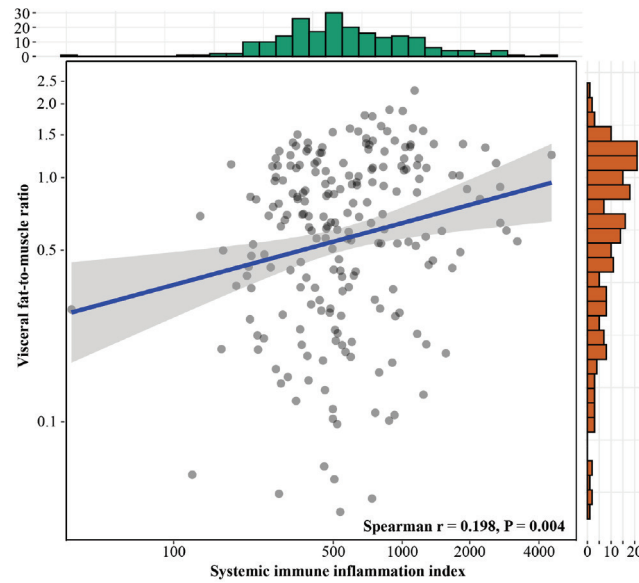


**Figure 2.** Scatter plot between systemic immune-inflammation and visceral fat-to-muscle ratio. Both parameters were normalized by natural logarithmic (ln) transformation.

Variables	Overall survival				Progression-free survival	
	Univariate		Multivariate		Multivariate	
	HR (95% CI)	<i>P</i> value	HR (95% CI)	<i>P</i> value	HR (95% CI)	<i>P</i> value
Age, per 1 year	1.008 (0.981–1.036)	0.550				
<b>Histology</b>		0.028		0.579		0.134
Squamous cell carcinoma	Reference		Reference		Reference	
Adenocarcinoma	2.235 (1.097–5.015)		1.259 (0.558–2.845)		1.722 (0.846–3.506)	
<b>FIGO stage</b>		<0.001		0.001		0.001
IB-II	Reference		Reference		Reference	
III-IVA	5.019 (2.820–8.931)		2.985 (1.534–5.809)		2.810 (1.546–5.107)	
<b>Pelvic lymph node</b>		0.005		0.158		0.062
Negative	Reference		Reference		Reference	
Positive	2.398 (1.302–4.416)		1.621 (0.829–3.169)		1.762 (0.973–3.190)	
<b>SCC-Ag level</b>		0.017		0.210		0.848
<10 ng/mL	Reference		Reference		Reference	
>10 ng/mL	2.004 (1.135–3.536)		1.468 (0.806–2.673)		1.055 (0.608–1.833)	
<b>Concurrent chemotherapy</b>		0.027		0.293		0.548
No	Reference		Reference		Reference	
Yes	0.467 (0.238–0.918)		0.672 (0.320–1.410)		0.813 (0.414–1.597)	
<b>SII level</b>		<0.001		<0.001		<0.001
<828	Reference		Reference		Reference	
>828	3.399 (1.924–6.003)		2.976 (1.647–5.378)		2.776 (1.629–4.728)	
<b>vFMR level</b>		<0.001		0.049		0.031
<1.1	Reference		Reference		Reference	
>1.1	3.443 (1.944–6.095)		2.803 (1.005–7.817)		2.689 (1.093–6.616)	
<b>SMI, per 1 cm<sup>2</sup>/m<sup>2</sup></b>	0.985 (0.956–1.015)	0.327				
<b>VAI, per 1 cm<sup>2</sup>/m<sup>2</sup></b>	1.015 (1.004–1.026)	0.008	0.996 (0.976–1.015)	0.660	0.996 (0.979–1.014)	0.663

FIGO, International Federation of Gynecology and Obstetrics; SCC-Ag, squamous cell carcinoma antigen; SII, systemic immune-inflammation index; vFMR, visceral fat-to-muscle ratio; SMI, skeletal muscle index; VAI, visceral adipose index; HR, hazard ratio; CI, confidence interval.

with a lower SII and higher vFMR (Figure 3a, c). Based on the above results, we defined three risk groups according to the SII and vFMR [systemic immune-inflammation and fat-to-muscle ratio (SFMR)]: patients with both lower SII and vFMR were regarded as low-risk, patients with either a higher SII or vFMR were regarded as middle-risk, and patients with both higher SII and vFMR were regarded as high-risk. Patients with a higher risk according to SFMR score were more likely to be older ( $P = 0.013$ ) and obese ( $P = 0.065$ ), and have a more advanced FIGO stage ( $P = 0.081$ ) (Supplementary Table 3).

### Prognostic value of systemic immune-inflammation and fat-to-muscle ratio

The 3-year OS rates for low-, middle-, and high-risk patients were 90.5%, 73.9%, and 46.8%, respectively ( $P < 0.05$ ); the 3-year PFS rates for low-, middle-, and high-risk patients were 86.0%, 58.4%, and 36.1%, respectively ( $P < 0.05$ ) (Figure 3b, d). After adjusting for FIGO stage and lymph node status, SFMR was found to be an independent risk factor for both OS and PFS (middle-risk vs. low-risk: HR: 3.783, 95% CI: 2.095–6.829; high-risk vs.

low-risk: HR: 6.062, 95% CI: 2.888–12.723;  $P < 0.001$ ) (Table 3).

The AUC values of SFMR for predicting 1-year, 3-year, and 5-year OS were 0.847, 0.704, and 0.730, respectively. The AUC values of SFMR for predicting 1-year, 3-year, and 5-year PFS were 0.723, 0.718, and 0.728, respectively (Figure 4). Hosmer–Lemeshow tests showed that SFMR was a good fit for predicting OS and PFS ( $P = 0.975$  and  $0.432$ , respectively). As depicted in Figure 5, the curve corresponding to the SFMR combined with FIGO stages was above, and the area under the decision curve it formed with the “treat none” and “treat all” lines was larger than that of the FIGO stages alone. Therefore, the clinical model consisting of the SFMR and FIGO stages has a higher net benefit compared with the FIGO stages, making it the superior model.

## Discussion

This is the first study to demonstrate the prognostic value of vFMR and its combined effect with the SII in patients with LACC undergoing definitive CCRT. Moreover, we

found that the co-occurrence of a high SII and vFMR (SFMR: high-risk) was related to a six-fold risk of death or progression in these patients. Our results suggest that these two easily identifiable biomarkers have great potential for prognostic stratification.

Excessive or persistent systemic inflammation, represented by the ratio of circulating blood cell counts, plays a significant role in cancer development and progression.<sup>19</sup> Calculated using peripheral neutrophil, lymphocyte, and platelet counts, SII has been demonstrated to be a powerful prognostic factor for various human malignancies.<sup>20</sup> Cumulative evidence has indicated a significant association between the SII and survival in cervical cancer.<sup>16,21,22</sup> In this study, it was found that a higher SII was independently associated with poorer OS and PFS. These findings can be attributed to the prognostic value of each SII component. Lymphocytes play a vital role in cell-mediated immune responses and secrete antitumor cytokines. Therefore, lymphocytopenia can lead to an unfavorable prognosis.<sup>23</sup> Second, neutrophils may promote a tumor-favorable environment by promoting neovascular-

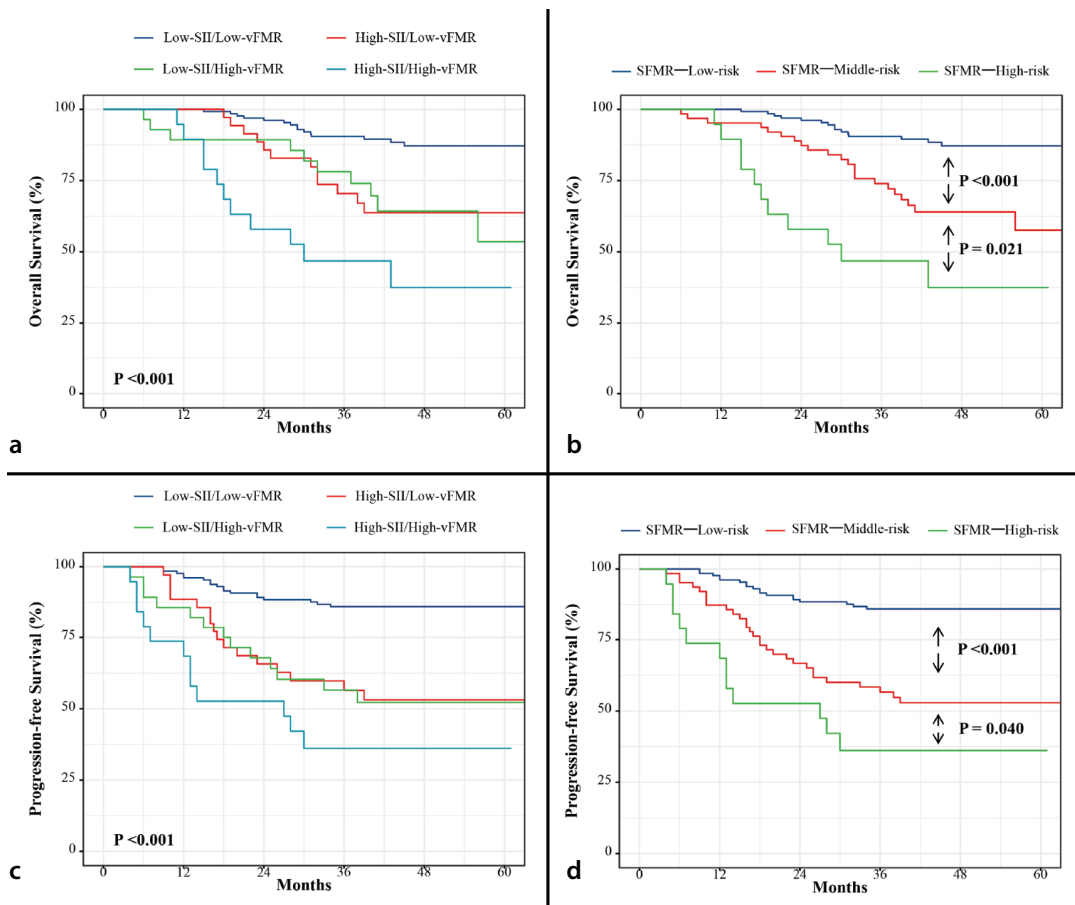


**Figure 3.** Kaplan–Meier curves for overall survival (a+b) and progression-free survival (c+d) according to the combination of systemic immune-inflammation (SII) and visceral fat-to-muscle ratio (vFMR) (a+c) and systemic immune-inflammation and fat-to-muscle ratio (SFMR) (b+d). The  $P$  values were calculated using the log-rank test.

ization and suppressing lymphocyte-mediated cytotoxicity.<sup>24</sup> Third, an increase in the number of platelets can directly promote tumor growth, invasion, and angiogenesis.<sup>25</sup> Hence, the SII, which is based on the three aforementioned types of blood cells, can more effectively demonstrate the equilibrium between antitumor and pro-tumor immune statuses.

Sarcopenia is an early manifestation of cancer and cachexia. Cumulative studies

have demonstrated that pretreatment sarcopenia is significantly associated with survival outcomes in patients with gastrointestinal<sup>26</sup> and gynecological tumors.<sup>27</sup> The prognostic value of pretreatment sarcopenia has also been extensively investigated in LACC, but with mostly negative results.<sup>9,28,29</sup> In addition, previous studies have reported the prognostic significance of the visceral fat area in various cancers.<sup>30-32</sup> Similarly, the prognostic value of adiposity in patients with LACC re-

mains controversial.<sup>9,22</sup> We speculated that considering individual muscle or fat parameters alone might not accurately describe the distribution of body composition, which could weaken the prognostic prediction ability. Therefore, we investigated the combined index of muscle and fat areas, vFMR, and confirmed its prognostic value. A feasible explanation is that patients with sarcopenia and/or visceral obesity are more likely to experience treatment-related adverse events, leading to low compliance with planned treatments.<sup>33-35</sup> The association between vFMR and CCRT response should be investigated further.

Systemic inflammation is the basis of and is intensified by sarcopenic obesity, forming a mutually reinforcing cycle that supports cancer progression. For instance, several cytokines released by inflammatory cells (e.g., interleukin 6) can regulate skeletal muscle metabolism, leading to protein degradation and decreased synthesis.<sup>36</sup> Excess adipose tissue is closely associated with low-grade systemic inflammation, which is characterized by abnormal cytokine production and muscle degradation.<sup>37,38</sup> Moreover, skeletal muscle wasting can drive local inflammation, systemic inflammation, and muscle degradation.<sup>39</sup> Our results also showed that higher vFMR was significantly associated with higher SII. The combination of the vFMR and SII better reflects the synergistic effect of systemic inflammation and sarcopenic obesity and exhibits promising prognostic significance.

This study has some limitations that need to be considered. First, as this was a retrospective, single-center study, selection bias and confounding factors were inevitable. Second, because all patients were Asian, the generalizability of our findings should be further confirmed. Third, although SII can possibly be influenced by various med-

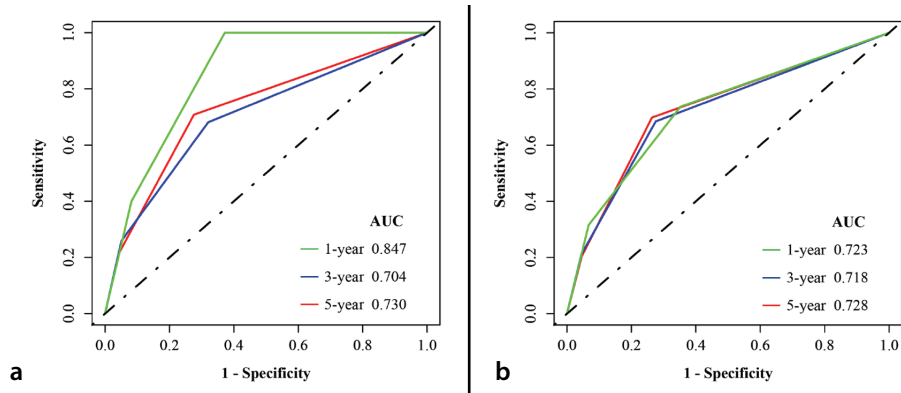


**Figure 4.** Time-dependent receiver-operating characteristic curves and area under the curves (AUCs) for predicting overall survival (a) and progression-free survival (b) by systemic immune-inflammation and fat-to-muscle ratio.

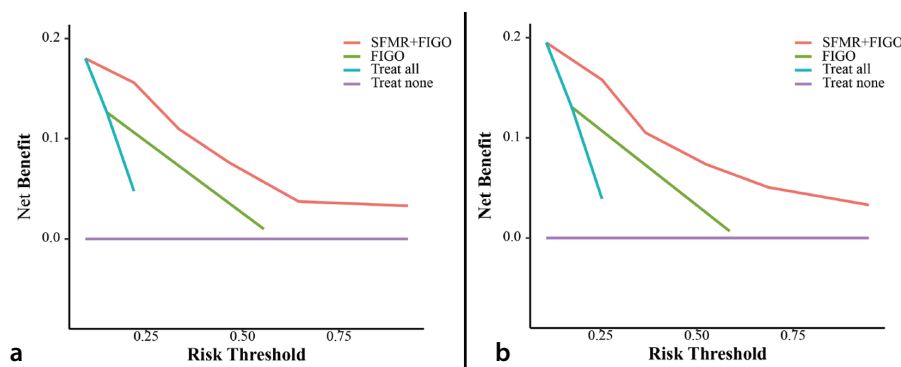


**Figure 5.** Decision curve analysis for overall survival (a) and progression-free survival (b).

Variables	Progression-free Survival		
	HR (95% CI)	HR (95% CI)	P value
<b>FIGO stage</b>			<0.001
IB-II	Reference	Reference	
III-IVA	3.653 (1.983–6.730)	3.457 (1.996–5.989)	
<b>Pelvic lymph node</b>			0.114
Negative	Reference	Reference	
Positive	1.593 (0.839–3.026)	1.594 (0.893–2.844)	
<b>SFMR</b>			<0.001
Low-risk	Reference	Reference	
Middle-risk	3.158 (1.633–6.108)	3.783 (2.095–6.829)	
High-risk	6.341 (2.873–13.996)	6.062 (2.888–12.723)	

FIGO, International Federation of Gynecology and Obstetrics; HR, hazard ratio; CI, confidence interval; SFMR, systemic immune-inflammation and fat-to-muscle ratio.

ical conditions, this inflammatory marker was calculated through routine laboratory test results. Other markers of systemic inflammation (e.g., C-reactive protein) were available for few patients and therefore not used. Fourth, laboratory blood and CT-derived body composition parameters were obtained from a single time point at the initial diagnosis. In future studies, data from subsequent CT scans should be incorporated to explore the prognostic significance of the changes in these markers. Finally, all patients received point A-based brachytherapy in this study. As image-guided brachytherapy is the current standard of treatment, further validation of our findings is needed in patients undergoing this procedure.

In conclusion, despite the above limitations, our study demonstrated that the SII and vFMR, as well as their composite indices, were independent prognostic factors in patients with LACC who received definitive CCRT. Future studies are needed to explore novel therapies to improve the outcomes in high-risk patients.

#### Conflict of interest disclosure

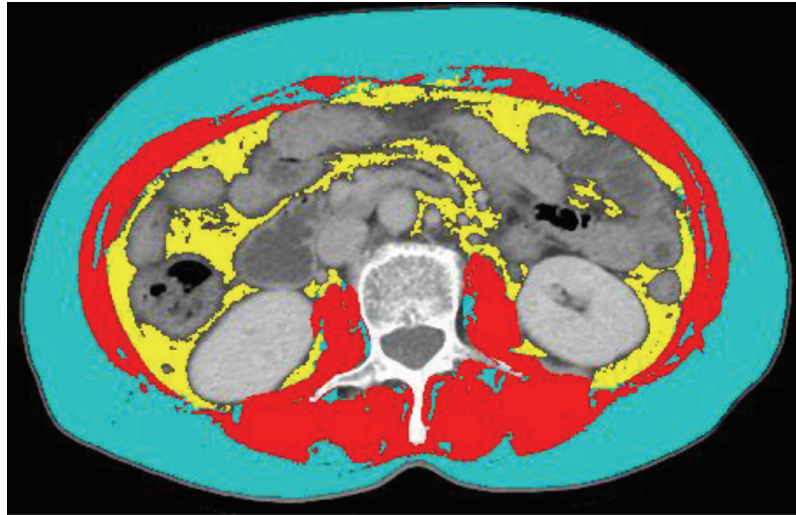
The authors declared no conflicts of interest.

#### References

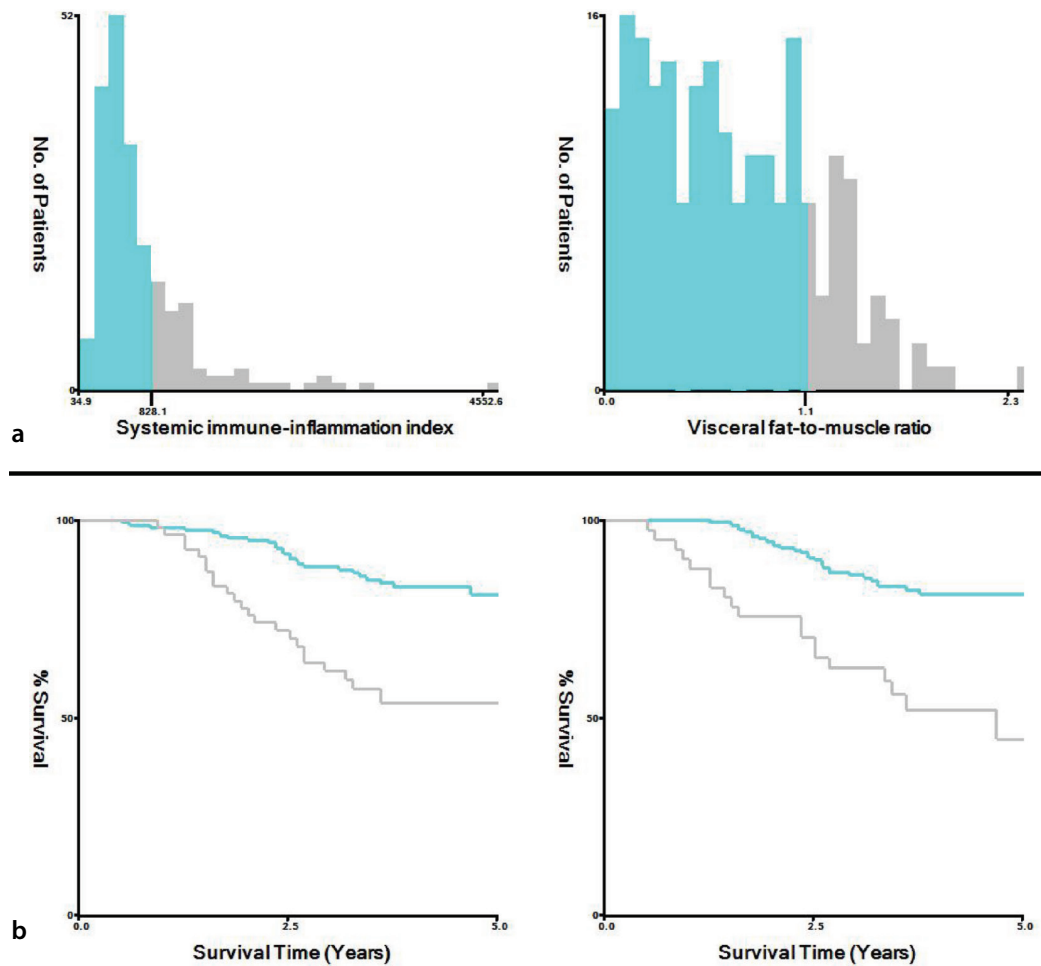
- Sung H, Ferlay J, Siegel RL, et al. Global Cancer Statistics 2020: GLOBOCAN estimates of incidence and mortality worldwide for 36 cancers in 185 countries. *CA Cancer J Clin.* 2021;71(3):209-249. [\[CrossRef\]](#)
- Grigsby PW, Massad LS, Mutch DG, et al. FIGO 2018 staging criteria for cervical cancer: Impact on stage migration and survival. *Gynecol Oncol.* 2020;157(3):639-643. [\[CrossRef\]](#)
- Meng Q, Wang W, Liu X, Wang D, Zhang F. Nomograms predicting survival of cervical cancer patients treated with concurrent chemoradiotherapy based on the 2018 FIGO staging system. *Front Oncol.* 2022;12:870670. [\[CrossRef\]](#)
- Feliciano EMC, Kroenke CH, Meyerhardt JA, et al. Association of systemic inflammation and sarcopenia with survival in nonmetastatic colorectal cancer: results from the C SCANS study. *JAMA Oncol.* 2017;3(12):e172319. [\[CrossRef\]](#)
- Lin JX, Lin JP, Xie JW, et al. Prognostic value and association of sarcopenia and systemic inflammation for patients with gastric cancer following radical gastrectomy. *Oncologist.* 2019;24(11):1091-1101. [\[CrossRef\]](#)
- Liang H, Peng H, Chen L. Prognostic Value of sarcopenia and systemic inflammation markers in patients undergoing definitive radiotherapy for esophageal cancer. *Cancer Manag Res.* 2021;13:181-192. [\[CrossRef\]](#)
- Elinav E, Nowarski R, Thaiss CA, Hu B, Jin C, Flavell RA. Inflammation-induced cancer: crosstalk between tumours, immune cells and microorganisms. *Nat Rev Cancer.* 2013;13(11):759-771. [\[CrossRef\]](#)
- Han X, Liu S, Yang G, et al. Prognostic value of systemic hemato-immunological indices in uterine cervical cancer: a systemic review, meta-analysis, and meta-regression of observational studies. *Gynecol Oncol.* 2021;160(1):351-360. [\[CrossRef\]](#)
- Lee J, Chang CL, Lin JB, et al. Skeletal muscle loss is an imaging biomarker of outcome after definitive chemoradiotherapy for locally advanced cervical cancer. *Clin Cancer Res.* 2018;24(20):5028-5036. [\[CrossRef\]](#)
- Abe A, Yuasa M, Imai Y, et al. Extreme leanness, lower skeletal muscle quality, and loss of muscle mass during treatment are predictors of poor prognosis in cervical cancer treated with concurrent chemoradiation therapy. *Int J Clin Oncol.* 2022;27(5):983-991. [\[CrossRef\]](#)
- Aichi M, Hasegawa S, Kurita Y, et al. Low skeletal muscle mass predicts poor prognosis for patients with stage III cervical cancer on concurrent chemoradiotherapy. *Nutrition.* 2023;109:111966. [\[CrossRef\]](#)
- Mauland KK, Eng Ø, Ytre-Hauge S, et al. High visceral fat percentage is associated with poor outcome in endometrial cancer. *Oncotarget.* 2017;8(62):105184-105195. [\[CrossRef\]](#)
- Eide AJ, Halle MK, Lura N, et al. Visceral fat percentage for prediction of outcome in uterine cervical cancer. *Gynecol Oncol.* 2023;176:62-68. [\[CrossRef\]](#)
- Ham S, Choi JH, Shin SG, Lee EJ. High visceral fat-to-muscle ratio is an independent factor that predicts worse overall survival in patients with primary epithelial ovarian, fallopian tube, and peritoneal cancer. *J Ovarian Res.* 2023;16(1):19. [\[CrossRef\]](#)
- Gien LT, Covens A. Lymph node assessment in cervical cancer: prognostic and therapeutic implications. *J Surg Oncol.* 2009;99(4):242-247. [\[CrossRef\]](#)
- Huang H, Liu Q, Zhu L, et al. Prognostic value of preoperative systemic immune-inflammation index in patients with cervical cancer. *Sci Rep.* 2019;9(1):3284. [\[CrossRef\]](#)
- Camp RL, Dolled-Filhart M, Rimm DL. X-tile: a new bio-informatics tool for biomarker assessment and outcome-based cut-point optimization. *Clin Cancer Res.* 2004;10(21):7252-7259. [\[CrossRef\]](#)
- Vickers AJ, Elkin EB. Decision curve analysis: a novel method for evaluating prediction models. *Med Decis Making.* 2006;26(6):565-574. [\[CrossRef\]](#)
- Ayhan S, Akar S, Kar İ, et al. Prognostic value of systemic inflammatory response markers in cervical cancer. *J Obstet Gynaecol.* 2022;42(6):2411-2419. [\[CrossRef\]](#)
- Yang R, Chang Q, Meng X, Gao N, Wang W. Prognostic value of systemic immune-inflammation index in cancer: a meta-analysis. *J Cancer.* 2018;9(18):3295-3302. [\[CrossRef\]](#)
- Liu P, Jiang Y, Zheng X, Pan B, Xiang H, Zheng M. Pretreatment systemic immune-inflammation index can predict response to neoadjuvant chemotherapy in cervical cancer at stages IB2-IIIB. *Pathol Oncol Res.* 2022;28:1610294. [\[CrossRef\]](#)
- Guo H, Feng S, Li Z, et al. Prognostic Value of Body Composition and Systemic Inflammatory Markers in Patients with Locally Advanced Cervical Cancer Following Chemoradiotherapy. *J Inflamm Res.* 2023;16:5145-5156. [\[CrossRef\]](#)
- Mei Z, Liu Y, Liu C, et al. Tumour-infiltrating inflammation and prognosis in colorectal cancer: systematic review and meta-analysis. *Br J Cancer.* 2014;110(6):1595-1605. [\[CrossRef\]](#)
- Shamamian P, Schwartz JD, Pocock BJ, et al. Activation of progelatinase A (MMP-2) by neutrophil elastase, cathepsin G, and proteinase-3: a role for inflammatory cells in tumor invasion and angiogenesis. *J Cell Physiol.* 2001;189(2):197-206. [\[CrossRef\]](#)
- Kusumanto YH, Dam WA, Hospers GA, Meijer C, Mulder NH. Platelets and granulocytes, in particular the neutrophils, form important compartments for circulating vascular endothelial growth factor. *Angiogenesis.* 2003;6(4):283-287. [\[CrossRef\]](#)
- Su H, Ruan J, Chen T, Lin E, Shi L. CT-assessed sarcopenia is a predictive factor for both long-term and short-term outcomes in gastrointestinal oncology patients: a systematic review and meta-analysis. *Cancer Imaging.* 2019;19(1):82. [\[CrossRef\]](#)
- Li YX, Xia WW, Liu WY. The influence process of sarcopenia on female cancer: a systematic review and meta-analysis. *J Obstet Gynaecol Res.* 2021;47(12):4403-4413. [\[CrossRef\]](#)
- Kiyotoki T, Nakamura K, Haraga J, et al. Sarcopenia is an important prognostic factor in patients with cervical cancer undergoing concurrent chemoradiotherapy. *Int J Gynecol Cancer.* 2018;28(1):168-175. [\[CrossRef\]](#)
- Matsuoka H, Nakamura K, Matsubara Y, et al. Sarcopenia is not a prognostic factor of outcome in patients with cervical cancer undergoing concurrent chemoradiotherapy or radiotherapy. *Anticancer Res.* 2019;39(2):933-939. [\[CrossRef\]](#)
- Harada K, Baba Y, Ishimoto T, et al. Low Visceral fat content is associated with poor prognosis in a database of 507 upper gastrointestinal cancers. *Ann Surg Oncol.* 2015;22(12):3946-3953. [\[CrossRef\]](#)

31. Fujiwara N, Nakagawa H, Kudo Y, et al. Sarcopenia, intramuscular fat deposition, and visceral adiposity independently predict the outcomes of hepatocellular carcinoma. *J Hepatol.* 2015;63(1):131-140. [\[CrossRef\]](#)
32. Caan BJ, Cespedes Feliciano EM, Prado CM, et al. Association of muscle and adiposity measured by computed tomography with survival in patients with nonmetastatic breast cancer. *JAMA Oncol.* 2018;4(6):798-804. [\[CrossRef\]](#)
33. Baracos VE, Arribas L. Sarcopenic obesity: hidden muscle wasting and its impact for survival and complications of cancer therapy. *Ann Oncol.* 2018;29(Suppl 2):ii1-ii9. [\[CrossRef\]](#)
34. Cespedes Feliciano EM, Chen WY, Lee V, et al. Body composition, adherence to anthracycline and taxane-based chemotherapy, and survival after nonmetastatic breast cancer. *JAMA Oncol.* 2020;6(2):264-270. [\[CrossRef\]](#)
35. Catikkas NM, Bahat Z, Oren MM, Bahat G. Older cancer patients receiving radiotherapy: a systematic review for the role of sarcopenia in treatment outcomes. *Aging Clin Exp Res.* 2022;34(8):1747-1759. [\[CrossRef\]](#)
36. Baracos VE. Regulation of skeletal-muscle-protein turnover in cancer-associated cachexia. *Nutrition.* 2000;16(10):1015-1018. [\[CrossRef\]](#)
37. Iyengar NM, Hudis CA, Dannenberg AJ. Obesity and cancer: local and systemic mechanisms. *Annu Rev Med.* 2015;66:297-309. [\[CrossRef\]](#)
38. Deng T, Lyon CJ, Bergin S, Caligiuri MA, Hsueh WA. Obesity, inflammation, and cancer. *Annu Rev Pathol.* 2016;11:421-449. [\[CrossRef\]](#)
39. Kalinkovich A, Livshits G. Sarcopenic obesity or obese sarcopenia: a cross talk between age-associated adipose tissue and skeletal muscle inflammation as a main mechanism of the pathogenesis. *Ageing Res Rev.* 2017;35:200-221. [\[CrossRef\]](#)





**Supplementary Figure 1.** Example of body composition analysis for measurement of tissue areas. The blue area represents subcutaneous adipose, the red area represents skeletal muscle, and the yellow area represents visceral adipose.



**Supplementary Figure 2.** X-tile software analysis to determine the optimal cut-off values for systemic immune-inflammation index (left) and visceral fat-to-muscle ratio (right). (a) The histogram of the both parameters. (b) Kaplan-Meier analysis for overall survival.

<b>Supplementary Table 1. The relationship between systemic immune-inflammation and clinicopathological parameters</b>			
Characteristics	SII ≤828 (n = 158)	SII >828 (n = 54)	P value
Age, mean ± SD, yrs	58.6 ± 10.4	59.4 ± 11.1	0.607
BMI, mean ± SD, kg/m <sup>2</sup>	22.9 ± 3.1	23.7 ± 3.0	0.116
<b>ECOG performance status, n (%)</b>			0.144
0	108 (68.4)	31 (57.4)	
1	50 (31.6)	23 (42.6)	
<b>Histology, n (%)</b>			0.522
Squamous cell carcinoma	145 (91.8)	48 (88.9)	
Adenocarcinoma	13 (8.2)	6 (11.1)	
<b>FIGO stage, n (%)</b>			0.417
IB-II	120 (75.9)	38 (70.4)	
III-IVA	38 (24.1)	16 (29.6)	
<b>Pelvic lymph node, n (%)</b>			1.000
Negative	79 (50.0)	27 (50.0)	
Positive	79 (50.0)	27 (50.0)	
<b>SCC-Ag level, n (%)</b>			0.949
≤10 ng/mL	109 (69.0)	37 (68.5)	
>10 ng/mL	49 (31.0)	17 (31.5)	
<b>vFMR level, n (%)</b>			0.008
≤1.1	130 (82.3)	35 (64.8)	
>1.1	28 (17.7)	19 (35.2)	

BMI, body mass index; ECOG, Eastern Cooperative Oncology Group; FIGO, International Federation of Gynecology and Obstetrics; SCC-Ag, squamous cell carcinoma antigen; vFMR, visceral fat-to-muscle ratio; SD, standard deviation; SII, systemic immune-inflammation.

**Supplementary Table 2.** The relationship between visceral fat-to-muscle ratio and clinicopathological parameters

Characteristics	vFMR ≤ 1.1 (n = 165)	vFMR > 1.1 (n = 47)	P value
Age, mean ± SD, yrs	57.4 ± 10.9	63.5 ± 7.9	<0.001
BMI, mean ± SD, kg/m <sup>2</sup>	22.1 ± 2.9	22.1 ± 3.7	0.989
<b>ECOG performance status, n (%)</b>			0.949
0	108 (65.5)	31 (66.0)	
1	57 (34.5)	16 (34.0)	
<b>Histology, n (%)</b>			0.648
Squamous cell carcinoma	151 (91.5)	42 (89.4)	
Adenocarcinoma	14 (8.5)	5 (10.6)	
<b>FIGO stage, n (%)</b>			0.056
IB-II	128 (77.6)	30 (63.8)	
III-IVA	37 (22.4)	17 (36.2)	
<b>Pelvic lymph node, n (%)</b>			0.069
Negative	88 (53.3)	18 (38.3)	
Positive	77 (46.7)	29 (61.7)	
<b>SCC-Ag level, n (%)</b>			0.625
≤10 ng/mL	115 (69.7)	31 (66.0)	
>10 ng/mL	50 (30.3)	16 (34.0)	
<b>SII level, n (%)</b>			0.008
≤550.1	130 (78.8)	28 (59.6)	
>550.1	35 (21.2)	19 (40.4)	

BMI, body mass index; ECOG, Eastern Cooperative Oncology Group; FIGO, International Federation of Gynecology and Obstetrics; SCC-Ag, squamous cell carcinoma antigen; SII, systemic immune-inflammation index; SD, standard deviation; vFMR, visceral fat-to-muscle ratio.

**Supplementary Table 3.** The relationship between the combination of systemic immune-inflammation and visceral fat-to-muscle ratio and clinicopathological parameters

Characteristics	SFMR			$P_{\text{linear}}$ value
	Low-risk (n = 130)	Middle-risk (n = 63)	High-risk (n = 19)	
<b>Age, n (%)</b>				0.013
<65 yrs	95 (73.1)	33 (52.4)	11 (57.9)	
≥65 yrs	35 (26.9)	30 (47.6)	8 (42.1)	
<b>BMI, n (%)</b>				0.065
<25 kg/m <sup>2</sup>	99 (76.2)	43 (68.3)	11 (57.9)	
≥25 kg/m <sup>2</sup>	31 (23.8)	20 (31.7)	8 (42.1)	
<b>ECOG performance status, n (%)</b>				0.352
0	89 (68.5)	38 (60.3)	12 (63.2)	
1	41 (31.5)	25 (39.7)	7 (36.8)	
<b>Histology, n (%)</b>				0.475
Squamous cell carcinoma	119 (91.5)	58 (92.1)	16 (84.2)	
Adenocarcinoma	11 (8.5)	5 (7.9)	3 (15.8)	
<b>FIGO stage, n (%)</b>				0.081
IB-II	102 (78.5)	44 (69.8)	12 (63.2)	
III-IVA	28 (21.5)	19 (30.2)	7 (36.8)	
<b>Pelvic lymph node, n (%)</b>				0.250
Negative	69 (53.1)	29 (46.0)	8 (42.1)	
Positive	61 (46.9)	34 (54.0)	11 (57.9)	
<b>SCC-Ag level, n (%)</b>				0.725
≤10 ng/mL	90 (69.2)	44 (69.8)	12 (63.2)	
>10 ng/mL	40 (30.8)	19 (30.2)	7 (36.8)	

BMI, body mass index; ECOG, Eastern Cooperative Oncology Group; FIGO, International Federation of Gynecology and Obstetrics; SCC-Ag, squamous cell carcinoma antigen; SFMR, systemic immune-inflammation and fat-to-muscle ratio



# Meta-research on reporting guidelines for artificial intelligence: are authors and reviewers encouraged enough in radiology, nuclear medicine, and medical imaging journals?

Burak Koçak  
 Ali Keleş  
 Fadime Köse

University of Health Sciences, Başakşehir Çam and Sakura City Hospital, Clinic of Radiology, Istanbul, Türkiye

## PURPOSE

To determine how radiology, nuclear medicine, and medical imaging journals encourage and mandate the use of reporting guidelines for artificial intelligence (AI) in their author and reviewer instructions.

## METHODS

The primary source of journal information and associated citation data used was the Journal Citation Reports (June 2023 release for 2022 citation data; Clarivate Analytics, UK). The first- and second-quartile journals indexed in the Science Citation Index Expanded and the Emerging Sources Citation Index were included. The author and reviewer instructions were evaluated by two independent readers, followed by an additional reader for consensus, with the assistance of automatic annotation. Encouragement and submission requirements were systematically analyzed. The reporting guidelines were grouped as AI-specific, related to modeling, and unrelated to modeling.

## RESULTS

Out of 102 journals, 98 were included in this study, and all of them had author instructions. Only five journals (5%) encouraged the authors to follow AI-specific reporting guidelines. Among these, three required a filled-out checklist. Reviewer instructions were found in 16 journals (16%), among which one journal (6%) encouraged the reviewers to follow AI-specific reporting guidelines without submission requirements. The proportions of author and reviewer encouragement for AI-specific reporting guidelines were statistically significantly lower compared with those for other types of guidelines ( $P < 0.05$  for all).

## CONCLUSION

The findings indicate that AI-specific guidelines are not commonly encouraged and mandated (i.e., requiring a filled-out checklist) by these journals, compared with guidelines related to modeling and unrelated to modeling, leaving vast space for improvement. This meta-research study hopes to contribute to the awareness of the imaging community for AI reporting guidelines and ignite large-scale group efforts by all stakeholders, making AI research less wasteful.

## CLINICAL SIGNIFICANCE

This meta-research highlights the need for improved encouragement of AI-specific guidelines in radiology, nuclear medicine, and medical imaging journals. This can potentially foster greater awareness among the AI community and motivate various stakeholders to collaborate to promote more efficient and responsible AI research reporting practices.

## KEYWORDS

Artificial intelligence, machine learning, guideline, checklist, reporting

Corresponding author: Burak Koçak

E-mail: drburakkocak@gmail.com

Received 10 November 2023; revision requested 03 January 2024; accepted 10 February 2024.



Epub: 20.02.2024

Publication date: 09.09.2024

DOI: 10.4274/dir.2024.232604

Poor or suboptimal reporting of medical research is regarded as a significant and widespread issue that contributes to the waste of scarce and valuable resources invested in research projects.<sup>1-5</sup> For such studies, readers cannot assess the validity of the method relative to existing knowledge, and thus the reliability and reproducibility of the findings.<sup>6</sup> This hinders the clinical translation of promising research findings<sup>7</sup> and their comparability with other publications for evidence synthesis or meta-analysis.<sup>8</sup> The adherence to consensus-based reporting standards (i.e., reporting guidelines) is one of the principal methods for reducing the risk of poor reporting. To promote this, vast projects, like Enhancing the QUALity and Transparency Of health Research (EQUATOR) network, were started, and several reporting guidelines were developed and published in the literature.<sup>9,10</sup> Typically, these guidelines take the form of online or offline checklists, flowcharts, or explicit texts that instruct authors on how to report their research. Several studies researched the effectiveness of adhering to reporting guidelines in various study types. They found that adherence is associated with improved manuscript quality in peer review,<sup>11</sup> favorable reviewer ratings and editorial decisions,<sup>12</sup> higher citation counts and opportunity to be published in journals with a higher impact factor,<sup>13</sup> and improved completeness and quality of the research.<sup>14-22</sup>

Similar to healthcare literature, medical artificial intelligence (AI) research faces poor or suboptimal reporting issues. With the massive growth of healthcare literature using AI, including medical imaging,<sup>23</sup> the need for complete and structured reporting of prognostic and diagnostic studies that use machine learning algorithms or models has

increased. An expanding body of research indicates that AI studies frequently fall short of expected reporting standards,<sup>24,25</sup> lacking sufficient details on modeling and its evaluation, and failing to adequately address potential sources of bias.<sup>26-32</sup> Multiple specific guidelines relevant to AI studies have been developed to address these issues.<sup>25,33-41</sup> Examples of these guidelines include Checklist for AI in Medical Imaging (CLAIM),<sup>42,43</sup> Fairness, Universality, Traceability, Usability, Robustness, and Explainability-AI (FUTURE-AI),<sup>44</sup> Minimum Information about Clinical AI Modelling (MI-CLAIM),<sup>45</sup> CheckList for Evaluation of Radiomics research (CLEAR),<sup>46</sup> and Methodological Radiomics Score (METRICS).<sup>47</sup> In addition, as a continuation of previous efforts, several guidelines are currently under development, such as Standards for the Reporting of Diagnostic Accuracy Studies-AI (STARD-AI) for AI-centered diagnostic test accuracy studies and Transparent Reporting of a Multivariable Prediction Model for Individual Prognosis or Diagnosis-AI (TRIPOD-AI) for those related to diagnostic models.<sup>48,49</sup> The most widely recognized AI guidelines and ones currently under development can be found in the following seminal papers.<sup>50,51</sup>

The availability of reporting guidelines and checklists has not yet resolved the problem of inadequate reporting. While editorial guidance advocating for transparent reporting is widespread and well-intentioned, authors frequently overlook or fail to adhere to these guidelines.<sup>52-57</sup> In a very recent citation analysis of an AI checklist on medical imaging and a meta-research on radiomics, claims regarding the use of checklists and quality scoring tools for self-reporting (i.e., reporting with filling checklists by study authors) have been supported.<sup>26,32</sup> Journals can significantly impact the quality of reporting by encouraging or mandating responsible reporting practices, such as the use of reporting guidelines and checklists in their author and reviewer instructions.<sup>58,59</sup> However, research on the encouragement of AI reporting guidelines by journals specialized in radiology, nuclear medicine, and medical imaging is scarce.<sup>60</sup> Investigating this issue could yield valuable insights to foster higher-quality research within these journals.

This meta-research study aims to determine how these journals encourage and mandate (i.e., requiring a filled-out checklist) the use of AI reporting guidelines in their author and reviewer instructions by comparing reporting guidelines that are specific to AI, related to modeling, and unrelated to modeling.

## Methods

Figure 1 presents the key study steps of this meta-research.

### Dataset

The primary source of journals and associated citation data used was the Journal Citation Reports (June 2023 release for 2022 citation data; Clarivate Analytics, UK). This report was based on data obtained from the Web of Science (WoS) (Clarivate Analytics, UK).

Journals indexed in the WoS category, radiology, nuclear medicine, and medical imaging, that met the following criteria were included in this study: inclusion in the Science Citation Index Expanded (SCIE) or Emerging Sources Citation Index (ESCI) and placement within the first quartile (Q1; top 25% of journals in the list) or second quartile (Q2; journals in the top 25%–50% group) based on the 2022 Journal Impact Factor. This analysis excluded journals that had a limited scope, specifically those that focused solely on review articles (i.e., not publishing original research articles), as these journals were not expected to publish articles using AI reporting guidelines.

Two readers, each in their third year of radiology residency and with prior experience conducting systematic reviews on reporting quality in AI or radiomics, accessed the author and reviewer instructions from the journals' websites and saved them as PDF files. The task was distributed evenly among the readers, and they also reviewed each other's resulting files. All author and reviewer instructions were accessed between September 4 and 7, 2023. In the case of multiple instructions, the most up-to-date version was selected.

To mitigate errors during the assessment of instructions, a custom Python script based on the PyMuPDF package was used to automatically annotate certain terms within the PDF documents. The terms covered AI, machine learning, reporting, guidelines, checklists, and their specific names or acronyms. The code and exact terms can be accessed at <https://github.com/radiomic/PDFhighlighter>.

### Evaluation of author and reviewer instructions

The author and reviewer instructions that were automatically annotated by the script were evaluated by the same readers who downloaded the instructions. All evaluations underwent a meticulous review process overseen by an additional reader possessing

#### Main points

- Based on author and reviewer instructions, artificial intelligence (AI)-specific guidelines are not commonly encouraged, and they are not mandated for submission as filled-out checklists by radiology, nuclear medicine, and medical imaging journals.
- The proportions of author and reviewer encouragements for AI-specific reporting guidelines were statistically significantly lower compared with those for other types of guidelines.
- The collaboration of all stakeholders, including guideline developers, journal managers, editors, reviewers, authors, and funders, is needed to further encourage these guidelines to make AI research less wasteful.

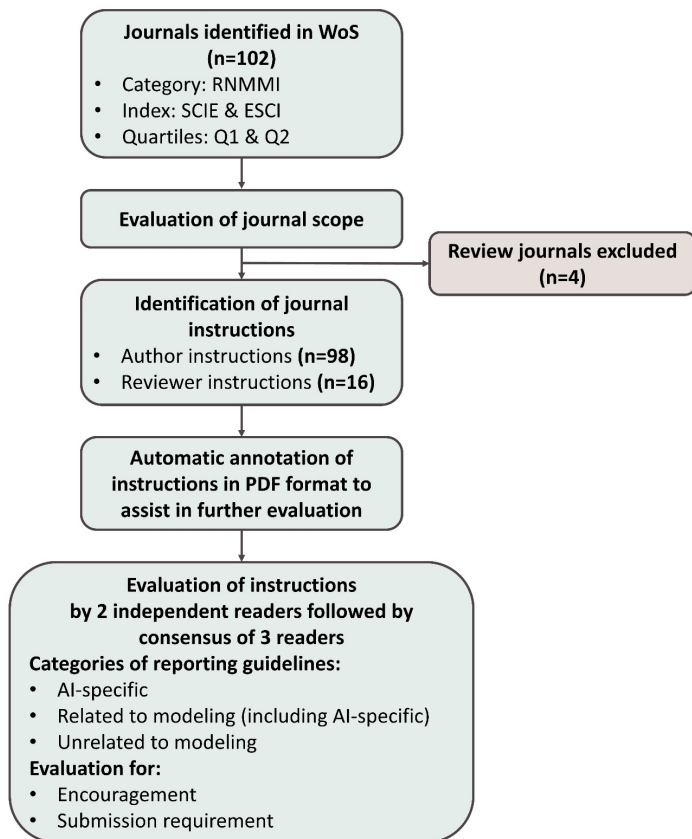


**Figure 1.** Key study steps. WoS, Web of Science; RNMMI, Radiology, Nuclear Medicine, and Medical Imaging; SCIE, Science Citation Index Expanded; ESCI, Emerging Sources Citation Index; Q1, first quartile; Q2, second quartile; PDF, portable document format; AI, artificial intelligence.

8 years of expertise as a radiology specialist, complemented by over 5 years of research experience in machine learning, radiomics, and systematic reviews. Final decisions were reached by consensus among all readers.

The collected data primarily fell into two categories: encouragement of authors or reviewers and the presence of submission requirements for filled-out checklists in case of encouragement. When evaluating the encouragement, to elicit a positive evaluation from readers, it was imperative to explicitly state the name of the reporting guideline or make a direct reference to it. In addition, encouragement was defined as any sort of mention of specific guidelines. For instance, if authors and reviewers are recommended for adherence, referral, or usage of the guidelines, even if not explicitly intended for integration into their workflow, it was considered encouragement. The inclusion of general references to the central source or hub of guidelines or checklists, such as the EQUATOR network website, was not regarded as a specific encouragement in this work. To fulfill the submission requirement (i.e., mandating), this study sought a clear indication that the filled-out checklist would be

uploaded to the submission system as an integral part of both the manuscript and peer review processes. The submission systems were only investigated when the submission requirements were unclear in the instructions. Checklists without an associated publication in a journal (i.e., checklists as part of journal instructions without a digital object identifier) were not considered as a reporting guideline.

Three types of reporting guidelines were analyzed as follows: i) AI-specific reporting guidelines; ii) those related to modeling (e.g., diagnostic or prognostic modeling; may or may not be associated with AI or machine learning); and iii) those unrelated to modeling. AI-specific reporting guidelines and those related to modeling included those specified in two recent seminal articles.<sup>50,51</sup> For AI-specific guidelines (e.g., CLAIM, Consolidated Standards of Reporting Trials for AI (CONSORT-AI), Standard Protocol Items: Recommendations for Interventional Trials for AI (SPIRIT-AI), FUTURE-AI, MI-CLAIM), this study referred to the publication of Klontzas et al.<sup>50</sup>, which did not limit its scope to a specific data type. For guidelines related to modeling, including AI-specific ones (e.g. TRIPOD), this

study referred to the paper of Klement and El Emam<sup>51</sup>, which primarily focused on structured data. Due to the potential omission of relevant reporting guidelines in these papers, this study refrained from confining its criteria to those listed in the aforementioned articles.

## Statistical analysis

Statistical analysis was performed using Jamovi (version 2.2.5). The majority of the findings were presented through descriptive statistics, wherein percentages were rounded to the nearest whole number. The inter-reader agreement analysis of the first two readers was conducted using Cohen's kappa or percentage agreement, as appropriate. The following grading system was used to interpret Cohen's kappa:  $\kappa \leq 0.00$ , no;  $0.00 < \kappa \leq 0.20$ , slight;  $0.20 < \kappa \leq 0.40$ , fair;  $0.40 < \kappa \leq 0.60$ , moderate;  $0.60 < \kappa \leq 0.80$ , substantial;  $0.80 < \kappa \leq 1$ , almost perfect agreement. Comparison of the distribution of quantitative variables was conducted using either the Student's t-test or the Mann-Whitney U test, depending on the statistical normality of the data. The chi-square test or Fisher's exact test was employed to assess differences in the distribution of categorical variables across various citation variables between subjects. Furthermore, McNemar's test was used for the same purpose within subjects, and the continuity correction was also applied. A *P* value of  $<0.05$  was considered statistically significant.

## Results

### Baseline characteristics of journals

Out of 102 Q1 and Q2 radiology, nuclear medicine, and medical imaging journals indexed in SCIE and ESCI databases, 98 were included in this study. Four journals were excluded because they published only review articles. Of the journals included, 66 were from SCIE (Q1/Q2, 32/34), with a median 2022 impact factor of 3.9 (interquartile range: 2.4). The remaining 32 journals were from ESCI (Q1/Q2, 16/16), with a median 2022 impact factor of 2.25 (interquartile range: 1.9).

For all 98 journals, instructions specific to authors were found. However, specific instructions for reviewers or referees were found for 16 journals only (16%).

### Analysis of author instructions

Table 1 summarizes the encouragement of authors to use reporting guidelines that are specific to AI, related to modeling, and

unrelated to modeling, as well as the requirement of submission for these reporting guidelines.

Considering all 98 journals, only five journals (5%) encouraged the authors to follow AI-specific reporting guidelines. Table 2 presents the AI-specific guidelines recommended in these journals: CLAIM (n = 3), Proposed Requirements for Cardiovascular Imaging-Related Machine Learning Evaluation (PRIME) (n = 1), and Checklist for AI in Medical Physics (CLAMP) (n = 1).<sup>42,61,62</sup> Of these, three (60%) required a filled-out checklist along with the submission.

In total, 30 journals (31% of 98) endorsed at least one reporting guideline related to modeling, including both general modeling guidelines and AI-specific ones: TRIPOD (n = 26), along with the three aforementioned AI reporting guidelines, namely CLAIM, PRIME, and CLAMP.<sup>42,61-63</sup> One journal encouraged two modeling-related guidelines (TRIPOD and CLAIM). Of the 30 journals, only four (13%) required a filled-out checklist along with the submission. Furthermore, only one of the journals, Ultrasound in Obstetrics and Gynecology, encouraged TRIPOD and mandated a filled-out checklist.

A total of 75 journals (77% of 98) encouraged at least one guideline unrelated to modeling. The frequency of the most well-known guidelines in these categories is as follows: CONSORT (n = 61), Preferred Reporting Items for Systematic Reviews and Meta-Analyses (PRISMA) (n = 51), Animal Research: Reporting of *In Vivo* Experiments (ARRIVE) (n = 45), STARD (n = 44), and Strengthening the Reporting of Observational Studies in Epidemiology (STROBE) (n = 42).<sup>64-68</sup> Of these journals, 36 (48%) required a filled-out checklist along with the submission.

The level of encouragement for authors, both with and without submission requirements, regarding the naming of reporting guidelines, is summarized in Figure 2, alongside a comparison with that of reviewers.

Statistically significant differences were observed in the proportions of author encouragement among pairwise comparisons of AI-specific reporting guidelines, those related to modeling, and those unrelated to modeling ( $P < 0.001$  for all). Notably, the encouragement level for guidelines unrelated to modeling was consistently higher across all pairs.

There were no statistically significant differences in the distribution of author encouragement status concerning the journal index (i.e., SCIE vs. ESCI) and quartile (i.e., Q1 vs. Q2) ( $P > 0.05$  for all).

Regarding the encouragement of reporting guidelines related to modeling in general, including AI-specific ones, as well as those unrelated to modeling, the inter-rater reliability analysis yielded almost perfect agreement, with Cohen's kappa values ranging between 0.916 and 0.950.

### Analysis of reviewer instructions

Table 1 summarizes the encouragement of reviewers to use reporting guidelines that are specific to AI, related to modeling, and unrelated to modeling, as well as the requirement of submission for these reporting guidelines.

Of the 16 journals that had instructions for reviewers, only one (6%), European Radiology, encouraged the reviewers to follow an AI-specific reporting guideline (CLAIM), which can also be regarded as a modeling-related guideline, without a filled-out checklist along with the submission of peer review.<sup>42</sup> The primary purpose was, however, to check whether the authors provided the checklist.

Regarding the guidelines that are not related to modeling, six journals (38% of 16) encouraged the reviewers to follow at least one of those. The journals most frequently recommended CONSORT (n = 4) and PRISMA (n = 4) without a filled-out checklist along with the submission of peer review.<sup>67,68</sup>

The summary of reviewer encouragement, both with and without submission requirements, regarding the naming of reporting guidelines, is depicted in Figure 2, alongside a comparison with that of the authors.

There was a statistically significant difference in the proportion of reviewer encouragement between AI-specific or modeling-related reporting guidelines and those unrelated to modeling ( $P < 0.025$ ), with the latter being the higher.

There were no statistically significant differences in the distribution of reviewer encouragement status against the journal index (i.e., SCIE vs. ESCI) and quartile (i.e., Q1 vs. Q2) ( $P > 0.05$  for all).

For reviewers, the encouragement of reporting guidelines related to modeling in general, including AI-specific ones, as well as those not related to modeling, resulted in high inter-rater reliability, with percentage agreement values ranging between 79% and 93%.

**Table 1.** Journal statistics for the encouragement and submission requirements of reporting guidelines

Instruction	Guideline	Number of journals			
		Encouragement		Submission requirement	
		Yes	No	Yes	No
For authors	AI-specific	5 (5%)	93 (95%)	3 (60%)	2 (40%)
	Related to modeling <sup>1</sup>	30 (31%)	68 (69%)	4 (13%)	26 (87%)
	Unrelated to modeling	75 (77%)	23 (23%)	36 (48%)	39 (52%)
For reviewers	AI-specific	1 (6%)	15 (94%)	0 (0%)	16 (100%)
	Related to modeling <sup>1</sup>	1 (6%)	15 (94%)	0 (0%)	16 (100%)
	Unrelated to modeling	6 (38%)	10 (62%)	0 (0%)	16 (100%)

<sup>1</sup>Including AI-specific ones. AI, artificial intelligence.

**Table 2.** Encouraged AI-specific reporting guidelines for authors and their submission requirements

Index	Journal title	2022 JIF	Q	AI-specific reporting guideline	
				Encouragement	Submission requirement
SCIE	JACC: Cardiovascular Imaging	14	Q1	PRIME	Yes
	European Radiology	5.9	Q1	CLAIM	No
	Journal of the American College of Radiology	4.5	Q1	CLAIM	No
	Medical Physics	3.8	Q2	CLAMP	Yes
ESCI	Radiology: Artificial Intelligence	9.8	Q1	CLAIM	Yes

SCIE, Science Citation Index Expanded; ESCI, Emerging Sources Citation Index; JIF, Journal Impact Factor; Q, quartile (according to the category radiology, nuclear medicine, and medical imaging); AI, artificial intelligence; Q1, first quartile; Q2, second quartile; PRIME, Proposed Requirements for Cardiovascular Imaging-Related Machine Learning Evaluation; CLAIM, Checklist for AI in Medical Imaging; CLAMP, Checklist for AI in Medical Physics.



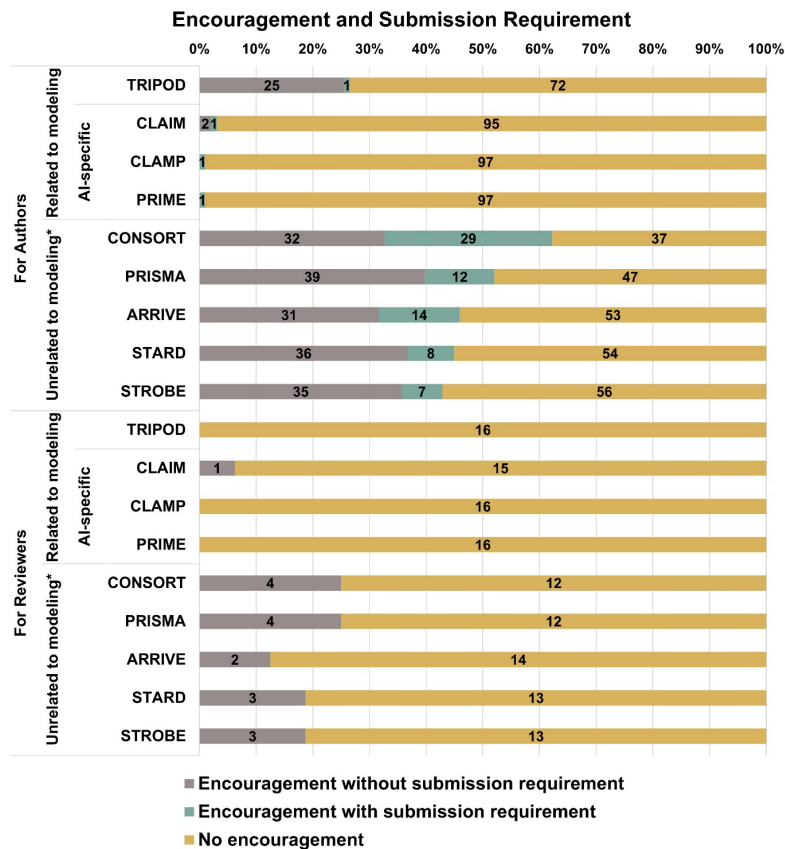


**Figure 2.** Encouragement of authors and reviewers for the reporting guidelines with and without submission requirements. AI, artificial intelligence. \*Only the top five most frequently encouraged reporting guidelines were included.

## Discussion

### Overview

This meta-research investigated how radiology, nuclear medicine, and medical imaging journals encourage and mandate (i.e., requiring a filled-out checklist) the use of AI reporting guidelines in their author and reviewer instructions. The results were presented by comparing reporting guidelines that are specific to AI, related to modeling, and unrelated to modeling. It was found that only a very small number of journals encouraged (5%, 5/98) and mandated (3%, 3/98) the use of AI reporting guidelines (i.e., CLAIM, PRIME, and CLAMP) for authors. In addition, only one journal (6% of 16 available reviewer instructions) encouraged the reviewers to follow AI reporting guidelines (i.e., CLAIM), without any requirement of submission. Encouragement and the mandated use of AI-specific guidelines and those related to modeling in the journals were generally lower compared with those unrelated to modeling.

### Previous related works

There is only one recent closely related study to this research in which the endorse-

ment of AI reporting guidelines in radiology journals has been systematically analyzed.<sup>60</sup> In their seminal study, Zhong et al.<sup>60</sup> investigated the endorsement of 15 general reporting guidelines and 10 AI reporting guidelines. Of the 117 SCIE journals included, the authors found that CLAIM (1.7%, 2/117) was the only and the most implemented AI reporting guideline, while the other nine AI reporting guidelines were not mentioned. This study found that five (5%) out of the 98 journals encouraged AI-specific guidelines. The disparity in rates can be attributed to two methodological issues. First, the journals differed in their index sources. Second, our study encompassed half of the journals indexed in SCIE and ESCI (i.e., Q1–Q2). In contrast, Zhong et al.<sup>60</sup> exclusively included all SCIE journals. Furthermore, the AI reporting guidelines considered for these works were different. This study referenced two prior works and imposed no additional restrictions on their use, provided that they were in the form of a publication (i.e., not a custom checklist that appears on the instructions of journals).<sup>50,51</sup> The authors of the prior investigation restricted their assessment to 10 AI reporting guidelines. Furthermore, both studies reached the same conclusion that the

endorsement or encouragement to follow AI reporting guidelines in these journals was remarkably low. Their main findings were complementary and mutually reinforcing.

Given the scarcity of literature on the encouragement of AI reporting guidelines in radiology, nuclear medicine, and medical imaging journals, it would be beneficial to discuss studies that are not specifically pertinent to AI but are nevertheless extremely relevant to the encouragement of and mandating reporting guidelines. In a cross-sectional study, Malički et al.<sup>69</sup> analyzed a representative sample of journal instructions for authors across multiple scientific fields, including health sciences. The instructions of 13% of journals suggested the use of reporting guidelines, while only 2% mandated its use. In addition, the authors discovered that journals in the health or life sciences, as well as those published by prominent publishers, were more likely to include reporting guidelines or standards in their author instructions. In a different study, Agha et al.<sup>70</sup> investigated the impact of the mandatory implementation of reporting guidelines on the quality of reporting in a surgical journal. Compliance with STROBE, CONSORT, and PRISMA dramatically improved after the policy implementation. The authors observed that implementing a policy demanding the submission of a completed reporting checklist for observational research, randomized controlled trials, and systematic reviews can increase compliance. In addition, they recommended similar approaches for various journals and study types. In another seminal study, Hirst and Altman focused on the encouragement of reviewers to utilize reporting guidelines for 116 health research publications.<sup>59</sup> They discovered that 41 (35%) of the journals offered reviewers with online instructions. In addition, they revealed that nearly half of the online instructions referred to these tools without providing clear instructions on how to use them.

### Potential reasons for low rates

Considering the relevant works above and the present study, it is evident that journals do not encourage and mandate AI reporting guidelines frequently. The potential causes can only be speculated because their analysis falls outside the scope of this study. The editorial team of the journals may wrongly presume that researchers are aware of these fundamental aspects of rigorous and transparent reporting and that authors are entirely responsible for implementing them, not the journals. The journals may also be hesitant to incorporate appropriate

reporting practices through reporting guidelines, and they may be unwilling to address scientific misconduct and correct publication errors.<sup>71-73</sup> The editors may also not want to unintentionally overburden the authors with too many instructions. Even if journals encourage good reporting practices, researchers may be resistant to fundamental change. Furthermore, despite the validity of these tools, journals may not agree on the importance of reporting guidelines and may be hesitant to recommend their usage in the absence of convincing proof of their effectiveness.

### What are the following steps?

In light of the outstanding and exponential growth of AI research on medical imaging over the past decade,<sup>23</sup> it is necessary to promote the highest-quality research. It would be advantageous to conduct additional research to define the effectiveness of AI reporting guidelines. Such research will help persuade journals to encourage and mandate them. Hence, there is a need for further assessment of AI reporting guidelines to determine their optimal utilization. This assessment should consider whether they should be incorporated into the study design, applied during ongoing research, utilized solely for reporting purposes post-study completion, or implemented at the request of journals, among other potential considerations. Enhancing our understanding of the factors that influence the dissemination and implementation of these tools and strategies is crucial for improving their efficacy and promoting their broader adoption. Future research should investigate the obstacles journals might experience when adopting such policy changes in their journals, as well as how automated tools could minimize their workload while guaranteeing adherence to these reporting guidelines. Furthermore, radiology, nuclear medicine, and medical imaging journals may collaborate to improve reporting standards for research. These group initiatives should also be supported by scientific organizations, universities, institutions, societies, and funding agencies. This would make it more difficult for authors receiving negative reviews due to inadequate reporting to choose journals with more flexible reporting policies. This could enhance the overall reporting quality of the scientific literature. In certain areas of medical research, such as rehabilitation and disability, the journals established such collaborations.<sup>74</sup> As of 2014, 28 prominent rehabilitation and disability journals have joined

a group to require the adherence to reporting guidelines to increase the quality of research reporting, not just inside their journal but also within their field of medicine and research. They jointly published an editorial, announcing their agreement and urging authors to adhere to appropriate EQUATOR reporting guidelines when preparing articles for submission. They also requested reviewers to utilize reporting guidelines when evaluating submissions.<sup>74</sup> A similar group effort is crucial to improve the overall reporting quality of AI research in radiology, nuclear medicine, and medical imaging journals.

### Limitations

This study has a few limitations. First, it assumed that instructions are the sole location where reporting guidelines that are encouraged or mandated can be found. However, some of the requirements editors put on authors and reviewers may not be necessarily outlined in the instructions. For instance, the submission systems of all the journals were not thoroughly analyzed to check whether they encouraged or requested the use of guidelines during the submission and/or review processes. It was presumed that this was not common practice. Nonetheless, their submission systems were only investigated when the submission requirements were not clear in the instructions. Second, only Q1 and Q2 SCIE and ESCI journals indexed in the WoS were included due to their well-known high standards for indexing. Therefore, it is unlikely to represent the editorial standards of all journals. To diversify the journal characteristics, Q1 and Q2 ESCI journals were included instead of Q3 and Q4 SCIE journals. However, achieving a perfect representation of journals in terms of diversity should not be a major concern in an exploratory study focusing on a new area of reporting guidelines. Third, while downloading the journal instructions, they were double-checked for accuracy. Due to the complex and multi-layered design of certain journal websites, some parts of the instructions may have been omitted. Additionally, this study aimed to evaluate the automatically annotated content of the instructions through independent readings by two readers, with consensus reached through consultation with a third reader. This study may have missed any reporting guidelines that were recommended or deemed necessary in the submission. However, the impact of missing instructions and their content analysis will likely be minor. Finally, the instructions were downloaded over a brief time frame (between September 4 and 7,

2023). If journals had improved their instructions after this period, these changes would not have been reflected in the results.

In conclusion, this meta-research study provides an overview of instructions for authors and peer reviewers across radiology, nuclear medicine, and medical imaging journals. It specifically examines the encouragement of AI-specific reporting guidelines and their submission requirements, comparing them with guidelines related to modeling and those unrelated to modeling. However, the findings indicate that these AI-specific guidelines are not commonly encouraged and mandated (i.e., requiring a filled-out checklist) by these journals, compared with other guidelines. To further encourage the use of these tools, all stakeholders, including developers, journal managers, editors, reviewers, authors, and funders, are required to collaborate. Given their position at the forefront of AI, if more of these journals enforce or encourage responsible reporting through guidelines, the value of articles and AI research may increase and become less wasteful.

### Conflict of interest disclosure

Burak Koçak, MD, is Section Editor in Diagnostic and Interventional Radiology. He had no involvement in the peer-review of this article and had no access to information regarding its peer-review. Other authors have nothing to disclose.

### References

1. Jin Y, Sanger N, Shams I, et al. Does the medical literature remain inadequately described despite having reporting guidelines for 21 years? - A systematic review of reviews: an update. *J Multidiscip Healthc*. 2018;11:495-510. [\[CrossRef\]](#)
2. Glasziou P, Altman DG, Bossuyt P, et al. Reducing waste from incomplete or unusable reports of biomedical research. *Lancet Lond Engl*. 2014;383(9913):267-276. [\[CrossRef\]](#)
3. Macleod MR, Michie S, Roberts I, et al. Biomedical research: increasing value, reducing waste. *Lancet*. 2014;383(9912):101-104. [\[CrossRef\]](#)
4. Chan AW, Altman DG. Identifying outcome reporting bias in randomised trials on PubMed: review of publications and survey of authors. *BMJ*. 2005;330(7494):753. [\[CrossRef\]](#)
5. Altman DG, Simera I. Responsible reporting of health research studies: transparent, complete, accurate and timely. *J Antimicrob Chemother*. 2010;65(1):1-3. [\[CrossRef\]](#)
6. Goodman SN, Fanelli D, Ioannidis JPA. What does research reproducibility mean? *Sci Transl Med*. 2016;8(341):341ps12. [\[CrossRef\]](#)

7. Casas JP, Kwong J, Ebrahim S. Telemonitoring for chronic heart failure: not ready for prime time. *Cochrane Database Syst Rev.* 2010;2011:ED000008. [\[CrossRef\]](#)
8. Fuller T, Pearson M, Peters J, Anderson R. What affects authors' and editors' use of reporting guidelines? Findings from an online survey and qualitative interviews. *PLoS One.* 2015;10(4):e0121585. [\[CrossRef\]](#)
9. Moher D, Weeks L, Ocampo M, et al. Describing reporting guidelines for health research: a systematic review. *J Clin Epidemiol.* 2011;64(7):718-742. [\[CrossRef\]](#)
10. Simera I, Moher D, Hirst A, Hoey J, Schulz KF, Altman DG. Transparent and accurate reporting increases reliability, utility, and impact of your research: reporting guidelines and the EQUATOR Network. *BMC Med.* 2010;8(1):24. [\[CrossRef\]](#)
11. Cobo E, Cortés J, Ribera JM, et al. Effect of using reporting guidelines during peer review on quality of final manuscripts submitted to a biomedical journal: masked randomised trial. *BMJ.* 2011;343:d6783. [\[CrossRef\]](#)
12. Botos J. Reported use of reporting guidelines among JNCI: Journal of the National Cancer Institute authors, editorial outcomes, and reviewer ratings related to adherence to guidelines and clarity of presentation. *Res Integr Peer Rev.* 2018;3:7. [\[CrossRef\]](#)
13. Stevanovic A, Schmitz S, Rossaint R, Schürholz T, Coburn M. CONSORT item reporting quality in the top ten ranked journals of critical care medicine in 2011: a retrospective analysis. *PLoS One.* 2015;10(5):e0128061. [\[CrossRef\]](#)
14. Plint AC, Moher D, Morrison A, et al. Does the CONSORT checklist improve the quality of reports of randomised controlled trials? A systematic review. *Med J Aust.* 2006;185(5):263-267. [\[CrossRef\]](#)
15. Moher D, Jones A, Lepage L; CONSORT Group (Consolidated Standards for Reporting of Trials). Use of the CONSORT statement and quality of reports of randomized trials: a comparative before-and-after evaluation. *JAMA.* 2001;285(15):1992-1995. [\[CrossRef\]](#)
16. Prady SL, Richmond SJ, Morton VM, Macpherson H. A systematic evaluation of the impact of STRICTA and CONSORT recommendations on quality of reporting for acupuncture trials. *PLoS One.* 2008;3(2):e1577. [\[CrossRef\]](#)
17. Hopewell S, Dutton S, Yu LM, Chan AW, Altman DG. The quality of reports of randomised trials in 2000 and 2006: comparative study of articles indexed in PubMed. *BMJ.* 2010;340:c723. [\[CrossRef\]](#)
18. Wynne KE, Simpson BJ, Berman L, Rangel SJ, Grosfeld JL, Moss RL. Results of a longitudinal study of rigorous manuscript submission guidelines designed to improve the quality of clinical research reporting in a peer-reviewed surgical journal. *J Pediatr Surg.* 2011;46(1):131-137. [\[CrossRef\]](#)
19. Smidt N, Rutjes AW, van der Windt DA, et al. The quality of diagnostic accuracy studies since the STARD statement: has it improved? *Neurology.* 2006;67(5):792-797. [\[CrossRef\]](#)
20. Turner L, Shamseer L, Altman DG, Schulz KF, Moher D. Does use of the CONSORT Statement impact the completeness of reporting of randomised controlled trials published in medical journals? A Cochrane review. *Syst Rev.* 2012;1:60. [\[CrossRef\]](#)
21. Tunis AS, McInnes MD, Hanna R, Esmail K. Association of study quality with completeness of reporting: have completeness of reporting and quality of systematic reviews and meta-analyses in major radiology journals changed since publication of the PRISMA statement? *Radiology.* 2013;269(2):413-426. [\[CrossRef\]](#)
22. Hong PJ, Korevaar DA, McGrath TA, et al. Reporting of imaging diagnostic accuracy studies with focus on MRI subgroup: Adherence to STARD 2015. *J Magn Reson Imaging.* 2018;47(2):523-544. [\[CrossRef\]](#)
23. Kocak B, Baessler B, Cuocolo R, Mercaldo N, Pinto Dos Santos D. Trends and statistics of artificial intelligence and radiomics research in radiology, nuclear medicine, and medical imaging: bibliometric analysis. *Eur Radiol.* 2023;33(11):7542-7555. [\[CrossRef\]](#)
24. Liu X, Faes L, Kale AU, et al. A comparison of deep learning performance against healthcare professionals in detecting diseases from medical imaging: a systematic review and meta-analysis. *Lancet Digit Health.* 2019;1(6):271-297. [\[CrossRef\]](#)
25. Cabitza F, Campagner A. The need to separate the wheat from the chaff in medical informatics: Introducing a comprehensive checklist for the (self)-assessment of medical AI studies. *Int J Med Inform.* 2021;153:104510. [\[CrossRef\]](#)
26. Kocak B, Keles A, Akinci D'Antonoli T. Self-reporting with checklists in artificial intelligence research on medical imaging: a systematic review based on citations of CLAIM. *Eur Radiol.* 2023. [\[CrossRef\]](#)
27. Marwaha JS, Chen HW, Habashy K, et al. Appraising the quality of development and reporting in surgical prediction models. *JAMA Surg.* 2023;158(2):214-216. [\[CrossRef\]](#)
28. Emam KE, Klement W, Malin B. Reporting and methodological observations on prognostic and diagnostic machine learning studies. *JMIR AI.* 2023;2(1):e47995. [\[CrossRef\]](#)
29. Ibrahim H, Liu X, Denniston AK. Reporting guidelines for artificial intelligence in healthcare research. *Clin Experiment Ophthalmol.* 2021;49(5):470-476. [\[CrossRef\]](#)
30. Shelmerdine SC, Arthurs OJ, Denniston A, Sebire NJ. Review of study reporting guidelines for clinical studies using artificial intelligence in healthcare. *BMJ Health Care Inform.* 2021;28(1):e100385. [\[CrossRef\]](#)
31. Rivera SC, Liu X, Chan AW, Denniston AK, Calvert MJ; SPIRIT-AI and CONSORT-AI Working Group. Guidelines for clinical trial protocols for interventions involving artificial intelligence: the SPIRIT-AI Extension. *BMJ.* 2020;370:m3210. [\[CrossRef\]](#)
32. Kocak B, Akinci D'Antonoli T, Ates Kus E, et al. Self-reported checklists and quality scoring tools in radiomics: a meta-research. *Eur Radiol.* 2024. [\[CrossRef\]](#)
33. Olczak J, Pavlopoulos J, Puijs J, et al. Presenting artificial intelligence, deep learning, and machine learning studies to clinicians and healthcare stakeholders: an introductory reference with a guideline and a Clinical AI Research (CAIR) checklist proposal. *Acta Orthop.* 2021;92(5):513-525. [\[CrossRef\]](#)
34. Padula WV, Kreif N, Vanness DJ, et al. Machine learning methods in health economics and outcomes research-the PALISADE checklist: a good practices report of an ISPOR task force. *Value Health.* 2022;25(7):1063-1080. [\[CrossRef\]](#)
35. Loftus TJ, Tighe PJ, Ozrazgat-Baslanti T, et al. Ideal algorithms in healthcare: explainable, dynamic, precise, autonomous, fair, and reproducible. *PLOS Digit Health.* 2022;1(1):e0000006. [\[CrossRef\]](#)
36. Weaver CGW, Basmadjian RB, Williamson T, et al. Reporting of model performance and statistical methods in studies that use machine learning to develop clinical prediction models: protocol for a systematic review. *JMIR Res Protoc.* 2022;11(3):e30956. [\[CrossRef\]](#)
37. Kotecha D, Asselbergs FW, Achenbach S, et al. CODE-EHR best-practice framework for the use of structured electronic health-care records in clinical research. *Lancet Digit Health.* 2022;4(10):757-764. [\[CrossRef\]](#)
38. Seedat N, Imrie F, van der Schaar M. DC-Check: a data-centric AI checklist to guide the development of reliable machine learning systems. Published online November 9, 2022. [\[CrossRef\]](#)
39. Vasey B, Nagendran M, Campbell B, et al. Reporting guideline for the early stage clinical evaluation of decision support systems driven by artificial intelligence: DECIDE-AI. *BMJ.* 2022;377:e070904. [\[CrossRef\]](#)
40. Lu JH, Callahan A, Patel BS, et al. Assessment of adherence to reporting guidelines by commonly used clinical prediction models from a single vendor: a systematic review. *JAMA Netw Open.* 2022;5(8):e2227779. [\[CrossRef\]](#)
41. Crossnohere NL, Elsaid M, Paskett J, Bose-Brill S, Bridges JFP. Guidelines for artificial intelligence in medicine: literature review and content analysis of frameworks. *J Med Internet Res.* 2022;24(8):e36823. [\[CrossRef\]](#)
42. Mongan J, Moy L, Kahn CE. Checklist for artificial intelligence in medical imaging

- (CLAIM): a guide for authors and reviewers. *Radiol Artif Intell.* 2020;2(2):e200029. [\[CrossRef\]](#)
43. Tejani AS, Klontzas ME, Gatti AA, et al. Updating the checklist for artificial intelligence in medical imaging (CLAIM) for reporting AI research. *Nat Mach Intell.* 2023;5(9):950-951. [\[CrossRef\]](#)
  44. Lekadir K, Osuala R, Gallin C, et al. FUTURE-AI: Guiding principles and consensus recommendations for trustworthy artificial intelligence in medical imaging. Published online October 1, 2023. [\[CrossRef\]](#)
  45. Norgeot B, Quer G, Beaulieu-Jones BK, et al. Minimum information about clinical artificial intelligence modeling: the MI-CLAIM checklist. *Nat Med.* 2020;26(9):1320-1324. [\[CrossRef\]](#)
  46. Kocak B, Baessler B, Bakas S, et al. Checklist for evaluation of radiomics research (CLEAR): a step-by-step reporting guideline for authors and reviewers endorsed by ESR and EuSoMIL. *Insights Imaging.* 2023;14:75. [\[CrossRef\]](#)
  47. Kocak B, Akinci D, Antonoli T, Mercaldo N, et al. Methodological radiomics score (METRICS): a quality scoring tool for radiomics research endorsed by EuSoMIL. *Insights Imaging.* 2024;15(1):8. [\[CrossRef\]](#)
  48. Sounderajah V, Ashrafian H, Golub RM, et al. Developing a reporting guideline for artificial intelligence-centred diagnostic test accuracy studies: the STARD-AI protocol. *BMJ Open.* 2021;11(6):e047709. [\[CrossRef\]](#)
  49. Collins GS, Dhiman P, Andaur Navarro CL, et al. Protocol for development of a reporting guideline (TRIPOD-AI) and risk of bias tool (PROBAST-AI) for diagnostic and prognostic prediction model studies based on artificial intelligence. *BMJ Open.* 2021;11(7):e048008. [\[CrossRef\]](#)
  50. Klontzas ME, Gatti AA, Tejani AS, Kahn CE Jr. AI reporting guidelines: how to select the best one for your research. *Radiol Artif Intell.* 2023;5(3):e230055. [\[CrossRef\]](#)
  51. Klement W, El Emam K. Consolidated reporting guidelines for prognostic and diagnostic machine learning modeling studies: development and validation. *J Med Internet Res.* 2023;25:e48763. [\[CrossRef\]](#)
  52. Leung V, Rousseau-Blass F, Beauchamp G, Pang DSJ. ARRIVE has not ARRIVED: support for the ARRIVE (animal research: reporting of in vivo experiments) guidelines does not improve the reporting quality of papers in animal welfare, analgesia or anesthesia. *PLoS One.* 2018;13(5):e0197882. [\[CrossRef\]](#)
  53. Reveiz L, Villanueva E, Iko C, Simera I. Compliance with clinical trial registration and reporting guidelines by Latin American and Caribbean journals. *Cad Saude Publica.* 2013;29(6):1095-1100. [\[CrossRef\]](#)
  54. Pussegoda K, Turner L, Garrity C, et al. Systematic review adherence to methodological or reporting quality. *Syst Rev.* 2017;6(1):131. [\[CrossRef\]](#)
  55. Page MJ, Shamseer L, Altman DG, et al. Epidemiology and reporting characteristics of systematic reviews of biomedical research: a cross-sectional study. *PLoS Med.* 2016;13(5):e1002028. [\[CrossRef\]](#)
  56. Diong J, Butler AA, Gandevia SC, Héroux ME. Poor statistical reporting, inadequate data presentation and spin persist despite editorial advice. *PLoS One.* 2018;13(8):e0202121. [\[CrossRef\]](#)
  57. Innocenti T, Giagio S, Salvioli S, et al. Completeness of reporting is suboptimal in randomized controlled trials published in rehabilitation journals, with trials with low risk of bias displaying better reporting: a meta-research study. *Arch Phys Med Rehabil.* 2022;103(9):1839-1847. [\[CrossRef\]](#)
  58. Diong J, Bye E, Djajadikarta Z, Butler AA, Gandevia SC, Héroux ME. Encouraging responsible reporting practices in the instructions to authors of neuroscience and physiology journals: there is room to improve. *PLoS One.* 2023;18(3):e0283753. [\[CrossRef\]](#)
  59. Hirst A, Altman DG. Are peer reviewers encouraged to use reporting guidelines? A survey of 116 health research journals. *PLoS One.* 2012;7(4):e35621. [\[CrossRef\]](#)
  60. Zhong J, Xing Y, Lu J, et al. The endorsement of general and artificial intelligence reporting guidelines in radiological journals: a meta-research study. *BMC Med Res Methodol.* 2023;23(1):292. [\[CrossRef\]](#)
  61. Sengupta PP, Shrestha S, Berthon B, et al. Proposed requirements for cardiovascular imaging-related machine learning evaluation (PRIME): a checklist: reviewed by the American College of Cardiology Healthcare Innovation Council. *JACC Cardiovasc Imaging.* 2020;13(9):2017-2035. [\[CrossRef\]](#)
  62. El Naqa I, Boone JM, Benedict SH, et al. AI in medical physics: guidelines for publication. *Med Phys.* 2021;48(9):4711-4714. [\[CrossRef\]](#)
  63. Collins GS, Reitsma JB, Altman DG, Moons KG. Transparent reporting of a multivariable prediction model for individual prognosis or diagnosis (TRIPOD): the TRIPOD statement. *BMJ. BMC Med.* 2015;13(1):1. [\[CrossRef\]](#)
  64. von Elm E, Altman DG, Egger M, et al. The strengthening of reporting of observational studies in epidemiology (STROBE) statement: guidelines for reporting observational studies. *Ann Intern Med.* 2007;147(8):573-577. [\[CrossRef\]](#)
  65. Bossuyt PM, Reitsma JB, Bruns DE, et al. STARD 2015: an updated list of essential items for reporting diagnostic accuracy studies. *BMJ.* 2015;351:h5527. [\[CrossRef\]](#)
  66. Percie du Sert N, Hurst V, Ahluwalia A, et al. The ARRIVE guidelines 2.0: Updated guidelines for reporting animal research. *PLoS Biol.* 2020;18(7):e3000410. [\[CrossRef\]](#)
  67. Page MJ, McKenzie JE, Bossuyt PM, et al. The PRISMA 2020 statement: an updated guideline for reporting systematic reviews. *BMJ.* 2021;372:n71. [\[CrossRef\]](#)
  68. Schulz KF, Altman DG, Moher D; CONSORT Group. CONSORT 2010 Statement: updated guidelines for reporting parallel group randomised trials. *BMJ.* 2010;8(1):18. [\[CrossRef\]](#)
  69. Malički M, Aalbersberg IJ, Bouter L, Ter Riet G. Journals' instructions to authors: a cross-sectional study across scientific disciplines. *PLoS One.* 2019;14(9):e0222157. [\[CrossRef\]](#)
  70. Agha RA, Fowler AJ, Limb C, et al. Impact of the mandatory implementation of reporting guidelines on reporting quality in a surgical journal: A before and after study. *Int J Surg.* 2016;30:169-172. [\[CrossRef\]](#)
  71. Bosch X, Hernández C, Pericas JM, Doti P, Marušić A. Misconduct policies in high-impact biomedical journals. *PLoS One.* 2012;7(12):e51928. [\[CrossRef\]](#)
  72. Williams P, Wager E. Exploring why and how journal editors retract articles: findings from a qualitative study. *Sci Eng Ethics.* 2013;19(1):1-11. [\[CrossRef\]](#)
  73. Wager E. Coping with scientific misconduct. *BMJ.* 2011;343:d6586. [\[CrossRef\]](#)
  74. Chan L, Heinemann AW, Roberts J. Elevating the quality of disability and rehabilitation research: mandatory use of the reporting guidelines. *Am J Phys Med Rehabil.* 2014;93(4):279-281. [\[CrossRef\]](#)



Copyright@Author(s) - Available online at dirjournal.org.  
Content of this journal is licensed under a Creative Commons  
Attribution-NonCommercial 4.0 International License.

# Application of deep learning and radiomics in the prediction of hematoma expansion in intracerebral hemorrhage: a fully automated hybrid approach

Mengtian Lu<sup>1</sup>

Yaqi Wang<sup>2</sup>

Jiaqiang Tian<sup>1</sup>

Haifeng Feng<sup>3</sup>

<sup>1</sup>The First Affiliated Hospital of Hubei University of Science and Technology, Xianning Central Hospital, Department of Radiology, Xianning, China

<sup>2</sup>The Second Affiliated Hospital of Hubei University of Science and Technology, Department of Radiology, Xianning, China

<sup>3</sup>The First Affiliated Hospital of Hubei University of Science and Technology, Xianning Central Hospital, Department of Ultrasound, Xianning, China

## PURPOSE

Spontaneous intracerebral hemorrhage (ICH) is the most severe form of stroke. The timely assessment of early hematoma enlargement and its proper treatment are of great significance in curbing the deterioration and improving the prognosis of patients with ICH. This study aimed to develop an automated hybrid approach to predict hematoma expansion in ICH.

## METHODS

The transfer learning method was applied to build a hybrid model based on a convolutional neural network (CNN) to predict the expansion of hematoma. The model integrated (1) a CNN for automated hematoma segmentation and (2) a CNN-based classifier for hematoma expansion prediction that incorporated both 2-dimensional images and the radiomics features of the 3-dimensional hematoma shape.

## RESULTS

The radiomics feature module had the highest area under the receiver operating characteristic curve (AUC) of 0.58, a precision of 0, a recall of 0, and an average precision (AP) of 0.26. The ResNet50 and Inception\_v3 modules had AUCs of 0.79 and 0.93, a precision of 0.56 and 0.86, a recall of 0.42 and 0.75, and an AP of 0.51 and 0.85, respectively. Radiomic with Inception\_v3 and Radiomic with ResNet50 had AUCs of 0.95 and 0.81, a precision of 0.90 and 0.57, a recall of 0.79 and 0.17, and an AP of 0.87 and 0.69, respectively.

## CONCLUSION

A model using deep learning and radiomics was successfully developed. This model can reliably predict the hematoma expansion of ICH with a fully automated process based on non-contrast computed tomography imaging. Furthermore, the radiomics fusion with the Inception\_v3 model had the highest accuracy.

## KEYWORDS

Convolutional neural network, radiomics, intracerebral hemorrhage, hematoma expansion, non-contrast computed tomography

Corresponding author: Haifeng Feng

E-mail: haifengfeng\_xn@yeah.net

Received 15 June 2023; revision requested 10 July 2023; last revision received 23 November 2024; accepted 10 February 2024.



Epub: 24.04.2024

Publication date: 09.09.2024

DOI: 10.4274/dir.2024.222088

Spontaneous intracerebral hemorrhage (ICH), the most severe form of stroke, accounts for 10%–15% of strokes in high-income nations and 20%–50% in developing nations.<sup>1</sup> Compared with ischemic stroke, ICH is associated with poor prognostic outcomes, with a mortality rate of 40% at 1 month and a disability rate of 80% in survivors.<sup>2-4</sup> Generally, ICH prognosis is influenced by many factors, including baseline volume and hematoma location, Glasgow Coma scale score, intraventricular hemorrhage, and age.<sup>5-7</sup> Of these factors, hematoma volume is the only one that is controllable and dynamic.<sup>5</sup> Clinical studies have shown that 33% of patients with ICH develop early hematoma enlargement within 24 h of ICH onset.<sup>8-10</sup> Early hematoma enlargement in patients with ICH is independently correlated with poor prognostic outcomes and death.<sup>3,8,11,12</sup> Therefore, the timely assessment of early hemato-

You may cite this article as: Lu M, Wang Y, Tian J, Feng H. Application of deep learning and radiomics in the prediction of hematoma expansion in intracerebral hemorrhage: a fully automated hybrid approach. *Diagn Interv Radiol.* 2024;30(5):299-312.

ma enlargement and appropriate treatment are crucial in improving the outcomes of patients with ICH.

Recent studies have identified numerous radiological features for predicting hematoma enlargement after ICH. For example, the computed tomography angiography (CTA) spot sign is a powerful predictive method of hematoma enlargement.<sup>13-15</sup> However, clinical applications have shown that some patients are allergic to the contrast agents used in CTA, and patients with renal insufficiencies are relatively contraindicated.<sup>16-18</sup> By contrast, non-contrast computed tomography (NCCT) serves as the first choice for diagnosis of patients with acute stroke. New markers based on NCCT, such as blend,<sup>19</sup> swirl,<sup>20</sup> black hole,<sup>21</sup> and island,<sup>22</sup> as well as satellite signs,<sup>23</sup> can reflect the density and shape heterogeneity of hematomas with high specificity. Therefore, they have been proposed as alternative predictors of hematoma enlargement in clinical settings.<sup>24-26</sup> However, these predictive indicators are only used for qualitative or semi-quantitative analyses and have relatively low sensitivity and accuracy in predicting hematoma enlargement.<sup>25</sup> Alternative quantitative methods with automated execution, which may have superior predictive power, are still needed.

Radiomics is a promising quantitative method that has performed excellently in various biomedical fields, where it has been used to extract large numbers of quantitative characteristics from conventional medical imaging.<sup>27,28</sup> As well as being extensively applied in oncology studies, radiomics has recently been used for the prediction of hematoma enlargement after ICH based on NCCT imaging. Although these models exhibit positive predictive performance,<sup>29-33</sup> only traditional or feature-based machine learning (ML) was utilized for the studies. Deep learning is an automatic method that can skip object segmentation, feature selection, and extraction from segmented objects to identify "effective features." Since it allows the whole process to be mapped from raw input images to final classifications and can exclude the requirement for hand-crafted

features, deep learning is also referred to as end-to-end ML.<sup>27</sup>

Convolutional neural networks (CNNs) based on deep learning are increasingly being used worldwide with promising outcomes. However, developing CNN-based methods requires large training datasets, which is challenging and laborious in clinical settings. Two approaches partially overcome this challenge. The first involves data augmentation, which utilizes affine transformations, including translation, scaling, and rotation, to produce more data from the available data. The other approach involves transfer learning, which is promising in medical image analysis.<sup>34</sup> In this study, we developed a CNN-based hybrid model using a data augmentation and transfer learning method for predicting hematoma expansion by integrating the following: (1) a CNN for automated hematoma segmentation, and (2) a CNN-centered classifier for hematoma expansion prediction that incorporates 2-dimensional (2D) images as well as radiomics features for the 3-dimensional (3D) hematoma shape.

## Methods

This was a retrospective study permitted by the Medical Ethics Committee of Xianning Central Hospital (no: 20211126011), and the informed consent was waived.

### Patients and image acquisition

Patients with spontaneous ICH diagnosed by the radiologist and admitted to the hospital between September 2017 and September 2021 were enrolled in this study. The inclu-

sion criteria were as follows: (1) patients aged >18 years; (2) patients who had received baseline NCCT within 24 h of symptomatic onset and follow-up computed tomography (CT) at ≤72 h. In this study, 506 patients met the inclusion criteria. The exclusion criteria were as follows: (1) patients diagnosed with trauma, aneurysm, vascular malformation, venous sinus embolism, or tumor-induced cerebral hemorrhage (151 cases); (2) patients with emergency surgery before CT review (53 cases); (3) patients with surgical intervention during the 72-h observation period, even in the absence of hematoma expansion (15 cases); (4) patients whose CT images revealed artifacts. In this study, two different CT scanners were used to minimize variability in image acquisition parameters (7 cases). Following the exclusion criteria, 226 cases were excluded from the study. Finally, 280 cases were included in this study. The original CT image of the patients with ICH was reconstructed into a standardized image with a thickness of 1.0 mm and a spacing of 0.7 mm before being exported from the picture archiving and communication system (PACS).

### Study design

The model architecture is shown in Figure 1. Briefly, the hybrid model comprised two deep learning models (models 1 and 2), with an automated pipeline between the two models. Model 1 was developed first for the automated generation of hematoma masks based on NCCT images. A hybrid classifier model (model 2) was then trained for the prediction of hemorrhage expansion based on radiomics and CNN features extracted from the NCCT images and hematoma masks in model 1.

**Main points**

- A model using deep learning and radiomics was successfully developed.
- The model was based on non-contrast computed tomography imaging.
- The model predicts hematoma expansion of an intracerebral hemorrhage with a fully automated process.

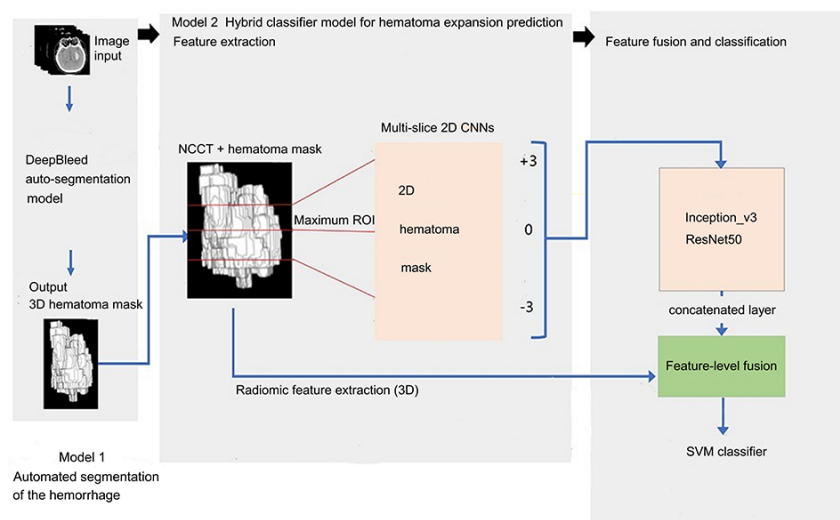


**Figure 1.** Fully automated hybrid model for predicting ICH expansion. ICH, intracerebral hemorrhage; NCCT, non-contrast computed tomography; ROI, region of interest; CNN, convolutional neural network; SVM, support vector machine.

## Image processing

The Siemens 64-slice CT (SOMATOM go.Top, Henkestr., Erlangen, Germany) scan parameters were as follows: positioning image, 140 kV, 60 mA; spiral scanning parameters, 120 kV, effective mAs 230, pitch 0.55, layer thickness 5 mm, layer spacing 5 mm. Before exporting the image from the PACS (USA), the original image was reconstructed into a standardized image with a thickness of 1.0 mm and a spacing of 0.7 mm. The CT images were exported from PACS in the Digital Imaging and Communications in Medicine format and were transformed into the Neuroimaging Informatics Technology Initiative format. Images were set to values of -1,024 and 3,052 HU. Image analysis was performed using the Ubuntu 18.04 operating system (London, UK) and Python (USA). First, all input sequences were acquired in a  $512 \times 512$  field. Next, the network output was set to only whole hematoma segmentation. After determining the hematoma volume and matching the original residual network, the original NCCT image and segmentation file ( $128 \times 128$  voxel) were reconstructed.

## Automated segmentation of the hemorrhage (model 1)

DeepBleed is an open-source tool for quick hemorrhage segmentation.<sup>35</sup> This automated deep neural network model preprocesses NCCT scans (including skull stripping), segments the hemorrhage area, and outputs a binary hemorrhage mask. Training and validation of this model using data from the Minimally Invasive Surgery Plus Alteplase for Intracerebral Hemorrhage Evacuation trial showed that the dice similarity coefficient, which evaluates spatial overlap extent between ground-truth segmentation by radiologists and the automatic model, was 0.919.<sup>35,36</sup> Contrary to manual segmentation, this model can rapidly and precisely segment ICH with a high level of agreement. To adapt it to this study, the code was partially modified and an interface was added for the automated calculation of hematoma volume.

## Labels

Previous studies have defined hematoma expansion as an outright volumetric ICH growth of  $>6$  mL or an increase of  $>33\%$  from the initial CT scan to the follow-up CT scan.<sup>3,12</sup> The binary label (negative or positive ICH expansion) was masked for each included study.

## Hybrid classifier model for hematoma expansion prediction (model 2)

The hybrid model for ICH hematoma expansion combines well-known radiomics

characteristic analysis and CNNs. Radiomics characteristic analysis was used to determine a wide range of researcher-defined quantitative features including shape, intensity, and texture of regions of interest on images. The CNN features were extracted based on CNN training.

The radiomics characteristic was extracted using the Python “pyradiomics” package (<https://www.radiomics.io/pyradiomics.html>).<sup>37</sup> The transformations were included with gradient, wavelet, original, square, exponential, logarithm, square root, and local binary pattern 3D. After image transformation, radiomics features were extracted.

The CNN model was executed using the well-known Inception\_v3<sup>38</sup> and ResNet50 modules to extract comprehensive 2D image information from the hematoma. Axial slices with maximum hematoma areas were automatically selected as “maximum ICH image”, and the other two images were extracted from three upper (+3) and three lower (−3) slices from the maximum ICH image. For small ICHs with a volume  $<1$  cm, the upper and lower slices may not be within the hematoma range; the extracted features after separation were therefore the same and did

not affect the data results. Hematomas  $<1$  cm are often negative. Typically, CNN features are extracted from the output of fully connected last hidden layers.<sup>39</sup> During CNN training, “warm-up training” of the convolutional residual network was achieved using image inputs to identify relevant imaging features. The weights of the pretrained conventional ResNet50 and Inception\_v3 modules were imported into model 2 and set as “non-trainable”. Meanwhile, data augmentation was performed by rotating, flipping, and resizing the training images to enrich the training data. This regular operation reduced the overfitting risk and boosted a classifier’s performance. The network was optimized using the Adam optimizer (beta1: 0.9, beta2: 0.999, initial learning rate: 0.0001), with an L2 penalty of 0.01, batch size of 50, and cross-entropy cost function. The maximum training epoch was set to 100, and the model was saved when the maximum accuracy was achieved on the testing set. The CNN models were then implemented using the “keras” and “tensorflow” packages and trained on an AMD Ryzen Threadripper 2970WX processor with 48 Gb RAM (USA).

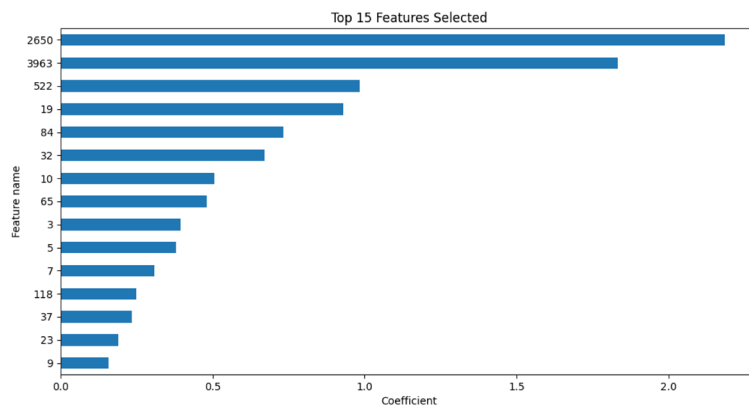


Figure 2. Top features selected.

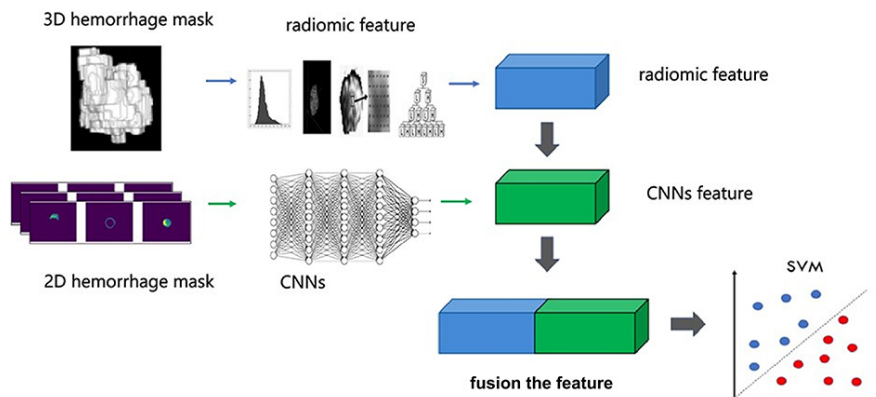


Figure 3. Schematic of 2D and 3D image feature fusion. CNN, convolutional neural network; SVM, support vector machine.

The features selected are shown in Figure 2. The feature-level fusion approaches were used to fuse the features to collect complementary information from radiomics and CNNs and improve diagnostic accuracy (Figure 3).<sup>40</sup> Following the fusion pipeline, sequential forward feature elimination was chosen for feature selection, which was able to automatically identify the subset of features that are highly appropriate to the problem. The grid search parameters consisted of many features that account for data complexity and separability. Next, the “support vector machine” was used as the ML model for classification. The training set was divided into two stratified sets for cross-validation, and the estimator with the best average accuracy in the cross-validation was chosen as the best estimator. Subsequently, 100 non-expanding (NEG-ICH) and expanding (POS-ICH) cases were randomly selected as the test set, and the remaining cases were used as training and validation sets. The radiomics-specific reporting [checklist for evaluation of radiomics research (CLEAR)<sup>41</sup> and radiomics quality score (RQS)<sup>42</sup>] are presented as Supplementary Materials S1 and S2. Thirty-seven items were addressed in the CLEAR checklist, and the RQS score was 10 (27.78%).

### Statistical analysis

Model performance was evaluated by metrics. The area under the receiver operating characteristic curve (AUC) was determined to assess the ability of a classifier to distinguish between classes. The confusion matrix (CM) denotes instances in a predicted class, whereas columns denote instances in an actual class. Precision indicates the accuracy of the classifier in identifying positive samples. Recall indicates the classifier’s ability to find all positive samples. The area under the precision-recall curve is the average precision (AP). Python software with the

“Scikit-Learn” package (<https://scikit-learn.org/stable/>) was used for statistical analyses.

## Results

The schematic of patient recruitment is shown in Figure 4. There were 280 cases included in the analysis, of which 180 were randomly grouped into the training and validation sets (43 POS-ICH cases and 137 NEG-ICH cases) and 100 were randomly grouped into the test sets (24 POS-ICH cases and 76 NEG-ICH cases). Model 1, which automatically labeled the hematoma area and calculated the hematoma volume (Figure 5), was able to efficiently mask the hematoma. The 213 NEG-ICH cases and 67 POS-ICH cases were then classified and labeled. The NEG-ICH group had a male/female ratio of 153:60, an average age of 64.4 years (range, 50–85 years), and a hematoma volume ranging from 0.271 to 79.6 mL. The POS-ICH group had a male/female ratio of 37:30, an average

age of 68.7 years (range, 53–89 years), and a hematoma volume ranging from 0.464 to 107.01 mL (Table 1a). These features were not markedly different between the training and testing datasets. The baseline features of the training, validation, and testing sets are shown in Table 1b.

In model 2, the “PyRadiomics” package was used for the extraction of shape-based characteristics from the hematoma masks, with some of the features extracted from the library being automatically deprecated. For each case, 107 features belonging to “Shape Features”, “First Order”, “Gray Level Dependence Matrix”, “Gray Level Co-occurrence Matrix”, “Gray Level Size Zone Matrix”, “Gray Level Run-Length Matrix”, and “Neighborhood Gray Tone Difference Matrix” were obtained using PyRadiomics. The results in the test dataset with the optimal estimator are presented in Figure 6 and Table 2. The radiomics feature module had the highest

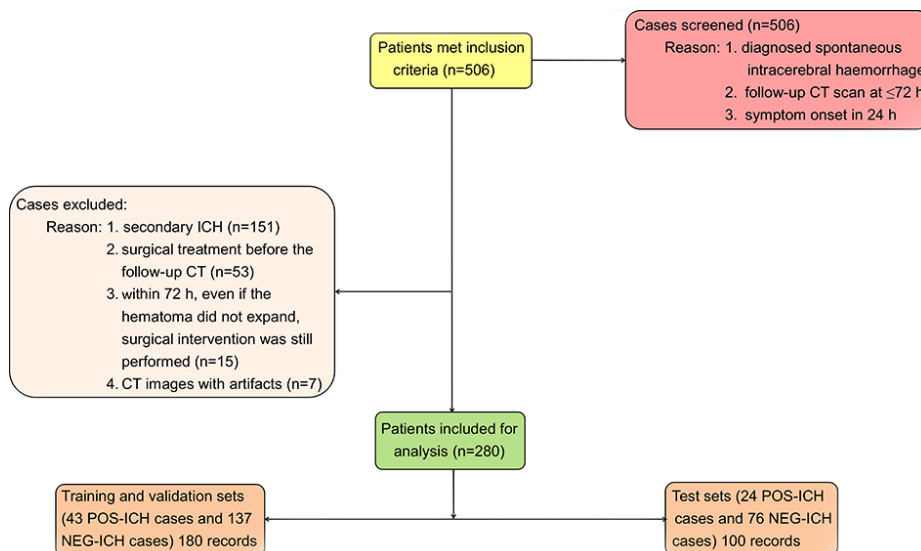


**Figure 4.** Flow diagram of ICH patient selection. ICH, intracerebral hemorrhage; CT, computed tomography; POS-ICH, positive hematoma expansion in intracerebral hemorrhage; NEG-ICH, negative hematoma expansion in intracerebral hemorrhage.

**Table 1. (a, b) Baseline clinical features of included participants**

#### a. NEG-ICH vs. POS-ICH

Variables	NEG-ICH	POS-ICH	P value*
Gender (male/female)	153/60	37/30	0.24
Age (years) [median (range)]	64.4 (50–85)	68.7 (53–89)	0.58
Hematoma volume (mL)	0.271–79.6	0.464–107.01	0.48

#### b. Training and validation vs. test sets

Variables	Training and validation sets		Test sets		P value*	
	NEG-ICH	POS-ICH	NEG-ICH	POS-ICH	NEG-ICH	POS-ICH
Gender (male/female)	98/39	24/19	55/21	13/11	0.27	0.21
Age (years) [median (range)]	64.3 (50–86)	68.4 (53–86)	64.5 (52–88)	68.9 (56–89)	0.61	0.56
Hematoma volume (mL)	0.271–79.3	0.464–106.02	0.273–79.6	0.466–107.01	0.50	0.45

\*P < 0.05. NEG-ICH, negative hematoma expansion in intracerebral hemorrhage; POS-ICH, positive hematoma expansion in intracerebral hemorrhage.



AUC of 0.58, a precision of 0, a recall of 0, and an AP of 0.26. The CM showed that all POS-ICH cases were identified as NEG-ICH cases, indicating that this module could not detect hematoma expansion.

For CNN features, the ResNet50 and Inception\_v3 modules were compared using various CNNs as feature extractors for the optimization of predictive performance, and the results of the multi-slice CNN performances in test sets are shown in Figures 7 and 8 and Table 2. The ResNet50 and Incep-

tion\_v3 modules had AUCs of 0.79 and 0.93, a precision of 0.56 and 0.86, a recall of 0.42 and 0.75, and an AP of 0.51 and 0.85, respectively.

Next, the radiomics and CNN features were fused to assess if the predictive capability could be improved. The CNN features were extracted from the last hidden layer of images before outputting (dimensional feature vectors, 4,096 for Inception\_v3, 6,144 for ResNet50). The results of the two fusion models are shown in Figures 9 and 10 and Table 2.

Radiomic with Inception\_v3 and Radiomic with ResNet50 had AUCs of 0.95 and 0.81, a precision of 0.90 and 0.57, a recall of 0.79 and 0.17, and an AP of 0.87 and 0.69, respectively. A summary of the analysis is included in doi: 10.5281/zenodo.10570452. The current analyses showed that the radiomics fusion with the Inception\_v3 model had the highest accuracy, indicating that improved performance was obtained relative to the radiomics and CNN modules alone.

## Discussion

In this study, we developed a hybrid model that incorporates data from 2D hematoma signal intensities and 3D hematoma shapes into one CNN, along with CNN-based automated hematoma segmentation and a fully automated pipeline, without any operator-dependent processes. The developed automated hybrid model can predict hematoma expansion prediction with high AUC (0.95), precision (0.90), recall (0.79), and AP (0.87) values. This strategy would also improve understanding of the synergistic nature of fusion classification using CNN-based transfer learning and radiomics features. The data obtained in this study highlight improved classification performance when using fusion strategies, radiomics-related features, or features extracted from CNN transfer learning alone. The performance of the CNN model using the Inception\_v3 algorithm based on a training dataset of 180 ICH cases for the prediction of hematoma expansion achieved an AUC of 0.93. With the addition of radiomics features, the hybrid model demonstrated a small improvement in the prediction performance. The performance was moderately effective based on a relatively small case series. The model had both radiological features and internal CNN features, and, therefore, the results were better.

Previous studies on the prediction of ICH expansion can be divided into two categories. The first category is a prediction model based on radiological characteristics, which are subjectively judged by image signs, including blend signs,<sup>19</sup> swirl signs,<sup>20</sup> black hole signs,<sup>21</sup> island signs,<sup>22</sup> and satellite signs.<sup>23</sup> These signs were combined with clinical factors to develop a predictive score table, such as the BAT score table,<sup>43</sup> NAG score,<sup>44</sup> HEAVN score,<sup>45</sup> HEP score,<sup>46</sup> the 9-point score,<sup>47</sup> and the BRAIN score.<sup>48</sup> Generally, these studies differ in indicators in their predictive scoring systems, but their radiological features may be associated with low sensitivity and low-quality results,

Module	AUC	Precision	Recall	AP
Radiomics	0.58	0	0	0.26
ResNet50	0.79	0.56	0.42	0.51
Inception_v3	0.93	0.86	0.75	0.85
Radiomic + Inception_v3	0.95	0.90	0.79	0.87
Radiomic + ResNet50	0.81	0.57	0.17	0.69

AUC, area under the receiver operating characteristic curve; AP, average precision.

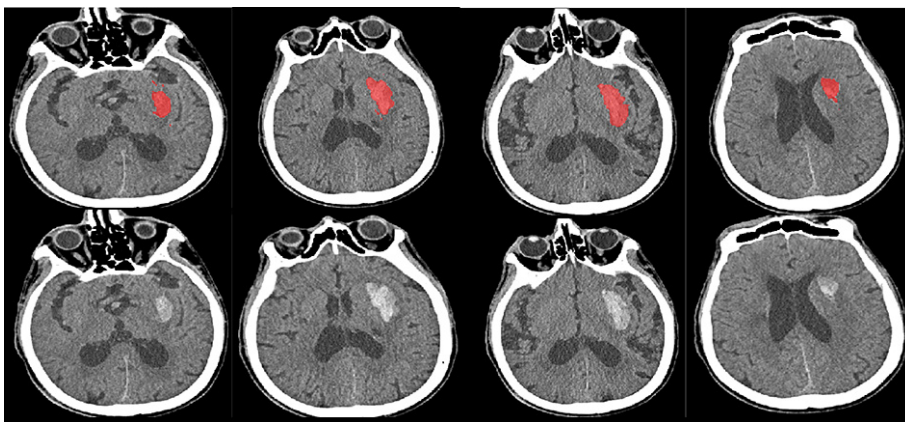


**Figure 5.** Regions of interest were auto-segmented (indicated in red).

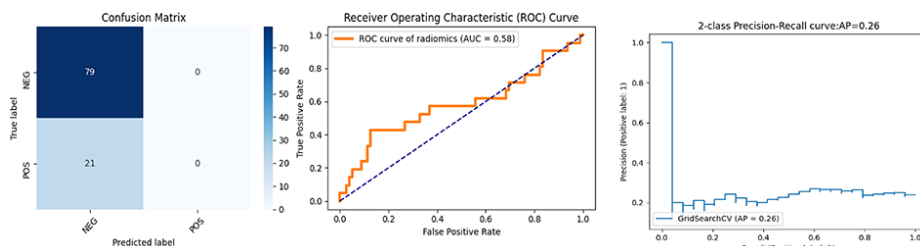


**Figure 6.** Predictive performance of the radiomics feature module. AP, average precision; AUC, area under the receiver operating characteristic curve.

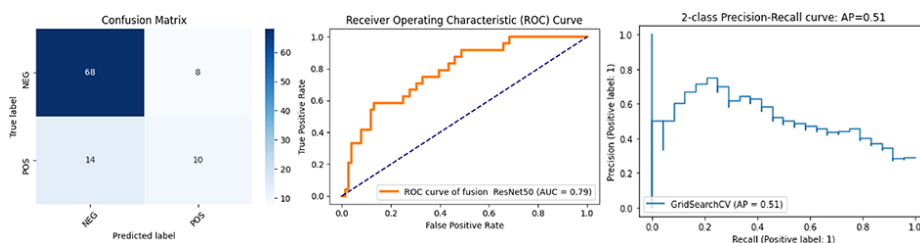


**Figure 7.** Predictive performance of the CNNs feature module with ResNet50. CNN, convolutional neural network; AP, average precision; AUC, area under the receiver operating characteristic curve.

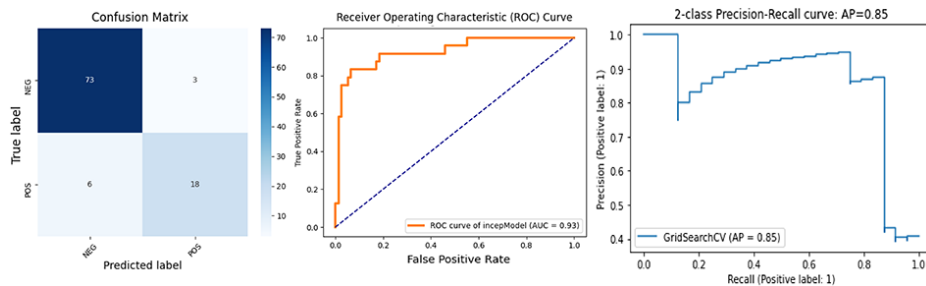


**Figure 8.** Predictive performance of the CNNs feature module with Inception\_v3. CNN, convolutional neural network; AP, average precision; AUC, area under the receiver operating characteristic curve.

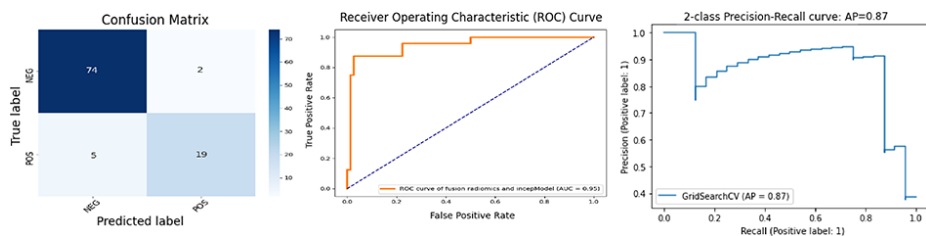


**Figure 9.** Predictive performance of the fusion model combining Radiomic and Inception\_v3. AP, average precision; AUC, area under the receiver operating characteristic curve.

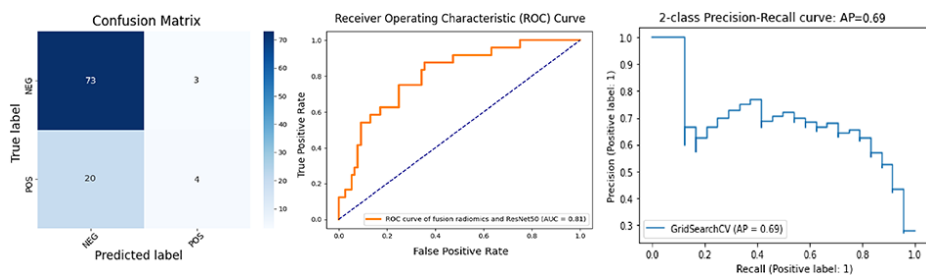


**Figure 10.** Predictive performance of the fusion model combining Radiomic and ResNet50. AP, average precision; AUC, area under the receiver operating characteristic curve.

as these visual assessments are susceptible to inter-observer variability. Furthermore, previous evaluation methods for ICH expansion were separated but not mixed. However, the relationship between predictors and hematoma enlargement is complex, which would make accurate predictions of hematoma enlargement challenging. As ML can potentially overcome these challenges, another prediction model based on radiomics has emerged. Previously, most prediction models using radiomics were based on traditional ML, which requires manual hematoma segmentation, feature extraction, screening, and reduction.<sup>30-33,49,50</sup> Although these models have effective predictive performance, the execution is not fully automated. Moreover, operator-dependent processes, including manual segmentation, are laborious and could cause interrater variability, which limits their clinical applications. Deep learning strategies, particularly CNN, have been used to solve this problem. CNNs and radiomics analyses are typical quantitative methods for image analysis

and can extract high-dimensional as well as abstract numeric data beyond what is perceivable through visual image analysis. Thus, in this study, we first used deep learning to develop a prediction model in which hematoma segmentation and feature extraction were automated, while the radiomics and CNN features were merged into a hybrid prediction model. This fusion model can combine complementary features and improve robustness by reducing the uncertainty of each feature or mode.

Although the radiomics feature module had a high AUC (0.58), 0 accuracy, and 0 recall, the predictive performance of feature-based radiomics in this study was not as effective as that reported in previous studies. This was probably because of a lack of clinical information in the current study. Generally, previous studies obtained various patients' features, including demographic factors, neurological status, and laboratory test parameters. However, these characteristics may not be accessible at all hospitals and may not cover the full spectrum of predictive infor-

mation that can be acquired from patients. Notably, the mixed model in this study has effective predictive performance without clinical information, indicating that it has greater clinical feasibility.

There are some limitations to this study. First, it is a single-center retrospective study with a small sample size. Further investigations with large sample sizes from multiple centers are required to verify the current results. In this study, we used CNNs to extract high-level features using two different modules (Inception\_v3 and ResNet50). Three axial slices were selected to yield three individual samples per patient. Therefore, the convolutional residual network and the CNN classifier were trained on 540 (180 × 3) samples and tested on 300 (100 × 3) samples. Second, even though CNNs exclude the processes of feature computation as well as selection using convolutions and can directly capture key characteristics from the images, signal intensity-based CNNs cannot directly capture 3D shapes of hematoma. Furthermore, model 2 can integrate a hematoma image and shape it into one CNN, but the developed model is not end to end. Model 1 for hematoma segmentation and model 2 for ICH status prediction were separately trained and pooled. However, the image preprocessing, models 1 and 2, and the pipeline in between are completely based on open-source modules that can be integrated into a Python-based pipeline, and a test sample can be automatically run through each step of our model.

In conclusion, we developed a model using deep learning and radiomics that can reliably predict hematoma expansion in ICH in a fully automated process based on NCCT imaging. Hematoma expansion was the only indicator of ICH outcome, and prognostic factors, such as neurological deterioration and mortality, were not included. Due to its high reproducibility and generalizability, this model can be applied more widely in predicting prognosis in acute ICH.

### Conflict of interest disclosure

The authors declared no conflicts of interest.

### References

1. Krishnamurthi RV, Feigin VL, Forouzanfar MH, et al. Global and regional burden of first-ever ischaemic and haemorrhagic stroke during 1990-2010: findings from the Global Burden of Disease Study 2010. *Lancet Glob Health*. 2013;1(5):259-281. [CrossRef]

2. van Asch CJ, Luitse MJ, Rinkel GJ, van der Tweel I, Algra A, Klijn CJ. Incidence, case fatality, and functional outcome of intracerebral haemorrhage over time, according to age, sex, and ethnic origin: a systematic review and meta-analysis. *Lancet Neurol.* 2010;9(2):167-176. [\[CrossRef\]](#)
3. Dowlatshahi D, Demchuk AM, Flaherty ML, et al. Defining hematoma expansion in intracerebral hemorrhage: relationship with patient outcomes. *Neurology.* 2011;76(14):1238-1244. [\[CrossRef\]](#)
4. Poon MT, Fonville AF, Al-Shahi Salman R. Long-term prognosis after intracerebral haemorrhage: systematic review and meta-analysis. *J Neurol Neurosurg Psychiatry.* 2014;85(6):660-667. [\[CrossRef\]](#)
5. Davis SM, Broderick J, Hennerici M, et al. Hematoma growth is a determinant of mortality and poor outcome after intracerebral hemorrhage. *Neurology.* 2006;66(8):1175-1181. [\[CrossRef\]](#)
6. Broderick JP, Brott TG, Duldner JE, Tomsick T, Huster G. Volume of intracerebral hemorrhage. A powerful and easy-to-use predictor of 30-day mortality. *Stroke.* 1993;24(7):987-993. [\[CrossRef\]](#)
7. Hemphill JC 3rd, Bonovich DC, Besmertis L, Manley GT, Johnston SC. The ICH score: a simple, reliable grading scale for intracerebral hemorrhage. *Stroke.* 2001;32(4):891-897. [\[CrossRef\]](#)
8. Delcourt C, Huang Y, Arima H, et al. Hematoma growth and outcomes in intracerebral hemorrhage: the INTERACT1 study. *Neurology.* 2012;79(4):314-319. [\[CrossRef\]](#)
9. Liotta EM, Prabhakaran S, Sangha RS, et al. Magnesium, hemostasis, and outcomes in patients with intracerebral hemorrhage. *Neurology.* 2017;89(8):813-819. [\[CrossRef\]](#)
10. Brouwers HB, Greenberg SM. Hematoma expansion following acute intracerebral hemorrhage. *Cerebrovasc Dis.* 2013;35(3):195-201. [\[CrossRef\]](#)
11. Hall AN, Weaver B, Liotta E, et al. Identifying modifiable predictors of patient outcomes after intracerebral hemorrhage with machine learning. *Neurocrit Care.* 2021;34(1):73-84. [\[CrossRef\]](#)
12. Yogendrakumar V, Ramsay T, Fergusson DA, et al. Redefining hematoma expansion with the inclusion of intraventricular hemorrhage growth. *Stroke.* 2020;51(4):1120-1127. [\[CrossRef\]](#)
13. Peng WJ, Reis C, Reis H, Zhang J, Yang J. Predictive value of CTA spot sign on hematoma expansion in intracerebral hemorrhage patients. *Biomed Res Int.* 2017;2017:4137210. [\[CrossRef\]](#)
14. Xu X, Zhang J, Yang K, Wang Q, Xu B, Chen X. Accuracy of spot sign in predicting hematoma expansion and clinical outcome: a meta-analysis. *Medicine (Baltimore).* 2018;97(34):e11945. [\[CrossRef\]](#)
15. Orito K, Hirohata M, Nakamura Y, et al. Leakage sign for primary intracerebral hemorrhage: a novel predictor of hematoma growth. *Stroke.* 2016;47(4):958-963. [\[CrossRef\]](#)
16. Huang Y, Zhang Q, Yang M. A reliable grading system for prediction of hematoma expansion in intracerebral hemorrhage in the basal ganglia. *Biosci Trends.* 2018;12(2):193-200. [\[CrossRef\]](#)
17. Dowlatshahi D, Brouwers HB, Demchuk AM, et al. Predicting intracerebral hemorrhage growth with the spot sign: the effect of onset-to-scan time. *Stroke.* 2016;47(3):695-700. [\[CrossRef\]](#)
18. Caplan LR. Recognizing and preventing intracerebral hematoma expansion. *JAMA Neurol.* 2016;73(8):914-915. [\[CrossRef\]](#)
19. Li Q, Zhang G, Huang YJ, et al. Blend sign on computed tomography: novel and reliable predictor for early hematoma growth in patients with intracerebral hemorrhage. *Stroke.* 2015;46(8):2119-2123. [\[CrossRef\]](#)
20. Yu Z, Zheng J, He M, et al. Accuracy of swirl sign for predicting hematoma enlargement in intracerebral hemorrhage: a meta-analysis. *J Neurol Sci.* 2019;399:155-160. [\[CrossRef\]](#)
21. Li Q, Zhang G, Xiong X, et al. Black hole sign: novel imaging marker that predicts hematoma growth in patients with intracerebral hemorrhage. *Stroke.* 2016;47(7):1777-1781. [\[CrossRef\]](#)
22. Li Q, Liu QJ, Yang WS, et al. Island sign: an imaging predictor for early hematoma expansion and poor outcome in patients with intracerebral hemorrhage. *Stroke.* 2017;48(11):3019-3025. [\[CrossRef\]](#)
23. Shimoda Y, Ohtomo S, Arai H, Okada K, Tominaga T. Satellite sign: a poor outcome predictor in intracerebral hemorrhage. *Cerebrovasc Dis.* 2017;44(3-4):105-112. [\[CrossRef\]](#)
24. Boulouis G, Morotti A, Charidimou A, Dowlatshahi D, Goldstein JN. Noncontrast computed tomography markers of intracerebral hemorrhage expansion. *Stroke.* 2017;48(4):1120-1125. [\[CrossRef\]](#)
25. Morotti A, Boulouis G, Dowlatshahi D, et al. Standards for detecting, interpreting, and reporting noncontrast computed tomographic markers of intracerebral hemorrhage expansion. *Ann Neurol.* 2019;86(4):480-492. [\[CrossRef\]](#)
26. Zhang D, Chen J, Xue Q, et al. Heterogeneity signs on noncontrast computed tomography predict hematoma expansion after intracerebral hemorrhage: a meta-analysis. *Biomed Res Int.* 2018;2018:6038193. [\[CrossRef\]](#)
27. Suzuki K. Overview of deep learning in medical imaging. *Radiol Phys Technol.* 2017;10(3):257-273. [\[CrossRef\]](#)
28. Gillies RJ, Kinahan PE, Hricak H. Radiomics: images are more than pictures, they are data. *Radiology.* 2016;278(2):563-577. [\[CrossRef\]](#)
29. Zhu DQ, Chen Q, Xiang YL, et al. Predicting intraventricular hemorrhage growth with a machine learning-based, radiomics-clinical model. *Aging (Albany NY).* 2021;13(9):12833-12848. [\[CrossRef\]](#)
30. Pszczolkowski S, Manzano-Patrón JP, Law ZK, et al. Quantitative CT radiomics-based models for prediction of haematoma expansion and poor functional outcome in primary intracerebral haemorrhage. *Eur Radiol.* 2021;31(10):7945-7959. [\[CrossRef\]](#)
31. Li H, Xie Y, Wang X, Chen F, Sun J, Jiang X. Radiomics features on non-contrast computed tomography predict early enlargement of spontaneous intracerebral hemorrhage. *Clin Neurol Neurosurg.* 2019;185:105491. [\[CrossRef\]](#)
32. Ma C, Zhang Y, Niyazi T, et al. Radiomics for predicting hematoma expansion in patients with hypertensive intraparenchymal hematomas. *Eur J Radiol.* 2019;115:10-15. [\[CrossRef\]](#)
33. Xie H, Ma S, Wang X, Zhang X. Noncontrast computer tomography-based radiomics model for predicting intracerebral hemorrhage expansion: preliminary findings and comparison with conventional radiological model. *Eur Radiol.* 2020;30(1):87-98. [\[CrossRef\]](#)
34. Guyon I, Dror G, Lemaire V, Silver DL, Taylor G, Aha DW. Analysis of the IJCNN 2011 UTL challenge. *Neural Netw.* 2012;32:174-178. [\[CrossRef\]](#)
35. Sharrock MF, Mould WA, Ali H, et al. 3D Deep neural network segmentation of intracerebral hemorrhage: development and validation for clinical trials. *Neuroinformatics.* 2021;19(3):403-415. [\[CrossRef\]](#)
36. Hanley DF, Thompson RE, Rosenblum M, et al. Efficacy and safety of minimally invasive surgery with thrombolysis in intracerebral haemorrhage evacuation (MISTIE III): a randomised, controlled, open-label, blinded endpoint phase 3 trial. *Lancet.* 2019;393(10175):1021-1032. [\[CrossRef\]](#)
37. van Griethuysen JJM, Fedorov A, Parmar C, et al. Computational radiomics system to decode the radiographic phenotype. *Cancer Res.* 2017;77(21):104-107. [\[CrossRef\]](#)
38. Szegedy C, Vanhoucke V, Ioffe S, Shlens J, Wojna Z. Rethinking the inception architecture for computer vision. *Cornell University.* 2015. [\[CrossRef\]](#)
39. Paul R, Hawkins SH, Balagurunathan Y, et al. Deep feature transfer learning in combination with traditional features predicts survival among patients with lung adenocarcinoma. *Tomography.* 2016;2(4):388-395. [\[CrossRef\]](#)
40. Afshar P, Mohammadi A, Plataniotis KN, Oikonomou A, Benali H. From hand-crafted to deep learning-based cancer radiomics. Challenges and opportunities. *Cornell University.* 2019. [\[CrossRef\]](#)

41. Kocak B, Baessler B, Bakas S, et al. CheckList for evaluation of radiomics research (CLEAR): a step-by-step reporting guideline for authors and reviewers endorsed by ESR and EuSoMII. *Insights Imaging*. 2023;14(1):75. [\[CrossRef\]](#)
42. Lambin P, Leijenaar RTH, Deist TM, et al. Radiomics: the bridge between medical imaging and personalized medicine. *Nat Rev Clin Oncol*. 2017;14(12):749-762. [\[CrossRef\]](#)
43. Morotti A, Dowlatshahi D, Boulouis G, et al. Predicting intracerebral hemorrhage expansion with noncontrast computed tomography: the BAT score. *Stroke*. 2018;49(5):1163-1169. [\[CrossRef\]](#)
44. Visser WE, Vrijmoeth P, Visser FE, Arts WF, van Toor H, Visser TJ. Identification, functional analysis, prevalence and treatment of monocarboxylate transporter 8 (MCT8) mutations in a cohort of adult patients with mental retardation. *J Stroke Cerebrovasc Dis*. 2018;27(10):2606-2612. [\[CrossRef\]](#)
45. Miyahara M, Noda R, Yamaguchi S, et al. New prediction score for hematoma expansion and neurological deterioration after spontaneous intracerebral hemorrhage: a hospital-based retrospective cohort study. *J Stroke Cerebrovasc Dis*. 2018;27(9):2543-2550. [\[CrossRef\]](#)
46. Yao X, Xu Y, Siwila-Sackman E, Wu B, Selim M. The HEP score: a nomogram-derived hematoma expansion prediction scale. *Neurocrit Care*. 2015;23(2):179-187. [\[CrossRef\]](#)
47. Brouwers HB, Chang Y, Falcone GJ, et al. Predicting hematoma expansion after primary intracerebral hemorrhage. *JAMA Neurol*. 2014;71(2):158-164. [\[CrossRef\]](#)
48. Wang X, Arima H, Al-Shahi Salman R, et al. Clinical prediction algorithm (BRAIN) to determine risk of hematoma growth in acute intracerebral hemorrhage. *Stroke*. 2015;46(2):376-381. [\[CrossRef\]](#)
49. Chen Q, Zhu D, Liu J, et al. Clinical-radiomics nomogram for risk estimation of early hematoma expansion after acute intracerebral hemorrhage. *Acad Radiol*. 2021;28(3):307-317. [\[CrossRef\]](#)
50. Song Z, Guo D, Tang Z, et al. Noncontrast computed tomography-based radiomics analysis in discriminating early hematoma expansion after spontaneous intracerebral hemorrhage. *Korean J Radiol*. 2021;22(3):415-424. [\[CrossRef\]](#)

## Supplementary Material 1.

### CLEAR Checklist v1.0

**Note:** Use the checklist in conjunction with the main text for clarification of all items.

Yes, details provided; No, details not provided; n/e, not essential; n/a, not applicable; Page, page number

Section	No.	Item	Yes	No	n/a	Page
<b>Title</b>						
	1	Relevant title, specifying the radiomic methodology	<input checked="" type="checkbox"/>	<input type="checkbox"/>	<input type="checkbox"/>	1
<b>Abstract</b>						
	2	Structured summary with relevant information	<input checked="" type="checkbox"/>	<input type="checkbox"/>	<input type="checkbox"/>	1
<b>Keywords</b>						
	3	Relevant keywords for radiomics	<input checked="" type="checkbox"/>	<input type="checkbox"/>	<input type="checkbox"/>	1
<b>Introduction</b>						
	4	Scientific or clinical background	<input checked="" type="checkbox"/>	<input type="checkbox"/>	<input type="checkbox"/>	1-2
	5	Rationale for using a radiomic approach	<input checked="" type="checkbox"/>	<input type="checkbox"/>	<input type="checkbox"/>	1-2
	6	Study objective(s)	<input checked="" type="checkbox"/>	<input type="checkbox"/>	<input type="checkbox"/>	2
<b>Method</b>						
<i>Study Design</i>	7	Adherence to guidelines or checklists (e.g., CLEAR checklist)	<input checked="" type="checkbox"/>	<input type="checkbox"/>	<input type="checkbox"/>	2
	8	Ethical details (e.g., approval, consent, data protection)	<input checked="" type="checkbox"/>	<input type="checkbox"/>	<input type="checkbox"/>	2
	9	Sample size calculation	<input type="checkbox"/>	<input type="checkbox"/>	<input checked="" type="checkbox"/>	
	10	Study nature (e.g., retrospective, prospective)	<input checked="" type="checkbox"/>	<input type="checkbox"/>	<input type="checkbox"/>	2
	11	Eligibility criteria	<input checked="" type="checkbox"/>	<input type="checkbox"/>	<input type="checkbox"/>	2
	12	Flowchart for technical pipeline	<input checked="" type="checkbox"/>	<input type="checkbox"/>	<input type="checkbox"/>	2
<i>Data</i>	13	Data source (e.g., private, public)	<input checked="" type="checkbox"/>	<input type="checkbox"/>	<input type="checkbox"/>	2
	14	Data overlap	<input type="checkbox"/>	<input type="checkbox"/>	<input checked="" type="checkbox"/>	
	15	Data split methodology	<input checked="" type="checkbox"/>	<input type="checkbox"/>	<input type="checkbox"/>	4
	16	Imaging protocol (i.e., image acquisition and processing)	<input checked="" type="checkbox"/>	<input type="checkbox"/>	<input type="checkbox"/>	2-3
	17	Definition of non-radiomic predictor variables	<input type="checkbox"/>	<input type="checkbox"/>	<input checked="" type="checkbox"/>	
	18	Definition of the reference standard (i.e., outcome variable)	<input checked="" type="checkbox"/>	<input type="checkbox"/>	<input type="checkbox"/>	3
<i>Segmentation</i>	19	Segmentation strategy	<input checked="" type="checkbox"/>	<input type="checkbox"/>	<input type="checkbox"/>	3
	20	Details of operators performing segmentation	<input type="checkbox"/>	<input type="checkbox"/>	<input checked="" type="checkbox"/>	
<i>Pre-processing</i>	21	Image pre-processing details	<input checked="" type="checkbox"/>	<input type="checkbox"/>	<input type="checkbox"/>	3
	22	Resampling method and its parameters	<input type="checkbox"/>	<input type="checkbox"/>	<input checked="" type="checkbox"/>	
	23	Discretization method and its parameters	<input type="checkbox"/>	<input checked="" type="checkbox"/>	<input type="checkbox"/>	

## Supplementary Material 1.

Section	No.	Item	Yes	No	n/a	Page
	24	Image types (e.g., original, filtered, transformed)	<input checked="" type="checkbox"/>	<input type="checkbox"/>	<input type="checkbox"/>	3
<i>Feature extraction</i>	25	Feature extraction method	<input checked="" type="checkbox"/>	<input type="checkbox"/>	<input type="checkbox"/>	3
	26	Feature classes	<input checked="" type="checkbox"/>	<input type="checkbox"/>	<input type="checkbox"/>	4
	27	Number of features	<input type="checkbox"/>	<input checked="" type="checkbox"/>	<input type="checkbox"/>	
	28	Default configuration statement for remaining parameters	<input type="checkbox"/>	<input checked="" type="checkbox"/>	<input type="checkbox"/>	
<i>Data preparation</i>	29	Handling of missing data	<input type="checkbox"/>	<input checked="" type="checkbox"/>	<input type="checkbox"/>	
	30	Details of class imbalance	<input checked="" type="checkbox"/>	<input type="checkbox"/>	<input type="checkbox"/>	3
	31	Details of segmentation reliability analysis	<input type="checkbox"/>	<input checked="" type="checkbox"/>	<input type="checkbox"/>	
	32	Feature scaling details (e.g., normalization, standardization)	<input checked="" type="checkbox"/>	<input type="checkbox"/>	<input type="checkbox"/>	3
	33	Dimension reduction details	<input checked="" type="checkbox"/>	<input type="checkbox"/>	<input type="checkbox"/>	3
<i>Modeling</i>	34	Algorithm details	<input checked="" type="checkbox"/>	<input type="checkbox"/>	<input type="checkbox"/>	3
	35	Training and tuning details	<input checked="" type="checkbox"/>	<input type="checkbox"/>	<input type="checkbox"/>	3-4
	36	Handling of confounders	<input type="checkbox"/>	<input checked="" type="checkbox"/>	<input type="checkbox"/>	
	37	Model selection strategy	<input checked="" type="checkbox"/>	<input type="checkbox"/>	<input type="checkbox"/>	2
<i>Evaluation</i>	38	Testing technique (e.g., internal, external)	<input checked="" type="checkbox"/>	<input type="checkbox"/>	<input type="checkbox"/>	4
	39	Performance metrics and rationale for choosing	<input checked="" type="checkbox"/>	<input type="checkbox"/>	<input type="checkbox"/>	4
	40	Uncertainty evaluation and measures (e.g., confidence intervals)	<input type="checkbox"/>	<input checked="" type="checkbox"/>	<input type="checkbox"/>	
	41	Statistical performance comparison (e.g., DeLong's test)	<input type="checkbox"/>	<input checked="" type="checkbox"/>	<input type="checkbox"/>	
	42	Comparison with non-radiomic and combined methods	<input type="checkbox"/>	<input type="checkbox"/>	<input checked="" type="checkbox"/>	
	43	Interpretability and explainability methods	<input type="checkbox"/>	<input checked="" type="checkbox"/>	<input type="checkbox"/>	
<b>Results</b>						
	44	Baseline demographic and clinical characteristics	<input checked="" type="checkbox"/>	<input type="checkbox"/>	<input type="checkbox"/>	4
	45	Flowchart for eligibility criteria	<input checked="" type="checkbox"/>	<input type="checkbox"/>	<input type="checkbox"/>	4
	46	Feature statistics (e.g., reproducibility, feature selection)	<input checked="" type="checkbox"/>	<input type="checkbox"/>	<input type="checkbox"/>	4-5
	47	Model performance evaluation	<input checked="" type="checkbox"/>	<input type="checkbox"/>	<input type="checkbox"/>	4-5
	48	Comparison with non-radiomic and combined approaches	<input type="checkbox"/>	<input type="checkbox"/>	<input checked="" type="checkbox"/>	
<b>Discussion</b>						
	49	Overview of important findings	<input checked="" type="checkbox"/>	<input type="checkbox"/>	<input type="checkbox"/>	5-6
	50	Previous works with differences from the current study	<input checked="" type="checkbox"/>	<input type="checkbox"/>	<input type="checkbox"/>	5-6
	51	Practical implications	<input checked="" type="checkbox"/>	<input type="checkbox"/>	<input type="checkbox"/>	5-6
	52	Strengths and limitations (e.g., bias and generalizability issues)	<input checked="" type="checkbox"/>	<input type="checkbox"/>	<input type="checkbox"/>	6

## Supplementary Material 1.

Section	No.	Item	Yes	No	n/a	Page
<b>Open Science</b>						
<i>Data availability</i>	53	Sharing images along with segmentation data [n/e]	<input checked="" type="checkbox"/>	<input type="checkbox"/>	<input type="checkbox"/>	4-5
	54	Sharing radiomic feature data	<input type="checkbox"/>	<input checked="" type="checkbox"/>	<input type="checkbox"/>	
<i>Code availability</i>	55	Sharing pre-processing scripts or settings	<input type="checkbox"/>	<input checked="" type="checkbox"/>	<input type="checkbox"/>	
	56	Sharing source code for modeling	<input type="checkbox"/>	<input checked="" type="checkbox"/>	<input type="checkbox"/>	
<i>Model availability</i>	57	Sharing final model files	<input type="checkbox"/>	<input checked="" type="checkbox"/>	<input type="checkbox"/>	
	58	Sharing a ready-to-use system [n/e]	<input type="checkbox"/>	<input checked="" type="checkbox"/>	<input type="checkbox"/>	

Kocak B, Baessler B, Bakas S, Cuocolo R, Fedorov A, Maier-Hein L, Mercaldo N, Müller H, Orhac F, Pinto Dos Santos D, Stanzione A, Ugga L, Zwanenburg A. CheckList for EvaluAtion of Radiomics research (CLEAR): a step-by-step reporting guideline for authors and reviewers endorsed by ESR and EuSoMII. *Insights Imaging*. 2023 May 4;14(1):75. doi: 10.1186/s13244-023-01415-8

## Supplementary Material 2.

2023/10/13 23:52

RQS - Radiomics.world

<p>Image protocol quality - well-documented image protocols (for example, contrast, slice thickness, energy, etc.) and/or usage of public image protocols allow reproducibility/replicability</p> <p><input checked="" type="checkbox"/> protocols well documented</p> <p><input checked="" type="checkbox"/> public protocol used</p> <p><input type="checkbox"/> none</p>
<p>Multiple segmentations - possible actions are: segmentation by different physicians/algorithms/software, perturbing segmentations by (random) noise, segmentation at different breathing cycles. Analyse feature robustness to segmentation variabilities</p> <p><input type="radio"/> yes</p> <p><input checked="" type="radio"/> no</p>
<p>Phantom study on all scanners - detect inter-scanner differences and vendor-dependent features. Analyse feature robustness to these sources of variability</p> <p><input type="radio"/> yes</p> <p><input checked="" type="radio"/> no</p>
<p>Imaging at multiple time points - collect images of individuals at additional time points. Analyse feature robustness to temporal variabilities (for example, organ movement, organ expansion/shrinkage)</p> <p><input type="radio"/> yes</p> <p><input checked="" type="radio"/> no</p>
<p>Feature reduction or adjustment for multiple testing - decreases the risk of overfitting. Overfitting is inevitable if the number of features exceeds the number of samples. Consider feature robustness when selecting features</p> <p><input checked="" type="radio"/> Either measure is implemented</p> <p><input type="radio"/> Neither measure is implemented</p>
<p>Multivariable analysis with non radiomics features (for example, EGFR mutation) - is expected to provide a more holistic model. Permits correlating/inferencing between radiomics and non radiomics features</p> <p><input type="radio"/> yes</p> <p><input checked="" type="radio"/> no</p>
<p>Detect and discuss biological correlates - demonstration of phenotypic differences (possibly associated with underlying gene-protein expression patterns) deepens understanding of radiomics and biology</p> <p><input type="radio"/> yes</p> <p><input checked="" type="radio"/> no</p>
<p>Cut-off analyses - determine risk groups by either the median, a previously published cut-off or report a continuous risk variable. Reduces the risk of reporting overly optimistic results</p> <p><input type="radio"/> yes</p> <p><input checked="" type="radio"/> no</p>

<https://www.radiomics.world/rqs>

1/3



## Supplementary Material 2.

2023/10/13 23:52

RQS - Radiomics.world

<p>Discrimination statistics - report discrimination statistics (for example, C-statistic, ROC curve, AUC) and their statistical significance (for example, p-values, confidence intervals). One can also apply resampling method (for example, bootstrapping, cross-validation)</p> <p><input type="checkbox"/> a discrimination statistic and its statistical significance are reported</p> <p><input checked="" type="checkbox"/> a resampling method technique is also applied</p> <p><input type="checkbox"/> none</p>
<p>Calibration statistics - report calibration statistics (for example, Calibration-in-the-large/slope, calibration plots) and their statistical significance (for example, P-values, confidence intervals). One can also apply resampling method (for example, bootstrapping, cross-validation)</p> <p><input type="checkbox"/> a calibration statistic and its statistical significance are reported</p> <p><input checked="" type="checkbox"/> a resampling method technique is applied</p> <p><input type="checkbox"/> none</p>
<p>Prospective study registered in a trial database - provides the highest level of evidence supporting the clinical validity and usefulness of the radiomics biomarker</p> <p><input type="radio"/> yes</p> <p><input checked="" type="radio"/> no</p>
<p>Validation - the validation is performed without retraining and without adaptation of the cut-off value, provides crucial information with regard to credible clinical performance</p> <p><input type="checkbox"/> No validation</p> <p><input checked="" type="checkbox"/> validation is based on a dataset from the same institute</p> <p><input type="checkbox"/> validation is based on a dataset from another institute</p> <p><input type="checkbox"/> validation is based on two datasets from two distinct institutes</p> <p><input type="checkbox"/> the study validates a previously published signature</p> <p><input type="checkbox"/> validation is based on three or more datasets from distinct institutes</p>
<p>Comparison to 'gold standard' - assess the extent to which the model agrees with/is superior to the current 'gold standard' method (for example, TNM-staging for survival prediction). This comparison shows the added value of radiomics</p> <p><input type="radio"/> yes</p> <p><input checked="" type="radio"/> no</p>
<p>Potential clinical utility - report on the current and potential application of the model in a clinical setting (for example, decision curve analysis).</p> <p><input type="radio"/> yes</p> <p><input checked="" type="radio"/> no</p>
<p>Cost-effectiveness analysis - report on the cost-effectiveness of the clinical application (for example, QALYs generated)</p> <p><input type="radio"/> yes</p> <p><input checked="" type="radio"/> no</p>

<https://www.radiomics.world/rqs>

2/3

## Supplementary Material 2.

2023/10/13 23:52

RQS - Radiomics.world

Open science and data - make code and data publicly available. Open science facilitates knowledge transfer and reproducibility of the study

- scans are open source
- region of interest segmentations are open source
- the code is open sourced
- radiomics features are calculated on a set of representative ROIs and the calculated features and representative ROIs are open source

Total score **10** (27.78%)



# Burnout and the role of mentorship for radiology trainees and early career radiologists

Richard J Fagan<sup>1</sup>  
 Dane Eskildsen<sup>1</sup>  
 Tara Catanzano<sup>2</sup>  
 Rachel Stanietzky<sup>3</sup>  
 Serageldin Kamel<sup>3</sup>  
 Mohamed Eltaher<sup>3</sup>  
 Khaled M. Elsayes<sup>3</sup>

<sup>1</sup>Baylor College of Medicine, Department of Radiology, Texas, United States of America

<sup>2</sup>University of Massachusetts Medical School-Baystate, Department of Radiology, UMass Chan-Baystate, Springfield, United States of America

<sup>3</sup>University of Texas MD Anderson Cancer Center, Department of Abdominal Imaging, Texas, United States of America

## ABSTRACT

Burnout is a widespread issue among physicians, including radiologists and radiology trainees. Long hours, isolation, and substantial stress levels contribute to healthcare workers experiencing a substantially higher rate of burnout compared with other professionals. Resident physicians, continuously exposed to stressors such as new clinical situations and performance feedback, are particularly susceptible. Mentorship has proven to be an effective strategy in mitigating burnout. Various mentorship delivery models exist, all aiming to have mentors serve as role models to mentees, thereby alleviating stress and anxiety. Physician groups and healthcare enterprises have actively implemented these programs, recognizing them as both successful and cost-effective. This article explores different mentorship models, their implementation processes, and the effectiveness of these programs as a standard component of academic departments.

## KEYWORDS

Burnout, mentees, mentorship, radiology trainees, work related stress

Healthcare workers are pivotal in fostering a healthy society. The issue of physician burnout, long overlooked within the healthcare setting, has now reached a critical point, prompting many physicians to leave the profession. Confronting and reversing this trend is imperative to sustain our legacy of outstanding and compassionate healthcare for future generations. Mentorship has emerged as a key strategy in combating the growing issue of physician burnout. This article discusses various mentorship models and their impact on improving physician mental health. Additionally, it presents a compelling business case for the establishment of institutional mentorship programs.

## The current state of burnout in medicine

Burnout is defined as a long-term stress reaction characterized by emotional exhaustion, depersonalization, and a diminished sense of personal accomplishment. The increasingly demanding healthcare workplace environment has accelerated burnout among physicians and other healthcare workers.<sup>1</sup> A 2011 study revealed that 45% of United States (U.S) physicians reported at least one manifestation of professional burnout and a decline in satisfaction with work-life balance compared with individuals of similar education levels working comparable weekly hours in non-healthcare fields. These gaps had widened by 2014, with 54% of physicians reporting burnout, a rate substantially higher than that of non-physicians.<sup>2</sup> This troubling trend was exacerbated by the coronavirus disease-2019 (COVID-19) pandemic, during which many specialties reported increasing rates of burnout. Notably, emergency department physicians experienced the highest levels of burnout, with an upward trend from 43% in 2020 to 60% in 2021, reaching 65% in 2022.<sup>3,4</sup> Increases in burnout among specialties involving high degrees of patient interaction are not surprising, as previous studies have demonstrated that healthcare workers in clinical settings experience more burnout than those in research or non-clinical settings.<sup>5</sup> The effects of burnout and other stressors induced by the COVID-19

Corresponding author: Khaled M. Elsayes

E-mail: kmelsayes@mdanderson.org

Received 25 April 2024; accepted 12 May 2024.



Epub: 05.06.2024

Publication date: 09.09.2024

DOI: 10.4274/dir.2024.242825

pandemic were pervasive throughout the physician workforce, also affecting radiologists. In 2022, 54% of radiologists reported feelings of burnout due to various factors, including long hours and feelings of isolation and inadequacy.<sup>4,6,7</sup> Resident physicians were also substantially impacted by the emotional stressors of the pandemic, experiencing an increase in clinical responsibilities, a reduction in educational opportunities, and less frequent and effective performance feedback compared with the period prior to the pandemic.<sup>8</sup>

In addition to burnout, physicians have reported a steady increase in depression, with 38% experiencing depressive symptoms in 2011, 40% in 2014, and 42% in 2017.<sup>2</sup> By 2021, 64% of physicians felt “down” or “sad,” with 21% reporting clinical depression.<sup>3</sup> The pandemic contributed to a continued rise in clinical depression rates, increasing to 23% in 2023.<sup>4</sup>

While the causes of burnout are undoubtedly multifactorial, commonly cited factors include increased regulations and oversight, reduced face-to-face time with patients, and a substantial administrative burden due to electronic health record usage, with physicians spending around half of their workday on these records. A pre-pandemic survey of neuroradiologists in the U.S revealed that 37% were likely to retire earlier than initially planned, with a statistically significant correlation between the inclination to retire early and the use of personal wellness measures alongside challenges in balancing clinical and non-clinical duties.<sup>9</sup> This survey also indicated that pre-pandemic increases in workload led to cutbacks in resident teaching and mentoring, activities that typically provide satisfaction to physicians in the workplace.<sup>9</sup> Moreover, economic constraints, along with increasing clinical volumes and escalating productivity demands in clinical

care, research, and teaching, contribute to emotional exhaustion.<sup>10</sup>

Certain groups within the physician population appear more prone to burnout. Women and those working in specific specialties such as emergency medicine and general internal medicine report higher rates of burnout and lower satisfaction with work-life balance.<sup>2,4,11</sup> Working additional weekly hours was also independently associated with an increased risk of burnout.<sup>2</sup> Among all healthcare workers, women, Caucasians, millennials, and those in supervisory roles have been identified as substantially more likely to experience burnout.<sup>5</sup> Interestingly, whereas women reported higher personal burnout scores than men, work-related and patient-related burnout did not show substantial differences between genders, suggesting that workplace factors are not the sole contributors to physician burnout.<sup>11</sup>

Multiple studies have demonstrated that physicians without a mentoring relationship exhibit higher levels of burnout.<sup>5,11</sup> Conversely, burnout scores are lower in workplaces that offer well-being consultation services.<sup>11</sup> The implementation of mentoring as an organizational objective is particularly crucial, as organization-directed interventions focusing on enhancing workplace communication and skills have proven more effective in treating and preventing burnout than interventions directed at individuals.<sup>12</sup> Moreover, hospital executives at leading U.S academic institutions, such as the Mayo Clinic, have implemented formal organizational strategies to identify, develop, and support physician leaders. These strategies are recognized as cost-neutral, and substantially promote physician well-being.<sup>13</sup> These executives also noted that mentorship and organizational efforts to engage physicians in work they find meaningful can dramatically reduce the risk of burnout.<sup>13</sup>

While not all causes of burnout are work-related, its effects are visibly manifested in the workplace. Outcomes such as early retirement, reduced working hours, and the desire to leave one’s current place of employment reflect burnout and dissatisfaction with work-life balance among U.S physicians.<sup>14</sup> For those choosing not to retire, decreased productivity, cynicism, depression, substance abuse, and an increased rate of clinical errors are well-documented consequences of burnout.<sup>10</sup> A Stanford University study conservatively estimates the annual cost of physician burnout in the U.S at \$4.6 billion, with other studies suggesting figures as high as \$10

billion.<sup>2,15</sup> Perhaps more alarming than the financial impact is the threat burnout poses to the already limited available physician workforce. Recruitment and retention strategies must address the effects of burnout and develop mitigating approaches to prevent a catastrophic workforce shortage that could substantially affect patient care.

### The role of mentorship in combating burnout

Efforts are underway to address burnout, with organizations such as the American Medical Association and the National Academy of Medicine initiating multidisciplinary efforts to engage regulators, healthcare organizations, and other groups in addressing system-wide issues contributing to burnout. Despite these efforts, the outcomes have been discouraging. For instance, the 2022 Physician Burnout and Depression Report revealed an increase in burnout, with several specialties reporting that over 50% of their members experience such feelings.<sup>16</sup> The COVID-19 pandemic has substantially contributed to these trends and may confound the assessment of the outcomes of these mitigation efforts.<sup>16</sup> Institutions have identified concrete steps to reduce burnout, including investing time and resources in leadership development and mentorship programs for employees.<sup>5</sup>

Mentorship is defined as a relationship in which a more experienced or knowledgeable person guides a less experienced or less knowledgeable person. At its core, mentorship focuses on the individual development of navigating challenges rather than acquiring specific knowledge or technical skills.<sup>10</sup> Various models of mentorship exist. The most common is the dyad model, in which one person mentors a single mentee. This model is straightforward to implement and facilitates the development of structure, goals, and accountability between the mentor and the mentee. However, the dyad model may not meet all the needs of its participants as it is limited by the expertise and skill set of a single mentor. In contrast, mosaic mentorship models offer a more comprehensive experience. These models involve multiple mentors and various forms of mentorship, such as group or peer mentorship, focusing on learning from and challenging peers at a similar expertise level. These less traditional mentorship models offer benefits such as enhanced support and more dynamic relationships while mitigating concerns related to perceived power differentials and providing access to a diverse array of mentors.<sup>17</sup>

#### Main points

- Burnout is an increasingly common problem among healthcare workers.
- Mentorship programs have been implemented to combat rising concern over burnout.
- Various mentorship delivery models have been rigorously studied and analyzed. We present and discuss the outcomes of these different models.
- The positive outcomes of mentorship programs, along with their substantial benefits to mentees, mentors, and the health organization, are illustrated.

The benefits of mentorship across various medical disciplines have been extensively researched and documented.<sup>18</sup> A notable study conducted at Massachusetts General Hospital investigated the impacts of a mentorship program that paired junior faculty with senior faculty. After 1 year, the junior faculty reported substantial increases in the department's emphasis on professional development, peer support, and their ability to balance work and family commitments.<sup>18</sup> In this cohort, 43% of junior faculty received grant funding, and 50% were honored with departmental awards during the study period. Remarkably, 10 junior faculty members, including three from under-represented minority groups, were promoted within the 1-year study period, a substantial increase from an average of 4.2 promotions per year prior to the mentorship program (with no promotions from under-represented minority groups).<sup>18</sup> These early career interventions are crucial, as evidenced by another study revealing that 36% of academic radiologists struggle to balance work and life demands, and a majority leave academic practices early in their careers.<sup>19,20</sup>

Additionally, the role of mentorship in mitigating burnout has been explored, with findings suggesting benefits for both mentors and mentees. Mentors often experience a renewed sense of purpose and rejuvenation, while mentees gain valuable insights and guidance for navigating workplace challenges.<sup>10</sup> Early interventions prove particularly effective. For example, a short-term study involving medical students on emergency medicine rotations demonstrated an increase in personal accomplishment and a trend toward reduced emotional exhaustion and depersonalization among participants in a mentorship program.<sup>21</sup> Institutions must implement early strategies to combat burnout, especially since only 13% of physicians seek professional help for burnout, 41% fear repercussions from their medical board or employer, and over half perceive a stigma associated with burnout and depression.<sup>4</sup> These findings underscore the need for early career interventions before symptoms manifest and call for the broader implementation of such programs.

The relationship between mentoring and burnout is not exclusive to the medical field. A large study among telecommunications workers demonstrated that mentoring and providing adequate resources to employees substantially reduced burnout and increased retention.<sup>22</sup> The study also highlighted the importance of flexible scheduling to en-

hance work-life balance, transparency in evaluations and pay, and avoiding overwork as key factors in mitigating burnout.<sup>22</sup>

Altruism is a commendable quality in mentors, and numerous benefits of mentorship have been identified. Studies show that physicians serving as mentors report an increase in leadership skills, heightened confidence in their mentoring abilities, a stronger sense of purpose, and renewed interest in their specialty.<sup>10,21</sup> Researchers from the University of South Florida studied healthcare employees at an undisclosed organization in the U.S and discovered that those with mentoring experience reported higher salaries and more promotions than those without mentoring experience.<sup>23</sup> The same study noted that the average timeframe for advancement within the company was approximately 1 year following the participants' initial mentoring experience. Furthermore, subjective assessments of personal success are substantially higher among mentors compared with non-mentors.<sup>23</sup>

Mentorship benefits also extend to the institutional level. Most radiologists who leave academic medicine do so within their first few years, with almost 70% departing after an average of 3.28 years, and the majority indicate that they would not consider returning to academic medicine.<sup>19</sup> A lack of mentorship has been identified as a critical factor in these physicians' decision to leave. This issue is particularly acute among women physicians, who often cite inadequate mentorship as a career obstacle. The disproportionately small number of women holding professorships and departmental leadership positions in academic medicine creates substantial barriers to securing mentorship for many women physicians.<sup>24</sup> This challenge is pronounced in fields with a lower percentage of women members. As of 2022, 73% of practicing radiologists and 72% of current ACGME radiology residents and fellows were identified as men.<sup>25</sup> Promoting and retaining a diverse workforce can aid in the future retention of underrepresented physicians by providing trainees and early career physicians access to a diverse set of mentors and leaders, as positive mentorship has been shown to increase job satisfaction and organizational commitment among healthcare workers.<sup>10,26-28</sup>

This institutional commitment to the retention of professionals can be demonstrated by incentivizing mentorship through financial means and promotions. While many institutions focus on the recruitment and

retention of "star" employees, implementing such measures with the average employee in mind will better foster diversity, versatility, and growth at the institutional level. Developing this breadth ensures that future employees do not need to find a "perfect" mentor, as a diverse network of mentors can offer benefits and guidance in various areas.<sup>10</sup>

### Implementing effective mentorship programs

There is robust evidence supporting the benefits of mentorship programs for physicians in training; however, the implementation of these programs often lacks clarity. A survey of radiology residency program directors revealed that while 85% recognized the importance of mentorship, only 52% reported that their residents utilized a mentor, and there was no consensus on the structure of mentorship programs.<sup>28</sup> Common goals for mentorship programs include focusing on the mentee's development and providing emotional and psychological support to foster the mentee's independent professionalism.<sup>29</sup> Most authors in our review advocated for the mosaic mentorship model, in which a mentee has multiple mentors who collectively address the specific needs of the mentee.<sup>29-32</sup> As Ayyala et al.<sup>27</sup> noted, the mosaic model is particularly beneficial for physicians from underrepresented groups, enabling these individuals to seek out specific mentors for needs that may not be met by a single mentor. For instance, studies have indicated that most women program directors believe having a female mentor is crucial for women radiology residents. However, this mentor may differ from those sought for research- or practice-specific advice.<sup>27,28,30,31</sup>

An initial barrier identified by trainees in forming productive mentoring relationships is the challenge of identifying a suitable mentor.<sup>33</sup> There are various approaches to pairing mentors with mentees. A formal, department-led process of assigning trainees to faculty mentors offers the advantage of being easier to structure, monitor, and evaluate. Conversely, an informal process in which trainees select their mentors can be more organic and potentially more aligned with the individual needs of the trainee.<sup>30</sup> In training programs with limited faculty resources, leveraging alumni networks or collaborating with local and national organizations can enhance mentorship opportunities.<sup>33,34</sup> An advantage of the mosaic mentorship model is that it allows for the simultaneous pursuit of these various methods.

Regardless of the method of mentor selection, several key elements of a productive mentor-mentee relationship have been identified. The mentee's responsibilities include respecting the mentor's time and expectations, being honest about their goals and abilities, and being receptive to feedback.<sup>29,30,33</sup> Conversely, the mentor's responsibilities include demonstrating enthusiasm, being available, and being transparent about the scope and timeline of projects.<sup>31,33</sup> Notably, one of the most substantial contributions a mentor can make is to direct a trainee toward another mentor better suited to address specific needs. Once mentorship is established, setting clear goals and mutually understanding how to achieve these goals is crucial. Articulating these objectives in a written mission statement can help hold both parties accountable.<sup>30</sup>

Peer and near-peer mentoring have also proven effective in physician training programs. A study of a peer mentoring cohort in an academic radiology residency found that the most commonly discussed topics included study strategies, rotation-specific advice, and preparation for on-call duties.<sup>35</sup> Peer and near-peer mentoring offers highly accessible relationships for trainees, allowing them to share the responsibility of teaching junior residents.

The clinical department plays a pivotal role in providing the institutional framework necessary for successful mentoring relationships. If reducing burnout is a departmental goal, an important initial step is to help members identify the drivers of burnout. The Mayo Clinic has developed an excellent model that outlines the challenges of physician burnout. The authors discuss integrating this model into everyday practice.<sup>36,37</sup> Once the drivers of burnout are recognized, mentorship can be leveraged to address them.

Departments can encourage mentorship by implementing several concrete steps: providing protected time for mentorship meetings -since a lack of such time has been identified as a major obstacle to effective mentorship- and offering mentorship training before the initiation of a mentoring partnership.<sup>30,32</sup> Benchmarks such as publications, promotions, and the implementation of new procedures can serve as opportunities for recognition by the department or individual mentors.<sup>30</sup> Other departmental incentives, such as formal recognitions or awards and the provision of continuing education credits, play a crucial role in promoting mentorship.<sup>29,32</sup>

Departmental leadership and committees are responsible for overseeing the matching of mentors with mentees, the allocation of resources and stipends, and the monitoring of progress and satisfaction within the pairings.<sup>31,32,38</sup> While departmental leaders, such as the department chair and program director, are instrumental in supporting mentorship programs, several authors recommend that these leaders refrain from holding personal mentorship positions to prevent perceived favoritism among trainees and to enable trainees to engage openly with their mentors without fear of repercussion regarding their evaluations.<sup>30,31</sup>

The benefits of mentorship extend beyond just residents. The transition from being a trainee to independent practice can be overwhelming, and early-career physicians face similar challenges. Establishing mentorships can help new faculty members quickly adapt to a new system or workload.<sup>38-40</sup> The mosaic model of mentorship is especially useful in this group, as young physicians often face financial strains and family responsibilities that can add to the pressure.<sup>32</sup> Additionally, physicians who are transitioning into new roles in private practice, administration, or legislative committees can benefit from mentors who are more experienced in these areas.<sup>31</sup> As radiologists progress in their careers, the concept of coaching, which focuses on enhancing an individual's awareness of their existing strengths, may become more substantial than traditional mentorship.<sup>41</sup>

## Conclusion

In conclusion, although there is no data to support the superiority of one mentorship style over another, ample data exists to support the benefits of mentorship in enhancing the well-being and progression of residents and early-career radiologists. These advantages are crucial in today's healthcare landscape, where burnout, depression, and job dissatisfaction are prevalent and contribute to medical errors, staff turnover, and financial losses. Productive mentorship has been demonstrated to be a low-cost or cost-neutral approach to enhancing physician retention, morale, and productivity.

## Conflict of interest disclosure

The authors declared no conflicts of interest.

## References

1. Agency for Healthcare Research and Quality. Physician Burnout. [\[CrossRef\]](#)

2. Shanafelt TD, West CP, Dyrbye LN, et al. Changes in burnout and satisfaction with work-life integration in physicians during the first 2 years of the COVID-19 pandemic. *Mayo Clin Proc.* 2022;97(12):2248-2258. [\[CrossRef\]](#)
3. Physician Burnout, Depression Compounded by COVID: Survey – Medscape. Accessed: Jan 21, 2022. [\[CrossRef\]](#)
4. Kane L. "I Cry but No One Cares": Physician Burnout & Depression Report 2023. [\[CrossRef\]](#)
5. Cavanaugh KJ, Lee HY, Daum D, et al. An examination of burnout predictors: understanding the influence of job attitudes and environment. *Healthcare (Basel).* 2020;8(4):502. [\[CrossRef\]](#)
6. Medscape National Physician Burnout, Depression & Suicide Report 2019. Kane, L. Medscape. Jan 16, 2019. [\[CrossRef\]](#)
7. Fishman MDC, Reddy SP. Coaching: a primer for the radiologist. *J Am Coll Radiol.* 2021;18(8):1192-1197. [\[CrossRef\]](#)
8. Lee LK, Krajewski KM, Suarez-Weiss KE, Silverman SG, Shinagare AB. Learning from experience- confronting challenges and adapting to change in a large academic abdominal radiology practice: insights from a faculty retreat. *Curr Probl Diagn Radiol.* 2022;51(6):818-822. [\[CrossRef\]](#)
9. Chen JY, Vedantham S, Lexa FJ. Burnout and work-work imbalance in radiology- wicked problems on a global scale. A baseline pre-COVID-19 survey of US neuroradiologists compared to international radiologists and adjacent staff. *Eur J Radiol.* 2022;155:110153. [\[CrossRef\]](#)
10. Fishman JA. Mentorship in academic medicine: competitive advantage while reducing burnout? *Health Sciences Review.* 2021;1:100004. [\[CrossRef\]](#)
11. Perumalswami CR, Takenoshita S, Tanabe A, et al. Workplace resources, mentorship, and burnout in early career physician-scientists: a cross sectional study in Japan. *BMC Med Educ.* 2020;20(1):178. [\[CrossRef\]](#)
12. Panagiotti M, Panagopoulou E, Bower P, et al. Controlled interventions to reduce burnout in physicians: a systematic review and meta-analysis. *JAMA Intern Med.* 2017;177(2):195-205. [\[CrossRef\]](#)
13. Shanafelt TD, Noseworthy JH. Executive leadership and physician well-being: nine organizational strategies to promote engagement and reduce burnout. *Mayo Clin Proc.* 2017;92(1):129-146. [\[CrossRef\]](#)
14. Shanafelt TD, Raymond M, Kosty M, et al. Satisfaction with work-life balance and the career and retirement plans of US oncologists. *J Clin Oncol.* 2014;32(11):1127-1135. [\[CrossRef\]](#)
15. Han S, Shanafelt TD, Sinsky CA, et al. Estimating the attributable cost of physician burnout in the United States. *Ann Intern Med.* 2019;170(11):784-790. [\[CrossRef\]](#)

16. Physician Burnout & Depression Report 2022: Stress, Anxiety and Anger. Kane L. Medscape. Jan 21, 2022. [\[CrossRef\]](#)
17. Khatchikian AD, Chahal BS, Kielar A. Mosaic mentoring: finding the right mentor for the issue at hand. *Abdom Radiol (NY)*. 2021;46(12):5480-5484. [\[CrossRef\]](#)
18. Bredella MA, Alvarez C, O'Shaughnessy SA, Lavigne SD, Brink JA, Thrall JH. Radiology Mentoring program for early career faculty-implementation and outcomes. *J Am Coll Radiol*. 2021;18(3 Pt A):451-456. [\[CrossRef\]](#)
19. Taljanovic MS, Hunter TB, Krupinski EA, Alcalá JN, Fitzpatrick KA, Ovitt TW. Academic radiology: the reasons to stay or leave. *Acad Radiol*. 2003;10:1461-1468. [\[CrossRef\]](#)
20. Cankurtaran CZ, Reddy S, Cen SY, Lei X, Walker DK. Work-life experience of academic radiologists: food for thought. *Acad Radiol*. 2023;30(4):579-584. [\[CrossRef\]](#)
21. Jordan J, Watcha D, Cassella C, Kaji AH, Trivedi S. Impact of a mentorship program on medical student burnout. *AEM Educ Train*. 2019;3(3):218-225. [\[CrossRef\]](#)
22. Jyoti J, Rani A. Role of burnout and mentoring between high performance work system and intention to leave: Moderated mediation model. *J Bus Res*. 2019;98:166-176. [\[CrossRef\]](#)
23. Allen TD, Lentz E, Day R. Career success outcomes associated with mentoring others: a comparison of mentors and nonmentors. *J Career Dev*. 2006;32(3):272-285. [\[CrossRef\]](#)
24. Farkas AH, Bonifacino E, Turner R, Tilstra SA, Corbelli JA. Mentorship of women in academic medicine: a systematic review. *J Gen Intern Med*. 2019;34(7):1322-1329. [\[CrossRef\]](#)
25. AAMC. Physician Specialty Data Report. 2022. Accessed 2/20/2023. [\[CrossRef\]](#)
26. Weng RH, Huang CY, Tsai WC, et al. Exploring the impact of mentoring functions on job satisfaction and organizational commitment of new staff nurses. *BMC Health Serv Res*. 2010;10:240. [\[CrossRef\]](#)
27. Ayyala RS, Artunduaga M, Morin CE, Coley BD. Leveraging diversity, equity and inclusion for promoting wellness in the radiology workplace. *Pediatr Radiol*. 2022;52(9):1724-1729. [\[CrossRef\]](#)
28. Donovan A. Views of radiology program directors on the role of mentorship in the training of radiology residents. *AJR Am J Roentgenol*. 2010;194(3):704-708. [\[CrossRef\]](#)
29. Vieira A, Cabri MM, Spijkers S, Vieira AC, Maas M. Mentoring in radiology: an asset worth exploring! *Eur J Radiol*. 2022;155:110133. [\[CrossRef\]](#)
30. Perry RE, Parikh JR. Developing effective mentor-mentee relationships in radiology. *J Am Coll Radiol*. 2018;15(2):328-333. [\[CrossRef\]](#)
31. Mainiero MB. Mentoring radiology residents: why, who, when, and how. *J Am Coll Radiol*. 2007;4(8):547-550. [\[CrossRef\]](#)
32. Perry RE, Parikh JR. Mentorship of junior faculty members in academic radiology. *J Am Coll Radiol*. 2017;14(10):1341-1344. [\[CrossRef\]](#)
33. Kikano EG, Ramaiya NH. Mentorship in academic radiology: a review from a Trainee's perspective-radiology in training. *Radiology*. 2022;303(1):E17-E19. [\[CrossRef\]](#)
34. Yedavalli VS, Shah P. Residents' perceptions of usage of the current alumni and attending network for a formal mentorship program in an academic affiliated community hospital radiology residency. *Curr Probl Diagn Radiol*. 2019;48(2):105-107. [\[CrossRef\]](#)
35. Cheng K, Grabowski C, Chong A, Yen A, Chung CB. Initial experience with formal near-peer mentoring in radiology residency. *Curr Probl Diagn Radiol*. 2022;51(3):304-307. [\[CrossRef\]](#)
36. Shanafelt TD, Noseworthy JH. Executive leadership and physician well-being: nine organizational strategies to promote engagement and reduce burnout. *Mayo Clin Proc*. 2017;92(1):129-146. [\[CrossRef\]](#)
37. Chong ST, Thrall JH, Fessell D. Addressing burnout: a model-based approach. *J Am Coll Radiol*. 2021;18(5):669-674. [\[CrossRef\]](#)
38. Retrouvey M, Grajo JR, Awan O, et al. Transitioning from radiology training to academic faculty: the importance of mentorship. *Curr Probl Diagn Radiol*. 2020;49(4):219-223. [\[CrossRef\]](#)
39. Patel MM, Kapoor MM, Whitman GJ. Transitioning to practice: getting up to speed in efficiency and accuracy. *J Breast Imaging*. 2020;3(5):607-611. [\[CrossRef\]](#)
40. Bredella MA, Fessell D, Thrall JH. Mentorship in academic radiology: why it matters. *Insights Imaging*. 2019;10(1):107. [\[CrossRef\]](#)
41. Gowda V, Jordan SG, Oliveira A, Cook TS, Enarson C. Support from within: coaching to enhance radiologist well-being and practice. *Acad Radiol*. 2022;29(8):1255-1258. [\[CrossRef\]](#)



# Percutaneous nephrostomy in infants: a 20-year single-center experience

- Onur Taydaş<sup>1</sup>  
 Emre Ünal<sup>2</sup>  
 Devrim Akıncı<sup>2</sup>  
 Mehmet Şeker<sup>3</sup>  
 Osman Melih Topçuoğlu<sup>4</sup>  
 Okan Akhan<sup>2</sup>  
 Türkmen Turan Çiftçi<sup>2</sup>

<sup>1</sup>Sakarya University Faculty of Medicine, Department of Radiology, Sakarya, Türkiye

<sup>2</sup>Hacettepe University Faculty of Medicine, Department of Radiology, Ankara, Türkiye

<sup>3</sup>Medipol University Faculty of Medicine, Department of Radiology, İstanbul, Türkiye

<sup>4</sup>Yeditepe University Faculty of Medicine, Department of Radiology, İstanbul, Türkiye

## PURPOSE

To investigate the safety and efficacy of the imaging-guided percutaneous nephrostomy (PCN) procedure in infants.

## METHODS

A total of 75 (50 boys; 66.7%) patients with a mean age of 121 days (range, 1–351 days) who underwent PCN over a period of 20 years were included in this retrospective study. For each patient, PCN indications, catheter size, the mean duration of catheterization, complications, and the procedure performed following nephrostomy were recorded. Technical success was determined based on the successful placement of the nephrostomy catheter within the pelvicalyceal system. Clinical success was defined as the complete resolution of hydronephrosis and improvement in renal function tests during follow-up. In patients with urinary leakage, technical and clinical success was determined based on the resolution of leakage.

## RESULTS

The technical success rate was 100%, and no procedure-related mortality was observed. In 11 patients (14.7%), bilateral PCN was performed. The most frequent indication of PCN was ureteropelvic junction obstruction (n = 41, 54.7%). Procedure-related major complications were encountered in two patients (methemoglobinemia and respiratory arrest caused by the local anesthetic agent in one patient and the development of urinoma caused by urinary leakage from the puncture site in the other). Mild urinary leakage was the only minor complication that occurred and only in one patient. Catheter-related complications were managed through replacement or revision surgery in 16 patients (21.3%).

## CONCLUSION

Imaging-guided PCN is a feasible and effective procedure with high technical success and low major complication rates, and it is useful for protecting kidney function in infants.

## KEYWORDS

Percutaneous nephrostomy, infants, interventional radiology, urinary tract obstruction, complications

Corresponding author: Onur Taydaş

E-mail: taydasonur@gmail.com

Received 20 April 2023; revision requested 11 June 2023; accepted 23 July 2023.



Epub: 18.08.2023

Publication date: 09.09.2024

DOI: 10.4274/dir.2023.232276

**P**ercutaneous nephrostomy (PCN) is the method of choice for external urinary diversion in patients with urinary obstruction or extravasation.<sup>1</sup> It is an indispensable tool, particularly for patients with malignant urinary obstruction because retrograde ureteral stenting is almost always challenging in these patients. The ultrasound-guided approach makes the procedure much safer than the conventional fluoroscopy-guided method. Access to the pelvicalyceal system through PCN may also serve as a feasible route for further interventions, including ureteral balloon dilatation, stenting, and foreign object or stone removal.<sup>2</sup>

Although PCN is routinely performed in adults at every major hospital and a large number of minor hospitals around the world, its applicability in infants and neonates is limited. The procedure can be more challenging in infants than in adults for various reasons, such as the smaller kidney size, lower cutaneous and subcutaneous tissue thickness, lack of perirenal fat

You may cite this article as: Taydaş O, Ünal E, Akıncı D, et al. Percutaneous nephrostomy in infants: a 20-year single-center experience. *Diagn Interv Radiol*. 2024;30(5):318-324.



tissue, more elastic and flexible renal parenchyma, and smaller volume of the pelvicalyceal system.<sup>3</sup> The elasticity of infant kidneys is the most commonly encountered problem. In infants, the kidney can be pushed or even kinked during needle puncturing, which is a rarely encountered incident in adults other than for patients with chronic kidney diseases. In addition, the rapid decompression of the pelvicalyceal system during the procedure may result in the loss of percutaneous access, further complicating the procedure.<sup>4</sup> Moreover, urinary leakage following kidney puncture may be negligible in adults, but it is particularly important for infants because of the smaller volume of their collecting systems. The management of infant patients following PCN is also very different from that of adults.<sup>5,6</sup>

Although PCN placement is an essential element of interventional radiology practice,<sup>3</sup> it is not widely practiced in infants for the reasons outlined above. Despite current studies on nephrostomy in pediatric and newborn patient groups in the literature,<sup>7,8</sup> there are no comprehensive and long-term studies on the infant age group. The fact that this age group includes the neonatal period, which marks an important period for kidney maturation, emphasizes that the evaluation of these patients should be of special interest.<sup>9</sup> In this study, we report our experience with imaging-guided PCN in infants, with an emphasis on the safety and efficacy of the procedure in this patient group.

## Methods

### Patients

Institutional approval for the study was granted by the Hacettepe University Clinical Research Ethics Committee (GO 16/609-06),

and all procedures were in accordance with the principles of the Helsinki Declaration. Informed consent was waived because of the retrospective nature of the study. Patient records were obtained from physical and electronic files, and the images of the patients were acquired from the picture archiving and communication systems of the hospital. The inclusion criteria were as follows: younger than 12 months at the date of the nephrostomy procedure; availability of clinical, imaging, and laboratory findings; and a post-procedure follow-up conducted in our hospital. The exclusion criteria were as follows: older than 12 months at the date of the procedure; incomplete data on clinical, imaging, and laboratory findings; or incomplete post-procedure follow-up. The clinical and radiological data of 75 infants who underwent PCN over a period of 20 years were retrospectively reviewed for the study. A total of 11 patients whose clinical or radiological findings could not be obtained were excluded from the study. The PCN indications, catheter size, duration of catheterization, complications, and any procedures performed following a nephrostomy were recorded for each patient. Technical success was determined based on the successful placement of the nephrostomy catheter within the pelvicalyceal system, whereas clinical success was defined as the complete resolution of hydronephrosis and improvement in renal function tests [blood urea nitrogen (BUN) and creatinine levels] during the follow-up. In patients with urinary leakage, clinical success was determined based on the resolution of leakage (successful urinary diversion).

The treatment results were also evaluated by reviewing the hospital records. Serum creatinine levels and the presence of hydronephrosis were routinely evaluated (at 3-month intervals) in all patients after the procedure. Complications were classified as major or minor according to the criteria of the Society of Interventional Radiology.<sup>10</sup>

### Preprocedural evaluation

Indications of PCN were evaluated using ultrasonography in each patient. Hydronephrosis was graded according to the Society for Fetal Urology classification.<sup>11</sup> Informed written consent was obtained from the parents of the patients prior to the procedure. In addition to routine blood biochemistry and hemogram analyses, coagulation parameters were also examined before each procedure. Nine patients (12%) were already using antibiotics because of bacteriuria iden-

tified through urine culture results; all the remaining patients received prophylactic broad-spectrum antibiotics prior to the procedure. All procedures were performed in an interventional radiology unit and were evaluated through ultrasonography before the procedure and at hour 6 after the procedure. The longitudinal length of the kidney and parenchyma thickness were measured and recorded.

### Procedures

The PCN procedure was performed while the patients were in the prone position. Ultrasound guidance was used to puncture the lower or middle calyx. The kidney was punctured with a 19-G, 18-G, and 21-G needle in 19 (38.7%), 37 (49.3%), and 9 (12%) patients, respectively. Two different techniques were used during the procedure:

1. In patients with severe hydronephrosis, following urine sampling through the needle, contrast material was administered to reveal the pelvicalyceal system under fluoroscopy. A stiff guide wire (Amplatz, Super Stiff; Boston Scientific, Marlborough, MA, USA) was then advanced through the renal pelvis and ureter. Consequently, the tract was dilated, and a nephrostomy catheter was placed in the renal pelvis over the guide wire (Figure 1).

2. In patients with urinary leakage or a mild degree of hydronephrosis, a 21-G needle was used to puncture the calyx. After revealing the pelvicalyceal system under fluoroscopy, a 0.018-inch guide wire was initially introduced through the renal pelvis, and then an introducer set (AccuStick, Boston Scientific) was placed. Finally, a 0.035-inch stiff guide wire was used for tract dilatation and catheter placement (Figure 2). These patients were not given diuretics before the procedure.

The procedure was performed with moderate-to-deep sedation without intubation, under local anesthesia, and under general anesthesia in 60 (80%), 8 (10.7%), and 7 (9.3%) patients, respectively. After the procedure, the patients were taken to the observation room and monitored for 6 hours.

According to the guidelines prepared by the Society of Interventional Radiology,<sup>10</sup> complications that require interventional procedures and hospitalization are classified as major, whereas those that do not require any intervention and are resolved during follow-up are considered minor. In light of this information, we classified the complications

#### Main points

- Percutaneous nephrostomy (PCN) is the method of choice for external urinary diversion in patients with urinary obstruction or extravasation.
- Although PCN is routinely performed in adults in multiple centers worldwide, its applicability in infants is limited.
- The main indication of PCN is urinary obstruction, but this procedure also plays a crucial role in patients with urinary leakage.
- Imaging-guided PCN is a feasible and effective procedure with high technical success and low major complication rates, and it is useful in protecting kidney function in infants.

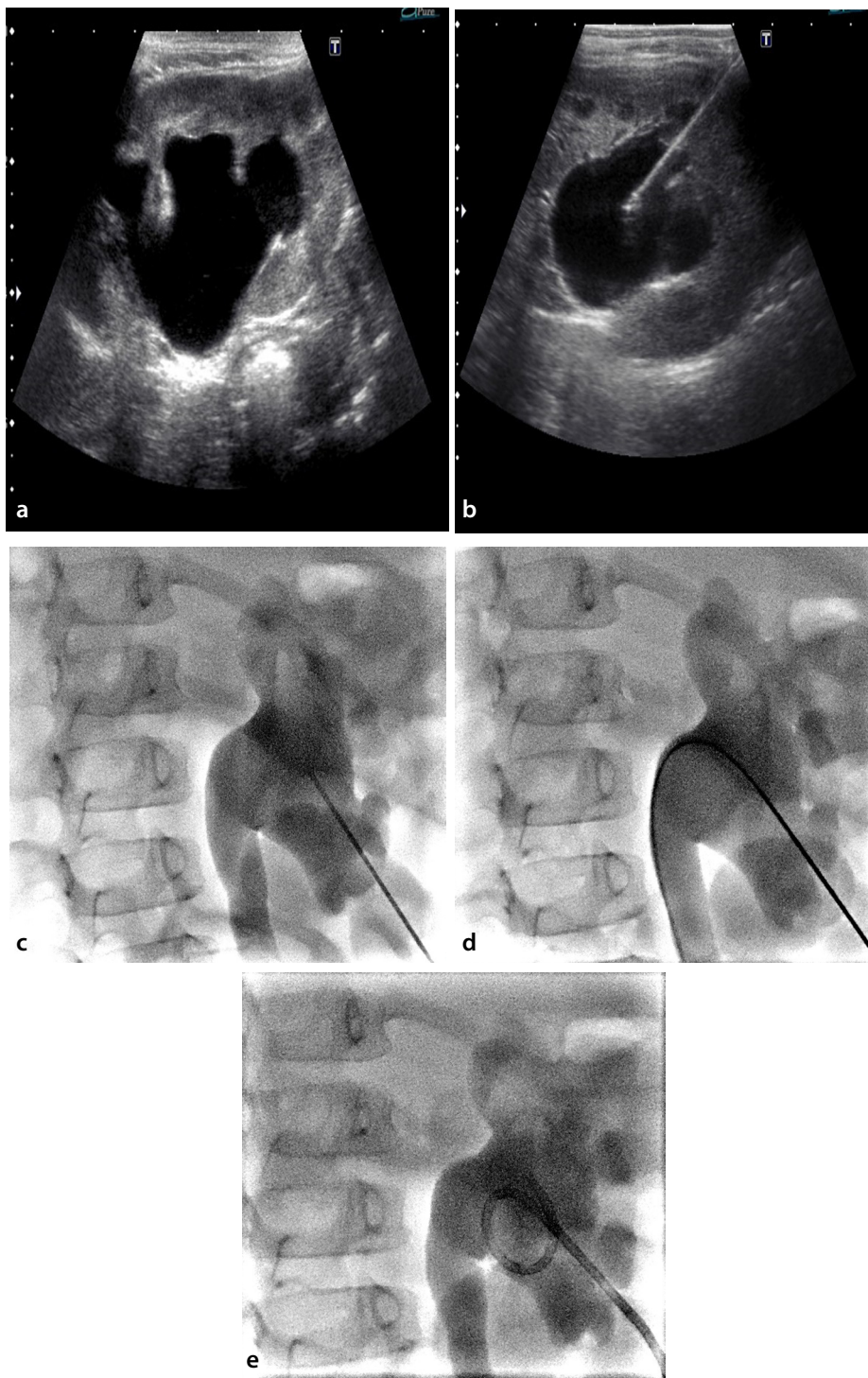


**Figure 1.** Percutaneous nephrostomy procedure in an 8-month-old girl with severe hydronephrosis caused by ureteropelvic junction obstruction. Sagittal (a) and axial (b) grayscale sonograms demonstrate severe hydronephrosis. The collecting system was punctured with an 18-G needle under ultrasonography guidance. (c-e) Contrast material was injected through the needle (c) to reveal the renal collecting system on fluoroscopy. The nephrostomy catheter was then advanced over the guide wire (d).

that developed in our patients after the procedure as major, minor, and catheter related. Catheter-related complications related to mechanical complications associated with the catheter, such as dislocation, obstruction, leakage, and malposition.

#### Statistical analysis

Statistical analysis was performed using the SPSS for Windows software package (v. 20.0; IBM, Chicago, IL, USA). Categorical variables are presented as numbers and percentages, and continuous variables are presented as average  $\pm$  standard deviation and median

(minimum and maximum) values. The Pearson chi-square test was used for the comparison of categorical variables, and continuous variables were compared using a non-parametric (Kruskal–Wallis) or parametric (One-Way analysis of variance) test according to the suitability of the data for normal distribution based on the evaluation undertaken using the Kolmogorov–Smirnov and Shapiro–Wilk tests. The results of the preprocedural and postprocedural renal function tests were compared using the Wilcoxon signed-rank test. Statistical significance was considered when a *P* value was less than 0.05.

## Results

Of the 75 patients enrolled in this study, 50 were male (66.7%) and 25 were female (33.3%), with a mean age of 121 days (range, 1–351 days). Twenty-five (33.3%) of the patients were in the neonatal period. PCN was performed on a total of 86 kidneys, with 11 patients (14.7%) undergoing bilateral nephrostomies. The hydronephrosis grade was 0 in 2 patients, 2 in 15 patients, 3 in 24 patients, and 4 in 34 patients.

Ureteropelvic junction obstruction (UPJO) (54.7%) was the most common indication of PCN, followed by ureterovesical junction obstruction (UVJO) (14.7%), and vesicoureteral reflux (VUR) (10.7%). The remaining indications of PCN are presented in Table 1. The sizes of the inserted catheters ranged from 6 to 8 Fr, with the majority being 6 Fr (77.3%). The median duration of catheterization was 24 days (interquartile range, 10–38; mean, 27.9  $\pm$  45.8; range, 2–345).

There was a significant decrease in serum creatinine and BUN levels following nephrostomy ( $P < 0.001$ ) (Table 2). In the subgroup analysis, renal function recovery was more apparent in patients with UPJO ( $P = 0.001$ ) (Table 3). There was no significant relationship between the BUN and creatinine values and age ( $P = 0.235$  and  $P = 0.345$ , respectively) or the degree of hydronephrosis ( $P = 0.341$  and  $P = 0.557$ , respectively).

Procedure-related major complications were encountered in two patients: methemoglobinemia and respiratory arrest caused by the local anesthetic agent in one patient and the development of urinoma caused by leakage from the puncture site in the other. Percutaneous urinoma drainage was successful in the patient with urinoma. The only minor complication was mild urine leakage in one patient, which was resolved without further intervention.

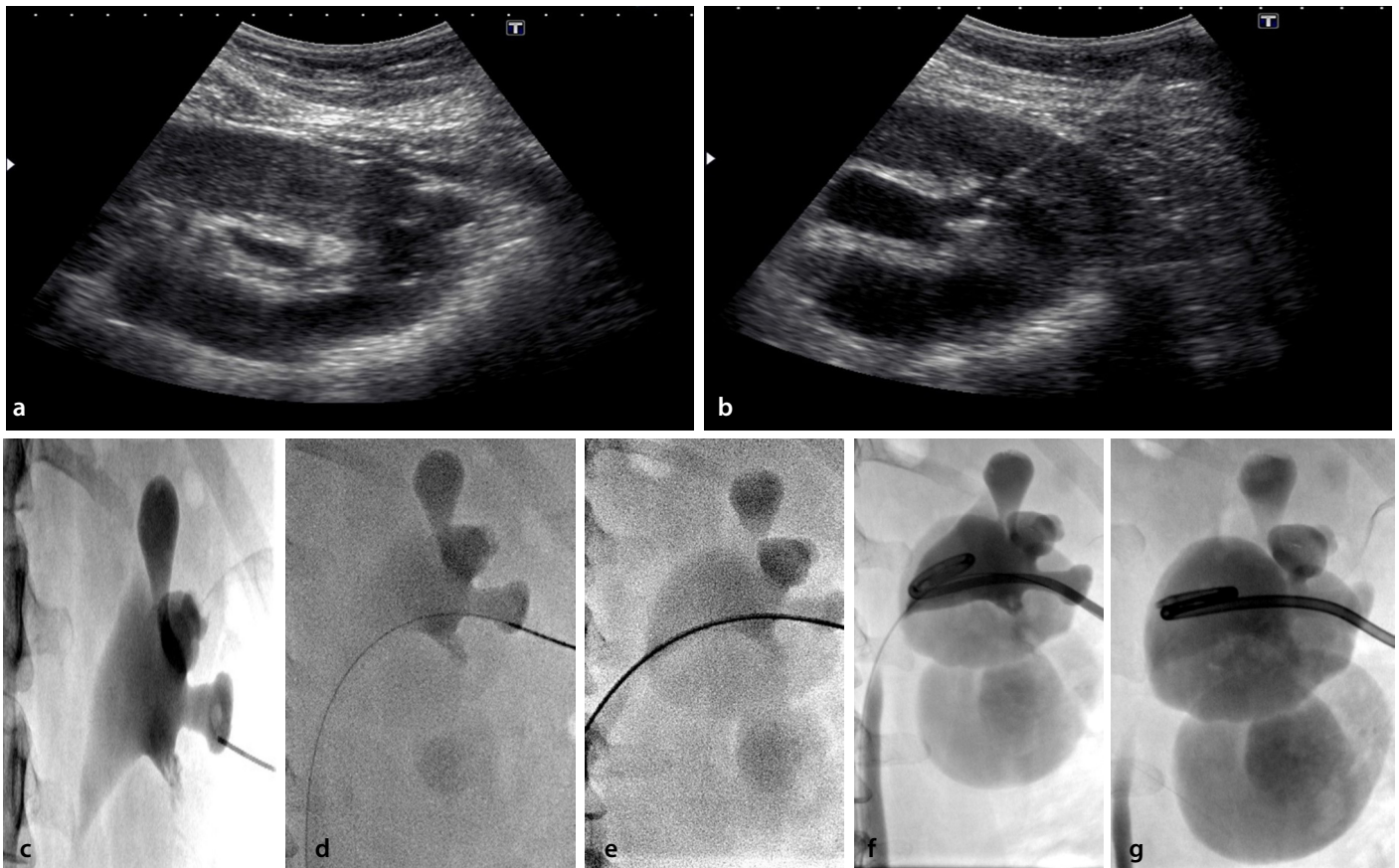


**Figure 2.** Percutaneous nephrostomy procedure in a 6-month-old boy with mild hydronephrosis caused by vesicoureteral reflux. Sagittal (a) and axial (b) grayscale sonograms demonstrate the mildly dilated renal collecting system. The lower pole calyx was punctured with a 21-G needle under ultrasonography guidance. (c-g) Contrast material was injected to reveal the renal collecting system on fluoroscopy (c). A 0.018-inch guide wire (d) was then introduced and exchanged with a 0.035-inch guide wire (e) using an introducer set. The 0.018-inch guide wire was kept in place to not lose the access route (f). The nephrostomy catheter (g) was advanced over the 0.035-inch guide wire. Finally, the 0.018-inch guide wire was removed following the successful insertion of the catheter.

**Table 1.** Distribution of the nephrostomy etiologies of patients

	n	%
Ureteropelvic junction obstruction	41	54.7
Ureterovesical junction obstruction	11	14.7
Vesicoureteral reflux	8	10.6
Congenital anomaly	5	6.7
Posterior urethral valve	3	4
Iatrogenic stenosis	2	2.7
Urinary leakage	2	2.7
Ureteral stone	1	1.3
Kidney stone	1	1.3
Pyonephrosis	1	1.3
Total	75	100

Catheter-related complications were managed through replacement or revision surgery in 16 patients (21.3%) (Table 4). The mean duration of catheterization was significantly longer in patients who experienced catheter-related complications (mean, 20 days) than in those without such complications (mean, 9 days) ( $P = 0.0035$ ).

Following successful urinary diversion, various surgical interventions were performed to eliminate the underlying disease (Table 5). The most common procedure performed following nephrostomy was pyeloplasty (38.7%). In seven of the patients (9.3%), no further surgical intervention was performed following the removal of the nephrostomy catheter. Of these patients, three

(42.9%) had VUR, three (42.9%) had UPJO, and one (14.2%) had multiple congenital anomalies. Only one patient (1.33%), who had undergone bilateral nephrostomy, required hemodialysis, and kidney failure in this patient was caused by multiple systemic anomalies. Nephrectomy was performed in eight patients (10.7%), of whom five had UPJO and the remaining three each had UVJO, VUR, and pyonephrosis.

There was a statistically significant difference between the preprocedural and postprocedural kidney sizes. The mean renal parenchymal thickness (pre-PCN:  $8.1 \pm 2.7$  vs. post-PCN:  $9 \pm 2.6$  mm;  $P = 0.016$ ) and longitudinal kidney diameter had an inverse correlation ( $56.9 \pm 9.8$  vs.  $51.9 \pm 9.4$  mm,  $P = 0.022$ ).

## Discussion

Our results demonstrate that PCN performed on infants has a technical success rate of 100%. No procedure-related mortality was identified in our study. According to the Society of Interventional Radiology Quality Improvement standards, the technical suc-

cess rate should be above 95% in pediatric PCN and is not affected by the patient's age, degree of hydronephrosis, or presence of renal calculi.<sup>12</sup> Similar to our study, the only study in the literature that included only infant patients reported a technical success rate of 100%.<sup>13</sup> In a multicenter study, technical failure was reported at a rate of 1%, and the loss of access was determined as the cause of technical failure.<sup>14</sup> In a recent study including newborn patients, the only technical failure resulted from multiple punctures that caused the rapid decompression of the obstructed pelvocalyceal system.<sup>7</sup>

PCN can be performed using the Seldinger or trocar method.<sup>15</sup> In our study, PCN was performed using the Seldinger technique with an 18–21-G needle in all patients. Koral et al.<sup>4</sup> used a modified trocar technique in addition to the standard Seldinger technique in newborns and infants. In that study, it was argued that the modified technique might be useful, especially for patients with UPJO.<sup>4</sup> Bas et al.<sup>16</sup> reported a technical success rate of 100% using the trocar technique in 6 neonates and 16 infants with urinary obstruction. The procedures were performed without fluoroscopic guidance; however, the size of the nephrostomy catheter used was 4 Fr.<sup>16</sup> In our study, all the procedures were performed under both ultrasound and fluor-

oscopic guidance; the catheter size ranged from 6 to 8 Fr, with the majority being 6 Fr.

The main indication of PCN is urinary obstruction, but this procedure also plays a crucial role in patients with urinary leakage. There is a lack of data in the literature regarding the utility of PCN in infants with urinary extravasation. In our study, two infants underwent PCN as a result of urinary extravasation. Shellikeri et al.<sup>14</sup> also performed PCN on 34 patients with urinary extravasation, with the major and minor complication rates being determined as 0.1% and 4.4%, respectively. We did not observe any procedure-related complications in either of our patients with urinary leakage.

In our study, the most common indication of PCN was UPJO. In the literature, several studies have also reported UPJO as the most common indication of PCN in infants.<sup>4,5,8,17,18</sup> In long-standing UPJO, the kidney can be visualized as a huge cyst; therefore, it may be difficult to differentiate the calyx from the renal pelvis. The kidney may become apparent following the drainage of the pelvocalyceal system.

Prophylactic antibiotic use is generally recommended before the PCN procedure.<sup>2,5,19</sup> However, Gray et al.<sup>20</sup> reported only one case of infection among 46 patients who

had not received prophylactic antibiotics prior to PCN. Cochran et al.<sup>21</sup> suggested that the risk of sepsis could not be eliminated with prophylactic antibiotic use in patients at higher risk of urinary sepsis (e.g., those with struvite stones, a urinary ostomy, and a positive urine culture test), and Millward<sup>22</sup> recommended prophylactic antibiotic use in patients with urinary stones. In our study, all the patients received third-generation cephalosporin prior to the procedure, with nine patients (12%) already using antibiotics because of bacteriuria identified through urine culture results. We did not observe any cases of urinary sepsis or infection following PCN. A recent study by Ključevšek et al.<sup>7</sup> in the newborn patient group reported that infections developed in 16.1% of the patients after PCN. The reason for the different results reported may be related to urosepsis and pyonephrosis constituting the indications of PCN in a high number of patients in the previous study.

According to the Society of Interventional Radiology Quality Improvement Standards for Percutaneous Nephrostomy in the Pediatric Population, the major complication threshold in PCN is 5% for sepsis, 4% for hemorrhage requiring treatment, and 1% for vascular/bowel injury and pleural complications.<sup>12</sup> We did not observe any procedure-related hematomas that required a blood transfusion or an extended hospital stay. The minor complication threshold is 5% for urinary tract infection, 3% for site infection, 3% for site oozing, and 10% for urine leak.<sup>12</sup> In our study, only one patient (1.3%) developed a urinoma that required percutaneous drainage. Although successful catheterization of the pelvocalyceal system was established, it was not possible to prevent urinary leakage in this patient. This may be because of catheter malfunction or dislodgement, primarily related to changes in patient posi-

**Table 2.** Comparison of the blood urea nitrogen and creatinine values of participants before and after nephrostomy

	Mean ± SD	Median	P*
<b>Creatinine</b>			
Before nephrostomy	1.1 ± 1.4	0.5	<0.001
After nephrostomy	0.7 ± 0.8	0.4	
<b>BUN</b>			
Before nephrostomy	22.6 ± 21.5	14	<0.001
After nephrostomy	15.2 ± 12.3	11.1	

\*Wilcoxon signed-rank test; BUN, blood urea nitrogen; SD, standard deviation.

**Table 3.** Subgroup analysis of blood urea nitrogen and creatinine values according to etiology

	Creatinine before PCN	Creatinine after PCN	P	BUN before PCN	BUN after PCN	P
Ureteropelvic junction obstruction	1.3	0.7	0.001	22.9	15.3	0.001
Ureterovesical junction obstruction	1.4	1.2	0.214	25.3	22.4	0.214
Vesicoureteral reflux	1	0.9	0.145	38.2	28.3	0.087
Congenital anomaly	0.9	0.7	0.174	23.4	20.1	0.098
Posterior urethral valve	1	0.8	0.121	27.3	25.4	0.147
Iatrogenic stenosis	1.4	1.2	0.154	30.5	25.4	0.068
Urinary leakage	0.8	0.7	0.584	14.3	13.4	0.471
Ureteral stone	1	0.9	0.662	18.8	17.4	0.547
Kidney stone	0.9	0.8	0.235	15.1	15.2	0.325
Pyonephrosis	1.4	1.3	0.337	22.8	21.2	0.447

BUN, blood urea nitrogen; PCN, percutaneous nephrostomy.

Table 4. Distribution of complications that developed after nephrostomy		
	Prevalence	%
<b>Major complications (n = 75)</b>		
No major complications	73	97.4
Urinoma	1	1.3
Local anesthesia-related methemoglobinemia	1	1.3
<b>Minor complications (n = 75)</b>		
No minor complications	74	98.7
Urinary extravasation not requiring intervention	1	1.3
<b>Catheter-related complications (n = 75)</b>		
None	59	78.7
Catheter dislocation	8	10.7
Catheter obstruction	3	4
Catheter leakage	3	4
Catheter malposition	2	2.6

Table 5. Procedures performed following nephrostomy		
	n	%
Pyeloplasty	29	38.7
Double-J stent placement	12	16
Ureteroneocystostomy	8	10.7
Nephrectomy	8	10.7
Medical treatment	7	9.3
Posterior urethral valve resection	3	4
Ureterocele excision	2	2.7
Subureteric teflon injection	2	2.7
Percutaneous nephrolithotomy	1	1.3
Pyelolithotomy	1	1.3
Cystostomy	1	1.3
Dialysis	1	1.3
<b>Total</b>	<b>75</b>	<b>100</b>

tion. We observed a significant improvement in serum creatinine and BUN levels following PCN; however, renal function recovery was most significant in patients with UPJO.

We observed methemoglobinemia and respiratory arrest associated with the local anesthetic agent in a 10-day-old newborn. Methemoglobinemia following the administration of local anesthetics is a serious complication for which care should be taken, particularly in neonates and low-weight infants. The use of prilocaine is not recommended in children younger than 6 months (except for transcutaneous administration), pregnant women, patients taking other oxidizing drugs, or those with glucose-6-phosphate dehydrogenase deficiency.<sup>23</sup> The maximum recommended doses of prilocaine are 2.5, 5.0, 3.2, and 1.3 mg/kg for patients older than 6 months, adults, patients with renal insufficiency, and those using other oxidizing drugs, respectively.<sup>23</sup> Methemoglobinemia is

a hemoglobinopathy caused by high methemoglobin levels resulting from the oxidation of iron to the ferric state in hemoglobin, leading to tissue hypoxia. In addition to tissue hypoxia, it may also cause respiratory depression, especially in infants and newborns<sup>24</sup> as in our patient.

Catheter-related complications are not defined clearly enough in the literature and are generally discussed as mechanical complications<sup>14</sup> or minor complications, as in the Society of Interventional Radiology Quality Improvement Standards for Percutaneous Nephrostomy in the Pediatric Population.<sup>12</sup> However, since catheter-related complications are especially common in the infant age group, we examined them in a separate category in our study. These complications are frequently encountered during the follow-up period of patients in the form of catheter occlusion, migration, or dislocation. In the first hours of catheter dislocation, access

to the pelvicalyceal system may remain patent; therefore, the nephrostomy catheter can be placed using the guide wire under fluoroscopy guidance (without a needle).<sup>25</sup> Catheter displacement or dislodgement is more frequently encountered in younger children and infants,<sup>26</sup> and in a recent study, the catheter-related complication rate was reported to be 18.6% in neonates.<sup>7</sup> Shellikeri et al.<sup>14</sup> detected catheter-related mechanical complications in 54 out of 675 patients (8%) and noted that the rate of catheter displacement/dislodgement was higher in infants (10%) than in the non-infant population (6%). In our study, we observed catheter displacement/dislodgement in 25 patients; however, 13 of these patients were under 1 year, and five were neonates. Our results are therefore consistent with those of Shellikeri et al.<sup>14</sup> We observed catheter-related mechanical complications more frequently in neonates (32%) than in the remainder of the patient population (21.3%). Therefore, we suggest that the fixation of the catheter to the skin should be carefully undertaken in neonates.

Results reported in studies conducted in the adult patient group and those reported for the pediatric patient group also reveal some differences. The most common indication of PCN in the adult age group is urinary stone disease, not UPJO.<sup>19</sup> Although a comprehensive study<sup>27</sup> determined the major complication rate as 9.6% and the minor complication rate as 9.9%, these rates vary depending on the location of the urinary obstruction,<sup>28</sup> dilatation status of the collecting system,<sup>29</sup> and the operator performing the procedure.<sup>30</sup> In this context, further studies are required to evaluate these parameters in the pediatric patient group. In studies conducted in the adult patient group, the rate of catheter-related problems varies between 2% and 38%, but it is generally around 7%.<sup>25,31,32</sup> As demonstrated in a recent study by Shah et al.<sup>33</sup>, this may be because the catheters used are designed specifically for adults.

The most important feature that makes our study unique is that it extensively discusses the 20 years of experience of a single center together with clinical and laboratory findings; however, our study also has some limitations. The first concerns the small number of patients and the single-center design, although the results obtained can still serve as a guide for further comprehensive studies. Second, the radiation dose information could not be recorded for all patients for technical reasons. Because of the importance of radiation exposure in this age group, future stud-

ies should evaluate radiation doses in these patients. Finally, because of the retrospective nature of the study, the indications of PCN were heterogeneously distributed, and there were very few patients in some subgroups. To address this, prospective studies should be undertaken.

In conclusion, imaging-guided PCN is a feasible and effective procedure with high technical success and low major complication rates, and it is useful in protecting kidney function in infants.

### Conflict of interest disclosure

The authors declared no conflicts of interest.

### References

- Dagli M, Ramchandani P. Percutaneous nephrostomy: technical aspects and indications. *Semin Intervent Radiol*. 2011;28(4):424-437. [\[CrossRef\]](#)
- Farrell TA, Hicks ME. A review of radiologically guided percutaneous nephrostomies in 303 patients. *J Vasc Interv Radiol*. 1997;8(5):769-774. [\[CrossRef\]](#)
- Trambert JJ. Percutaneous nephrostomy placement in neonates: not simply "miniature adults". *Cardiovasc Intervent Radiol*. 2020;43(9):1329-1330. [\[CrossRef\]](#)
- Koral K, Saker MC, Morello FP, Rigsby CK, Donaldson JS. Conventional versus modified technique for percutaneous nephrostomy in newborns and young infants. *J Vasc Interv Radiol*. 2003;14(1):113-116. [\[CrossRef\]](#)
- Hogan MJ, Coley BD, Jayanthi VR, Shiels WE, Koff SA. Percutaneous nephrostomy in children and adolescents: outpatient management. *Radiology*. 2001;218(1):207-210. [\[CrossRef\]](#)
- Laurin S, Sandström S, Ivarsson H. Percutaneous nephrostomy in infants and children. *Acad Radiol*. 2000;7(7):526-529. [\[CrossRef\]](#)
- Ključevšek T, Pirnovar V, Ključevšek D. Percutaneous nephrostomy in the neonatal period: indications, complications, and outcome—a single centre experience. *Cardiovasc Intervent Radiol*. 2020;43(9):1323-1328. [\[CrossRef\]](#)
- Hwang JY, Shin JH, Lee YJ, Yoon HM, Cho YA, Kim KS. Percutaneous nephrostomy placement in infants and young children. *Diagn Interv Imaging*. 2018;99(3):157-162. [\[CrossRef\]](#)
- Quigley R. Developmental changes in renal function. *Curr Opin Pediatr*. 2012;24(2):184-190. [\[CrossRef\]](#)
- Sacks D, McClenny TE, Cardella JF, Lewis CA. Society of Interventional Radiology clinical practice guidelines. *J Vasc Interv Radiol*. 2003;14(9 Pt 2):199-202. [\[CrossRef\]](#)
- Fernbach SK, Maizels M, Conway JJ. Ultrasound grading of hydronephrosis: introduction to the system used by the Society for Fetal Urology. *Pediatr Radiol*. 1993;23(6):478-480. [\[CrossRef\]](#)
- Cahill AM, Annam A, Baskin KM, et al. Society of Interventional Radiology Quality Improvement Standards for Percutaneous Nephrostomy in the Pediatric Population. *J Vasc Interv Radiol*. 2021;32(1):146-149. [\[CrossRef\]](#)
- O'Brien WM, Matsumoto AH, Grant EG, Gibbons MD. Percutaneous nephrostomy in infants. *Urology*. 1990;36(3):269-272. [\[CrossRef\]](#)
- Shellikeri S, Daulton R, Sertic M, et al. Pediatric percutaneous nephrostomy: a multicenter experience. *J Vasc Interv Radiol*. 2018;29(3):328-334. [\[CrossRef\]](#)
- Hsu L, Li H, Pucheril D, et al. Use of percutaneous nephrostomy and ureteral stenting in management of ureteral obstruction. *World J Nephrol*. 2016;5(2):172-181. [\[CrossRef\]](#)
- Bas A, Gülşen F, Emre S, et al. Ultrasound-guided percutaneous nephrostomy performed on neonates and infants using a "14-4" (trocar and cannula) technique. *Cardiovasc Intervent Radiol*. 2015;38(6):1617-1620. [\[CrossRef\]](#)
- Yavascan O, Aksu N, Erdogan H, et al. Percutaneous nephrostomy in children: diagnostic and therapeutic importance. *Pediatr Nephrol*. 2005;20(6):768-772. [\[CrossRef\]](#)
- Stanley P, Bear JW, Reid BS. Percutaneous nephrostomy in infants and children. *AJR Am J Roentgenol*. 1983;141(3):473-477. [\[CrossRef\]](#)
- Hausegger KA, Portugaller HR. Percutaneous nephrostomy and antegrade ureteral stenting: technique-indications-complications. *Eur Radiol*. 2006;16(9):2016-2030. [\[CrossRef\]](#)
- Gray RR, So CB, McLoughlin RF, Pugash RA, Saliken JC, Macklin NI. Outpatient percutaneous nephrostomy. *Radiology*. 1996;198(1):85-88. [\[CrossRef\]](#)
- Cochran ST, Barbaric ZL, Lee JJ, Kashfian P. Percutaneous nephrostomy tube placement: an outpatient procedure? *Radiology*. 1991;179(3):843-847. [\[CrossRef\]](#)
- Millward SF. Percutaneous nephrostomy: a practical approach. *J Vasc Interv Radiol*. 2000;11(8):955-964. [\[CrossRef\]](#)
- Guay J. Methemoglobinemia related to local anesthetics: a summary of 242 episodes. *Anesth Analg*. 2009;108(3):837-845. [\[CrossRef\]](#)
- Iolascon A, Bianchi P, Andolfo I, et al. Recommendations for diagnosis and treatment of methemoglobinemia. *Am J Hematol*. 2021;96(12):1666-1678. [\[CrossRef\]](#)
- Wah TM, Weston MJ, Irving HC. Percutaneous nephrostomy insertion: outcome data from a prospective multi-operator study at a UK training centre. *Clin Radiol*. 2004;59(3):255-261. [\[CrossRef\]](#)
- Riedy MJ, Lebowitz RL. Percutaneous studies of the upper urinary tract in children, with special emphasis on infants. *Radiology*. 1986;160(1):231-235. [\[CrossRef\]](#)
- Degirmenci T, Gunlusoy B, Kozacioglu Z, et al. Utilization of a modified Clavien Classification System in reporting complications after ultrasound-guided percutaneous nephrostomy tube placement: comparison to standard Society of Interventional Radiology practice guidelines. *Urology*. 2013;81(6):1161-1167. [\[CrossRef\]](#)
- Kumar S, Dutt UK, Singh S, et al. Prospective audit of complications after ultrasonography-guided percutaneous nephrostomy for upper urinary tract obstruction using modified Clavien classification system. *Urol Ann*. 2020;12(1):31-36. [\[CrossRef\]](#)
- Ho Won J, Jin Yang W, Hoon Shin J, et al. Percutaneous nephrostomy for nondilated renal collecting system with ultrasound and fluoroscopic guidance: the results of a 10-year experience. *Diagn Interv Radiol*. 2022;28(3):244-248. [\[CrossRef\]](#)
- Yonguc T, Bozkurt İH, Değirmenci T, et al. Urologist directed percutaneous nephrostomy tube placement: 6 years experience. *J Clin Anal Med*. 2015;5(1):213-218. [\[CrossRef\]](#)
- Kaskarelis IS, Papadaki MG, Malliaraki NE, Robotis ED, Malagari KS, Piperopoulos PN. Complications of percutaneous nephrostomy, percutaneous insertion of ureteral endoprosthesis, and replacement procedures. *Cardiovasc Intervent Radiol*. 2001;24(4):224-228. [\[CrossRef\]](#)
- Montvilas P, Solvig J, Johansen TE. Single-centre review of radiologically guided percutaneous nephrostomy using "mixed" technique: success and complication rates. *Eur J Radiol*. 2011;80(2):553-558. [\[CrossRef\]](#)
- Shah R, Minhas K, Patel PA. Is There really no kit for kids? Quantification of manufacturer recommendations regarding paediatric use for high-volume IR devices. *Cardiovasc Intervent Radiol*. 2023;46:1046-1052. [\[CrossRef\]](#)



# Use of gelatin sponge to seal the biliary tract after percutaneous transhepatic biliary drainage in patients with liver transplants

Ali Özgen

Bahçeşehir University Faculty of Medicine, İstanbul,  
Türkiye

## ABSTRACT

Percutaneous transhepatic biliary drainage (PTBD) is commonly used in the treatment of malign and benign biliary pathologies. Certain complications after PTBD may occur, such as biliary fistula, biliary leakage, bilioma, and hematoma. The purpose of this study was to evaluate the safety and effectiveness of using a sterile gelatin sponge to seal the biliary tract after PTBD in patients with liver transplants to prevent complications. A total of 131 biliary drainages were introduced in 97 patients, and a sterile gelatin sponge was used to seal the biliary tract after removal of the biliary drainage catheter. The patients were immediately examined for complications using ultrasound and then followed up clinically unless imaging was required. Five fluid collections within the liver with a diameter <2 cm, consistent with hematoma or bilioma, were resolved spontaneously. No hematoma or bilioma required treatment, and no biliary leakage or fistula was detected. No complications related to the use of the sponge were observed. The use of a sterile gelatin sponge is a safe and effective method for sealing the biliary tract to prevent complications after PTBD in patients with liver transplants.

## KEYWORDS

Biliary tract, catheter, fistula, liver, transplantation

Percutaneous transhepatic biliary drainage (PTBD) is commonly used in the treatment of malign and benign biliary pathologies. Although considered rare and with an unknown probability, complications after PTBD may occur in daily practice, such as biliary fistula, biliary leakage, bilioma, and hematoma. Many interventional and surgical treatment approaches can be used when such complications are observed.<sup>1-8</sup> In daily practice, materials such as coils, liquid embolics, and vascular plugs may be used to close the biliary tract. One study demonstrated the efficacy of using a gelatin sponge to close the tract in patients with biliary drainage caused by benign or malignant diseases using a slightly different technique.<sup>9</sup> The aim of the present study was to evaluate the safety and effectiveness of using sterile gelatin sponge to seal the biliary tract after PTBD in patients with liver transplants to prevent possible complications.

## Technique

Institutional review board approval was obtained for this retrospective study, and the requirement to obtain written informed consent was waived. We included adult patients with living-donor liver transplants with long-term internal PTBD performed in two liver transplant centers. The indication for biliary drainage was anastomotic and/or non-anastomotic biliary strictures unresponsive to or not suitable for endoscopic interventions. The study involved 97 adult patients, 61 male and 36 female, requiring a total of 131 biliary drainages (30 patients with two and two patients with three biliary drainages). The catheterization time was between two and 19 weeks, with a mean of 13 weeks.

All patients were heavily sedated or placed under general anesthesia. Proper antibiotic prophylaxis was administered to all patients. All PTBDs were performed by the same interven-

Corresponding author: Ali Özgen

E-mail: draliozgen@hotmail.com

Received 03 June 2023; revision requested 28 June 2023;  
accepted 26 July 2023.



Epub: 31.08.2023

Publication date: 09.09.2024

DOI: 10.4274/dir.2023.232344

You may cite this article as: Özgen A. Use of gelatin sponge to seal the biliary tract after percutaneous transhepatic biliary drainage in patients with liver transplants. *Diagn Interv Radiol.* 2024;30(5):325-327.

tional radiologist, with more than 15 years' experience in hepatobiliary procedures. A 14F multipurpose drainage catheter (Cook Medical, Bloomington, IN, USA) was used in four patients with a single drainage catheter, and a 12F SKATER catheter (Argon Medical Devices, Dallas, TX, USA) was used for the rest of the patients with single drainage catheters. A 10F SKATER catheter was used for the patients who required two or three drainage catheters. This procedure was not performed in patients with skin infections near the catheter insertion site.

The catheters were flushed with saline, and a contrast medium was injected into the catheter to examine the biliary system. Amplatz stiff guidewire (Boston Scientific, Marlborough, MA, USA) was introduced into the biliary drainage catheter, and then the catheter was removed over the wire. An 11F Radifocus Introducer II sheath (Terumo Corporation, Shibuya-ku, Tokyo, Japan) for 12F and 14F catheters and 10F sheath for 10F catheters were immediately placed over the wire. Cholangiography was then performed through the sheath to fully evaluate the biliary system (Figure 1a). If and when biliary drainage was considered successful, a commercially available sterile gelatin sponge was used to seal the biliary tract.

A piece of sponge (7 x 1 x 1 cm) was cut. It was then squeezed by hand and formed into a 7-cm-long cylinder with a diameter of approximately 3 mm, similar to that described in a previous study.<sup>9</sup> The tip of the sheath was pulled back into the liver parenchyma under fluoroscopic guidance. The length of the sponge was adjusted to approximately equal the distance between the tip of the sheath and the liver capsule. The tip of the dilator was cut so that the sponge could be pushed without being punctured, and the head of the sheath was then cut-off and the sponge placed inside the sheath. Under fluoroscopic guidance and using the dilator, the sponge was pushed until it reached the tip of the

sheath (Figure 1b). If the sponge softened following long contact with bile, the procedure was repeated using a new sponge. The sheath was removed while the sponge was placed using the dilator (Figure 1c). If the patient had more than one catheter, the procedure was repeated for each catheter. The skin was cleansed and then covered using a sterile pad. Routine ultrasound examination was performed before the patient left (Figure 1d). The patients were then followed up clinically, and imaging was performed only if indicated for any other reason (Figure 2).

## Results

All the biliary tracts were sealed successfully using this technique. There were five local fluid collections with a diameter <2 cm near the tract in the liver consistent with bilioma or hematoma, discovered using the first ultrasound; however, no treatment was indicated. They were followed up using ultrasound and were all resolved spontaneously. No other complications, such as biliary fistula, bile leakage, or hematoma, were ob-

served. No complications related to the use of the sponge were observed.

## Discussion

This study demonstrates that using a sterile gelatin sponge after PTBD may be a safe and effective method for preventing possible complications. Using sterile gelatin sponges is also cost-effective because they are relatively cheap and widely available. The implementation of this technique is also simple and takes only a couple of minutes. To our knowledge, this is the first study to present a specific technique to prevent complications after PTBD.

Spongostan is a sterile water-insoluble, absorbable, porcine gelatin used to maintain local hemostasis. These gelatin sponges have been used in surgical operations for decades. They have also been successfully used to close biliary tracts in patients with various benign and malignant disorders that require biliary drainage<sup>9</sup> and to occlude vessels and seal tracts in various situations. We also successfully occluded a biliary cutaneous fistula

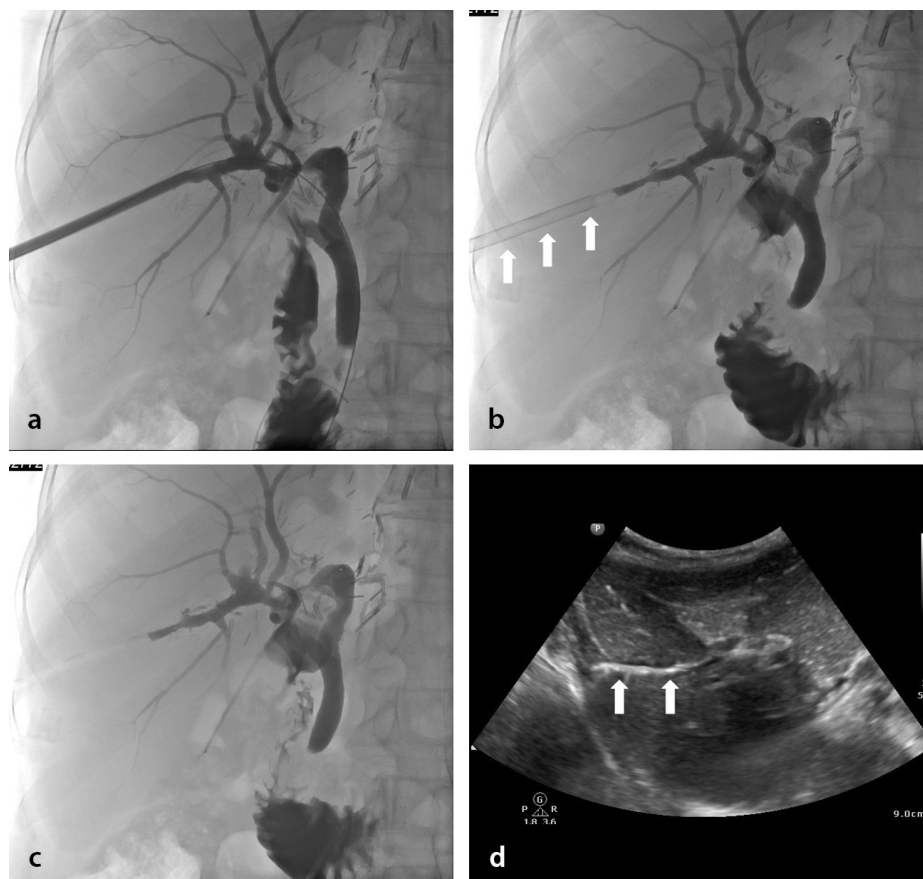


**Figure 1.** (a-d) Fifty seven-year-old patient with a liver transplant and long-term PTBD. (a) Cholangiography through the sheath after removal of the catheter revealing filling of the intrahepatic biliary tree and passage of contrast medium through the duodenum. (b) The sheath was pulled into the liver parenchyma and the sponge inserted (arrows). (c) The sheath was removed while the sponge was placed. (d) Ultrasound showing the sponge within the liver parenchyma (arrows). PTBD, percutaneous transhepatic biliary drainage.

### Main points

- Complications after percutaneous transhepatic biliary drainage (PTBD) procedures may occur.
- Many interventional and surgical treatment approaches may be used when such complications are observed.
- Using a gelatin sponge to seal the biliary tract after removal of the PTBD catheter may help prevent some of these possible complications.



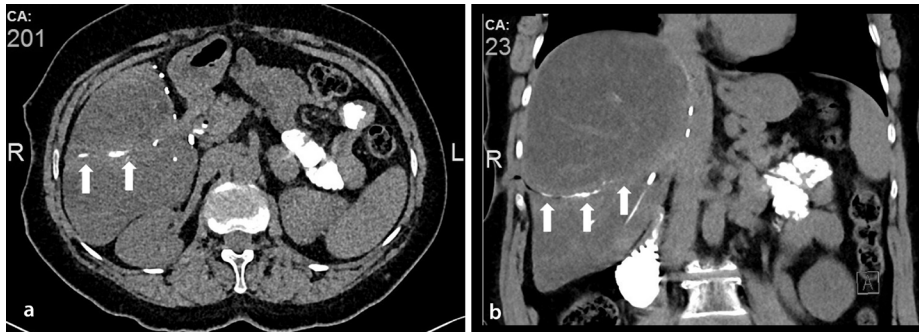


**Figure 2.** (a, b) Forty-eight-year-old patient with a liver transplant after the removal of a long-term PTBD catheter. Non-enhanced computed tomography immediately after removal of the catheter: (a) axial and (b) coronal reformatted images showing a gelatin sponge with contrast medium within the biliary tract (arrows). PTBD, percutaneous transhepatic biliary drainage.

that developed after prolonged biliary drainage in two patients using this material. In fact, we developed the concept of routinely closing the biliary tract after successfully occluding the tract of a patient with a biliary cutaneous fistula following the failure of glue and coil closure attempts at another center. The rationale behind sealing the tract with an absorbable sponge is to give the liver time to expand and then fill the tract naturally.

This study has some limitations. First, this was a retrospective study with no control group. Second, given the rarity of such complications, the number of patients was relatively limited. Third, although post-procedure imaging follow-up is not included in our routine practice, we did not perform any specific imaging follow-up other than ultrasound after the use of this material.

In conclusion, use of a sterile gelatin sponge to seal the biliary tract after PTBD may be a safe and effective method for preventing possible complications in patients

with liver transplants. This technique might also potentially be used for other patients with PTBD. Further comparative studies with a larger number of patients are necessary to confirm our findings.

#### Conflict of interest disclosure

The author declared no conflicts of interest.

#### References

1. Giurazza F, Ierardi A, Spinazzola A, et al. Percutaneous embolization of biliary leaks: initial experience with extravascular application of a PTFE-covered microplug. *Cardiovasc Intervent Radiol.* 2023;46(3):400-405. [\[Crossref\]](#)
2. Ierardi AM, Fontana F, Mangini M et al. Use of amplatzer vascular plug to treat a biliary cutaneous fistula. *Korean J Radiol.* 2013;14(5):801-804. [\[Crossref\]](#)
3. Al-Qahtani HH. Biliopleural fistula with cholethorax. A rare complication of

percutaneous transhepatic biliary drainage. *Saudi Med J.* 2011;32(11):1189-1192.

[\[Crossref\]](#)

4. Çakır MS, Guzelbey T, Kinacı E, Sevinc MM, Kilickesmez O. Delayed bilhemia complicating percutaneous transhepatic biliary drainage: successful treatment with primary coil embolization. *Radiol Case Rep.* 2018;14(2):269-272. [\[Crossref\]](#)
5. Eicher CA, Adelson AB, Himmelberg JA, Chintalapudi U. Laser ablation of a biliary duct for treatment of a persistent biliary-cutaneous fistula. *J Vasc Interv Radiol.* 2008;19(2):294-297. [\[Crossref\]](#)
6. Yu EYY, Yang FS, Chiu YJ, Tsai FJ, Lu CC, Yang JS. Late onset of biliopleural fistula following percutaneous transhepatic biliary drainage: a case report. *Biomedicine (Taipei).* 2018;8(1):6. [\[Crossref\]](#)
7. Li H, Ge N, He C, et al. Portal vein embolization in the treatment of portal vein bleeding after percutaneous transhepatic biliary drainage: a case report and literature review. *J Interv Med.* 2022;16(4):217-220. [\[Crossref\]](#)
8. Chanyaputhipong J, Lo RHG, Tan BS, Chow PKH. Portobiliary fistula: successful transcatheter treatment with embolisation coils. *Singapore Med J.* 2014;55(3):34-36. [\[Crossref\]](#)
9. Augustin AM, Cao V, Fluck F, Kunz J, Bley T, Kickuth T. Percutaneous transhepatic biliary tract embolization using gelatin sponge. *Acta Radiol.* 2019;60(10):1194-1199. [\[Crossref\]](#)



# Cortical and subcortical structural changes in pediatric patients with infratentorial tumors

Barış Genç<sup>1</sup>  
 Kerim Aslan<sup>1</sup>  
 Derya Bako<sup>1</sup>  
 Semra Delibalta<sup>2</sup>  
 Meltem Necibe Ceyhan Bilgici<sup>1</sup>

<sup>1</sup>Ondokuz Mayıs University Faculty of Medicine,  
Department of Neuroradiology, Samsun, Türkiye

<sup>2</sup>Acıbadem University, Atakent Hospital, Clinic of  
Radiology, Istanbul, Türkiye

## PURPOSE

This study aimed to detect supratentorial cortical and subcortical morphological changes in pediatric patients with infratentorial tumors.

## METHODS

The study included 24 patients aged 4–18 years who were diagnosed with primary infratentorial tumors and 41 age- and gender-matched healthy controls. Synthetic magnetization-prepared rapid gradient echo images of brain magnetic resonance imaging were generated using deep learning algorithms applied to T2-axial images. The cortical thickness, surface area, volume, and local gyrification index (LGI), as well as subcortical gray matter volumes, were automatically calculated. Surface-based morphometry parameters for the patient and control groups were compared using the general linear model, and volumes between subcortical structures were compared using the t-test and Mann–Whitney U test.

## RESULTS

In the patient group, cortical thinning was observed in the left supramarginal, and cortical thickening was observed in the left caudal middle frontal (CMF), left fusiform, left lateral orbitofrontal, left lingual gyrus, right CMF, right posterior cingulate, and right superior frontal ( $P < 0.050$ ). The patient group showed a volume reduction in the pars triangularis, paracentral, precentral, and supramarginal gyri of the left hemisphere ( $P < 0.05$ ). A decreased surface area was observed in the bilateral superior frontal and cingulate gyri ( $P < 0.05$ ). The patient group exhibited a decreased LGI in the right precentral and superior temporal gyri, left supramarginal, and posterior cingulate gyri and showed an increased volume in the bilateral caudate nucleus and hippocampus, while a volume reduction was observed in the bilateral putamen, pallidum, and amygdala ( $P < 0.05$ ). The ventricular volume and tumor volume showed a positive correlation with the cortical thickness in the bilateral CMF while demonstrating a negative correlation with areas exhibiting a decreased LGI ( $P < 0.05$ ).

## CONCLUSION

Posterior fossa tumors lead to widespread morphological changes in cortical structures, with the most prominent pattern being hypoglyria.

## CLINICAL SIGNIFICANCE

This study illuminates the neurological impacts of infratentorial tumors in children, providing a foundation for future therapeutic strategies aimed at mitigating these adverse cortical and subcortical changes and improving patient outcomes.

## KEYWORDS

Medulloblastoma, neoplasms, brain, primary, hippocampus, amygdala

Corresponding author: Barış Genç

E-mail: barisgenc12@gmail.com

Received 09 January 2024; revision requested 06  
February 2024; last revision received 15 April 2024;  
accepted 15 May 2024.



Epub: 03.06.2024

Publication date: 09.09.2024

DOI: 10.4274/dir.2024.242652

Central nervous system neoplasms are the most common solid tumors in children. With advancing therapies, the 10-year survival rate in these patients is approximately 70%. Posterior fossa tumors are more frequently observed in childhood, and the most common pediatric posterior fossa tumors are medulloblastomas and astrocytomas.<sup>1</sup> Although

You may cite this article as: Genç B, Aslan K, Bako D, Delibalta S, Ceyhan Bilgici MN. Cortical and subcortical structural changes in pediatric patients with infratentorial tumors. *Diagn Interv Radiol.* 2024;30(5):328-334.

astrocytomas can achieve a cure with total resection, medulloblastomas require chemotherapy and radiotherapy treatments after resection.<sup>2</sup>

Neuroplasticity is the brain's ability to change functionally, connectively, or structurally in physiological or pathological conditions. Recent advancements in neuroimaging have demonstrated that the brain can reorganize itself after pathologies, such as traumatic brain injury, stroke, and tumors, particularly in adults.<sup>3</sup> Children are more successful than adults in learning complex skills, such as learning a new language or playing a new instrument.<sup>4,5</sup> Children with unilateral left-brain damage at an early age can develop normal language skills, while lesions of similar location and extent in the adult brain cause more aphasia.<sup>6</sup>

Recent studies have been conducted on changes occurring in the contralateral hemisphere secondary to supratentorial gliomas in adults, but these studies are generally voxel-based morphometry (VBM) studies investigating changes in gray matter volume.<sup>7</sup> Surface-based morphometry (SBM) provides parameters such as cortical thickness, sulcal folding, and surface area that cannot be obtained with VBM. Furthermore, SBM is more successful than VBM at the intersections of gray and white matter.<sup>8</sup> In their SBM study, Zhang et al.<sup>9</sup> detected widespread changes in the contralateral hemisphere in adult patients with frontal low-grade glioma (LGG) for the first time using virtual brain grafting, and these changes were not detected in a VBM study conducted in a similar group.<sup>7</sup>

The posterior fossa contains the cerebellum and the brainstem. The dentate nucleus in the cerebellum is highly advanced in monkeys and humans, with dentothalamic and thalamocortical pathways projecting to the prefrontal cortex.<sup>10,11</sup> Recent studies show that the cerebellum is no longer merely an organ associated with balance but actively

participates in cognitive events, speech, and complex motor functions.<sup>10</sup> Cerebellar cognitive affective syndrome is a condition of cognitive decline in patients with cerebellar lesions, and its physiopathology is not fully understood.<sup>12</sup> A VBM study conducted on children who were cured after a posterior fossa tumor detected reduced gray matter volume in the entorhinal cortex, thalamus, hypothalamus, corpus callosum, and cuneus.<sup>13</sup> However, this could be due to the disease itself or secondary to chemoradiotherapy.<sup>14</sup>

There are no studies investigating cortical and subcortical changes at the time of diagnosis in children with posterior fossa tumors. There are several reasons for this. First, although they are the most common solid tumors in childhood, they are relatively rare.<sup>1</sup> Myelination is rapid in the first 2 years of life, and medulloblastomas peak at the age of 3 years.<sup>15</sup> Surface construction algorithms, such as Freesurfer, require good image contrast and can be applied to anatomically normal or near-normal brains without significant morphological abnormalities. In the presence of an intracranial tumor, Freesurfer has a failure rate of up to 30% in cortical reconstruction.<sup>16</sup> Therefore, it has prevented the detection of cortical and subcortical changes in pediatric tumors. Although virtual brain grafting studies have made this possible, they require neuroanatomical experience and time.<sup>17</sup> Recently, however, software developed using deep learning has made surface reconstruction possible in tumoral diseases by producing synthetic

magnetization-prepared rapid gradient echo (MP-RAGE) images.<sup>18</sup>

Our aim in this study is to investigate supratentorial cortical and subcortical morphological changes in pediatric posterior fossa tumors.

## Methods

This study was designed retrospectively. Ondokuz Mayıs University Clinical Research and Ethics Committee (decision no: 2023/300, date: 10.10.2023) approval has been obtained. All participants were fully informed and gave their written informed consent prior to each examination. Guidelines from Strengthening the Reporting of Observational Studies in Epidemiology were carefully followed.<sup>19</sup>

### Participants

Patients aged <18 years who underwent brain magnetic resonance imaging (MRI) due to intracranial tumor in the unit between 2015 and 2023 were retrospectively screened. Among these patients, those with a posterior fossa tumor who did not receive any treatment (chemoradiotherapy, surgery, steroids) before the MRI and who were diagnosed pathologically after the MRI were included in the study. Children aged <4 years were excluded from the study due to insufficient myelination. Children who did not have any chronic diseases, who presented with non-specific symptoms, whose brain MRI did not reveal any pathology, and who were age- and gender-matched formed the control group (Figure 1).

### Main points

- Pediatric posterior fossa tumors cause widespread hypogyrification and reductions in surface and volume, while also leading to an increase in cortical thickness.
- Pediatric posterior fossa tumors lead to an increase in volume in the hippocampus and caudate nucleus, while also causing an increase in the volume of the putamen, pallidum, and amygdala.
- Cortical and subcortical morphological changes have shown a correlation with ventricular volume and tumor volume.

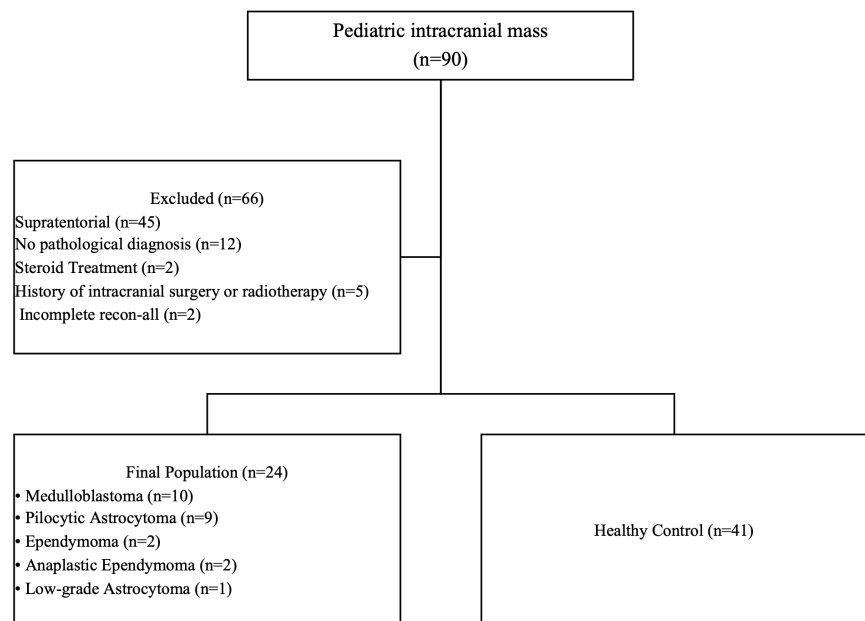


Figure 1. Flowchart of study.

## Magnetic resonance imaging acquisition

MRI was performed on the patient and control groups with one of two devices with a magnetic field strength of 1.5 Tesla (Philips, Achieva, Best, the Netherlands) or 3 Tesla (Philips, Ingenia, Best, the Netherlands).

The MRI protocol for patients who had a 3 Tesla scan was as follows: T2W-axial turbo spin-echo sequence [repetition time (TR)/echo time (TE), 3,000/80 ms; section thickness, 5 mm; matrix, 261 × 384; number of excitations (NEX), 3], 3D fluid attenuation inversion recovery (FLAIR) coronal (TR/TE/TI, 4,800/381/1,650 ms; section thickness, 3 mm; NEX, 2). For patients who had a 1.5 Tesla scan, the protocol was as follows: T2W-axial turbo spin-echo sequence (TR/TE, 8,078/100 ms; section thickness, 4 mm; matrix, 242 × 250; NEX, 4), T2-FLAIR coronal (TR/TE/TI, 7,000/140/2,800 ms; section thickness, 4 mm; NEX, 2).

## Magnetic resonance imaging processing

Due to the different devices and a heterogeneous data set, SynthSR 2.0 was used in the FreeSurfer developer version. SynthSR is a deep learning-based tool that enables the creation of synthetic MP-RAGE images for surface-based analyses with high accuracy, even if the images obtained clinically are heterogeneous. Moreover, it is challenging to perform surface-based analysis with FreeSurfer in patients with intracranial tumors. SynthSR overcomes this challenge.

The synthetic MP-RAGE images were generated from T2-axial images with SynthSR.<sup>18</sup> Then, pre-processing for cortical thickness,

surface area, volume, and local gyrification index (LGI) analyses and cortical reconstruction were performed using the standard FreeSurfer (V 7.4.0). To increase the accuracy of surface reconstruction, synthetic MP-RAGE images were used together with T2-FLAIR images (Figure 2).

## Tumor masking

A proficient general radiologist judiciously utilized the volume of interest procedure within the ITK-SNAP software suite to construct masks representing tumor volumes.

## Statistical analysis

Demographic information of the patient and control groups, the magnetic field strength, estimated total intracranial volume (eTIV), and normalized subcortical volume (structure volume × 1.000/eTIV); data were compared using the chi-squared test, t-test, or Mann-Whitney U test.

Maps of cortical thickness, volume, and surface area for each patient were registered to the “fsaverage” template included in FreeSurfer, and a generalized linear model (GLM) was then generated. Age, gender, and magnetic field strength were used as covariates for the GLM. Smoothing was applied to the cortical thickness, to volume maps with a full width at half maximum (FWHM) of 10 mm, to surface area maps with an FWHM of 15 mm, and to LGI maps with an FWHM of 25 mm. The patient and control groups were compared using “mri\_glmfit” and the main results were analyzed using “mri\_glmfit-sim,” with 1,000 random permutations. To prevent false positive results, the cluster-wise *P* threshold

was set at 0.05, and the vertex-wise cluster threshold was set at  $10^{-3}$ .<sup>20</sup>

When a significant group difference was detected, the mean cortical thickness, surface area, volume, and LGI parameters in the significant cluster for each participant were extracted using the “mri\_segstats” command. Volumes of subcortical structures were calculated using “asegstats2table.” The Spearman correlation coefficient ( $\rho$ ) was calculated to evaluate the correlation between these parameters and the total volume of the lateral ventricles and the volume of the tumor. A *P* value of <0.05 was considered statistically significant.

## Results

Clinical and demographic characteristics: the final population of the study consisted of 24 patients with posterior fossa tumors and 41 age- and gender-matched healthy controls. The patient group was aged  $8.2 \pm 4.2$  years, and the control group was aged  $10.9 \pm 3.7$  years; there was no statistically significant difference in ages between the groups ( $P = 0.11$ ). No significant difference was detected in the magnetic field strength between the patient and control groups in the chi-squared test ( $P = 0.08$ ). In the patient group, 10 received pathological diagnoses of medulloblastoma, 9 of pilocytic astrocytoma, 2 of ependymoma, 2 of anaplastic ependymoma, and 1 of low-grade astrocytoma. All lesions were located in the posterior fossa. The median size of the tumors was 22.1 mL (interquartile range: 22.3 mL). Seventeen of the lesions caused hydrocephalus, and the average lateral ventricular volume for the patient group was  $39.9 \pm 26.0 \text{ cm}^3$ .

## Cortical morphological changes

**Cortical thickness:** The patient group demonstrated a reduction in cortical thickness in the left supramarginal gyrus ( $P = 0.010$ , size: 221 mm<sup>2</sup>) and left superior frontal gyrus ( $P = 0.018$ , size: 200 mm<sup>2</sup>); an increase in cortical thickness was observed in the left caudal middle frontal (CMF) gyrus ( $P = 0.0002$ , size: 1,249 mm<sup>2</sup>), left fusiform gyrus ( $P = 0.001$ , size: 327 mm<sup>2</sup>), left lateral orbitofrontal gyrus ( $P = 0.04$ , size: 168 mm<sup>2</sup>), left lingual gyrus ( $P = 0.033$ , size: 179 mm<sup>2</sup>), right CMF gyrus ( $P = 0.0002$ , size: 727 mm<sup>2</sup>), right posterior cingulate gyrus ( $P = 0.0002$ , size: 363 mm<sup>2</sup>), right superior frontal gyrus ( $P = 0.004$ , size: 256 mm<sup>2</sup>), and right lateral orbitofrontal gyrus ( $P = 0.049$ , size: 162 mm<sup>2</sup>) (Figure 3, Table 1).

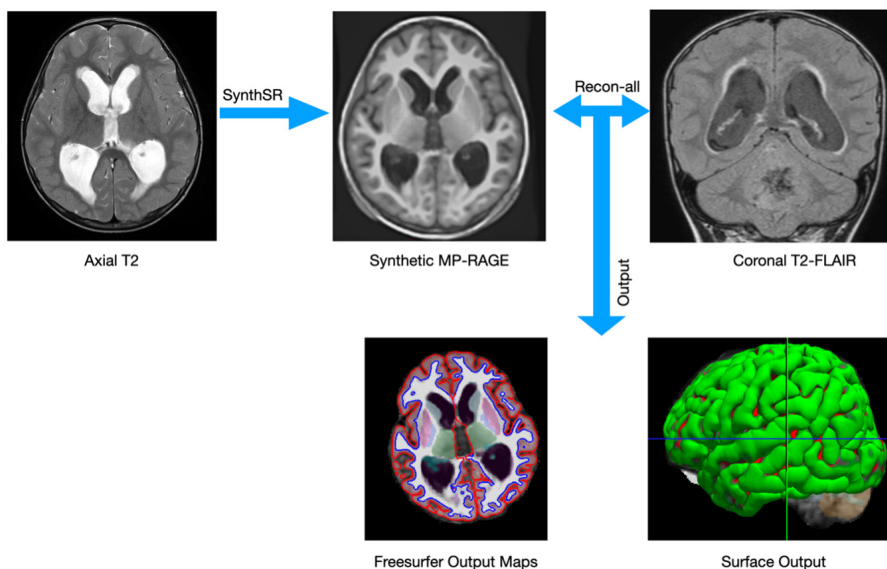


**Figure 2.** The cortical reconstruction pipeline. MP-RAGE, magnetization-prepared rapid gradient echo; FLAIR, fluid attenuation inversion recovery.

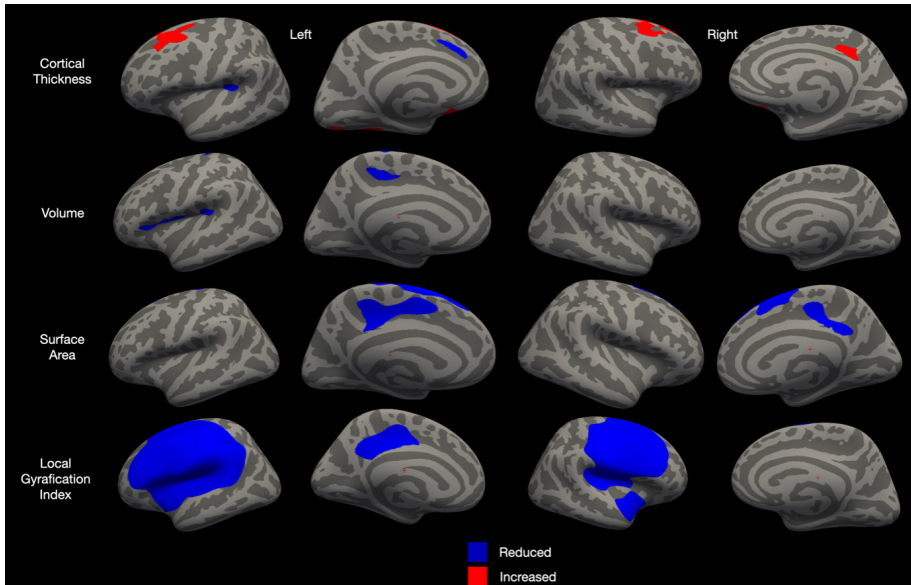


**Figure 3.** Areas showing changes in cortical thickness, surface area, volume, and local gyrification index in cases with posterior fossa tumors.

**Table 1.** The comparison of cortical morphology at the vertex level reveals significant clusters

Measurement	Group comparison	Cluster	Peak MNI coordinates	Size (mm <sup>2</sup> )	P value of CWP
Cortical thickness	HC > patient	L. supramarginal	-34, -35, 17	221	0.010
		L. superior frontal	-10, 31, 31	200	0.018
		L. caudal middle frontal	-34, 13, 50	1,249	<0.001
		L. fusiform	-28, -48, -18	327	0.001
		L. lingual	-19, -85, -10	179	0.033
	Patient > HC	L. lateral orbitofrontal	-14, 12, -15	168	0.049
		R. caudal middle frontal	32, 13, 50	727	<0.001
		R. posterior cingulate	12, -36, 50	363	<0.001
		R. superior frontal	14, 38, 46	256	0.004
		R. lateral orbitofrontal	17, 23, -22	162	0.049
Volume	HC > patient	L. pars triangularis	-33, 27, 8	385	0.001
		L. paracentral	17, -26, 42	248	0.009
		L. precentral	-10, -25, 74	238	0.012
		L. supramarginal	-35, -33, 20	217	0.023
Local gyrification index	HC > patient	L. supramarginal	-52, -31, 35	23,075	<0.001
		L. posterior cingulate	-9, -26, 39	1,647	<0.001
		R. precentral	52, -5, 43	14,342	<0.001
		R. superior temporal	48, 6, -20	1,357	<0.001

All clusters survived correction for multiple comparisons using a Monte Carlo simulation, resulting in a corrected cluster-wise  $P < 0.05$ . L, left; R, right; HC, healthy control; MNI, The Montreal Neurological Institute; CWP, cluster-wise probability.

**Volume:** The patient group showed a decrease in volume in the left pars triangularis ( $P = 0.001$ , size: 385 mm<sup>2</sup>), left paracentral gyrus ( $P = 0.009$ , size: 248 mm<sup>2</sup>), left precentral ( $P = 0.012$ , size: 238 mm<sup>2</sup>), and left supramarginal gyrus ( $P = 0.023$ , size: 217 mm<sup>2</sup>). No statistically significant volume change was observed in the right hemisphere (Figure 3, Table 1).

**Surface area:** The patient group showed a decrease in surface area in the left posterior cingulate ( $P = 0.0004$ , size: 986 mm<sup>2</sup>), left superior frontal ( $P = 0.001$ , size: 554 mm<sup>2</sup>), right superior frontal ( $P = 0.0002$ , size: 1,737 mm<sup>2</sup>), and right isthmus cingulate ( $P = 0.003$ , size: 774 mm<sup>2</sup>). No area increase in the patient group was observed (Figure 3, Table 1).

**Local gyrification index:** In the patient group, a decrease in the LGI was observed in the right hemisphere's precentral gyrus ( $P = 0.0002$ , size: 14,342 mm<sup>2</sup>), right superior temporal gyrus ( $P = 0.0002$ , size: 1,357 mm<sup>2</sup>), left hemisphere's supramarginal gyrus ( $P = 0.0002$ , size: 23,075 mm<sup>2</sup>), and posterior cingulate gyrus ( $P = 0.0002$ , size: 1,647 mm<sup>2</sup>) (Figure 3, Table 1).

### Correlation

The ventricular volume showed a positive correlation with cortical thickness in the areas of bilateral CMF gyrus where a cortical thickness increase was observed [right: ( $P < 0.0001$ , rho: 0.74); left: ( $P = 0.0049$ , rho: 0.57)]. The cortical thickness of the cluster in the right CMF gyrus showed a positive correlation with tumor volume ( $P = 0.015$ , rho: 0.50) but did not correlate with the left cluster.

The LGI showed a negative correlation with the ventricular volume in the cluster containing the right precentral gyrus ( $P = 0.0001$ , rho: -0.72), right superior temporal gyrus ( $P = 0.0011$ , rho: -0.64), left supramarginal gyrus ( $P < 0.0001$ , rho: -0.77), and the left posterior cingulate gyrus ( $P = 0.0003$ , rho: -0.70). The LGI showed a negative correlation with the tumor volume in the cluster containing the right precentral gyrus ( $P = 0.015$ , rho: -0.50), left supramarginal gyrus ( $P = 0.033$ , rho: -0.44), and the peak cluster in the left posterior cingulate gyrus ( $P = 0.0021$ , rho: -0.61).

No significant correlation was observed between the tumor volume and ventricular volume in areas where the cortical volume changed ( $P > 0.05$ ).

### Subcortical volumetric findings

When compared with the control group, the posterior fossa tumor group showed volume increases in the left caudate ( $d = 1.37$ ,  $P < 0.0001$ ), right caudate ( $d = 1.50$ ,  $P < 0.0001$ ), left hippocampus ( $d = 0.99$ ,  $P = 0.0006$ ), and right hippocampus ( $d = 1.02$ ,  $P = 0.0049$ ), and volume decreases in the left putamen ( $d = -1.16$ ,  $P < 0.0001$ ), right putamen ( $d = -1.45$ ,  $P < 0.0001$ ), left pallidum ( $d = 0.99$ ,  $P = 0.0006$ ), right pallidum ( $d = 0.77$ ,  $P = 0.0131$ ), left amygdala ( $d = -0.47$ ,  $P = 0.024$ ), and right amygdala ( $d = 1.11$ ,  $P = 0.0003$ ). No statistically significant volume difference was observed in the bilateral thalamus between the groups (Table 2).

### Correlation of subcortical structures

The tumor volume showed a negative correlation with the volume of the left amygdala ( $P = 0.02$ ,  $\rho = -0.48$ ) and the left accumbens area ( $P = 0.047$ ,  $\rho = -0.41$ ) but showed a positive correlation with the volume of the bilateral caudate nucleus [right: ( $P = 0.001$ ,  $\rho = 0.62$ ); left: ( $P = 0.027$ ,  $\rho = 0.46$ )]. No statistically significant correlation was observed with other subcortical structures (Figure 4, Table 3).

The total ventricular volume showed a negative correlation with the bilateral putamen [right: ( $P = 0.003$ ,  $\rho = -0.59$ ); left: ( $P = 0.023$ ,  $\rho = -0.46$ )], bilateral pallidum

[right: ( $P = 0.006$ ,  $\rho = -0.54$ ); left: ( $P = 0.0002$ ,  $\rho = -0.71$ )], bilateral accumbens area [right: ( $P = 0.017$ ,  $\rho = -0.48$ ); left: ( $P = 0.0001$ ,  $\rho = -0.72$ )], and a positive correlation with the bilateral caudate nucleus [right: ( $P = 0.011$ ,  $\rho = 0.51$ ); left: ( $P = 0.02$ ,  $\rho = -0.47$ )], and left hippocampus ( $P = 0.012$ ,  $\rho = 0.51$ ) (Figure 4, Table 3).

### Discussion

In this study, we investigated the cortical morphological and subcortical volumetric changes at the time of diagnosis and their relationship with tumor size and ventricular volume in children with posterior fossa tumors. Our findings demonstrated a cortical

thickening, particularly in the bilateral CMF region, even at the time of diagnosis. We observed volume reduction in the left supramarginal gyrus, surface area reduction in the posterior cingulate and superior frontal gyrus, and widespread hypogyrification in the bilateral fronto-temporo-parietal areas. Whereas the volume of the caudate nucleus and hippocampus increased, the putamen, amygdala, and nucleus accumbens showed volume reduction. These cortical and subcortical changes exhibited a significant association with ventricular volume, whereas only a partial relationship was observed with tumor size.

To our knowledge, the question of whether there are structural changes in the brain in childhood tumors has not been investigated. Large-scale studies are challenging due to the relative rarity of these tumors. Additionally, for such research, appropriate analysis of children's brain images and standardization of MRI devices are necessary. The SynthSR 2.0 used in our study enables the creation of suitable images for surface-based analysis and allows surface-based analysis even in the presence of intracranial tumors, making it feasible to work with heterogeneous datasets.<sup>18</sup>

Clinical and neuroimaging studies have shown that the cerebellum is not only involved in motor control or balance but also plays a role in a range of cognitive functions, such as language, emotion processing, and attention.<sup>10</sup> The cerebellum contains circuits associated with various areas, including the prefrontal cortex, parietal cortex, thalamus, superior temporal region, and limbic system.<sup>21</sup> Cerebellar cognitive affective syndrome is an entity described in the last 25

**Table 2.** The comparison of subcortical gray matter volume of patient and healthy control group

Structure volume (mL)	HC (n = 41)	Patient (n = 24)	Cohen's D	P
Left thalamus	4.71 ± 0.37	4.75 ± 0.41	-0.10	0.697
Left caudate	2.29 ± 0.25	2.76 ± 0.46	1.37	<0.001*
Left putamen	3.42 ± 0.28	3.05 ± 0.38	-1.16	0.001*
Left pallidum	1.13 ± 0.1	1.06 ± 0.15	-0.51	0.084
Left hippocampus	2.87 ± 0.2	3.31 ± 0.68	0.99	<0.001*
Left amygdala	1.01 ± 0.1	0.94 ± 0.22	-0.47	0.025*
Left accumbens area	0.47 ± 0.06	0.37 ± 0.06	-1.67	<0.001
Right thalamus	4.51 ± 0.32	4.48 ± 0.34	-0.09	0.736
Right caudate	2.36 ± 0.28	2.86 ± 0.42	1.50	<0.001*
Right putamen	3.38 ± 0.26	2.95 ± 0.34	-1.45	<0.001
Right pallidum	1.21 ± 0.13	1.08 ± 0.22	-0.77	0.013
Right hippocampus	2.89 ± 0.25	3.33 ± 0.62	1.02	0.005*
Right amygdala	1.16 ± 0.11	1.03 ± 0.15	-1.11	<0.001
Right accumbens area	0.44 ± 0.07	0.38 ± 0.06	-0.91	<0.001
Total lateral ventricle	8.18 ± 3	39.94 ± 26.04	2.00	<0.001*

\*The Mann-Whitney U test performed. HC, healthy control.

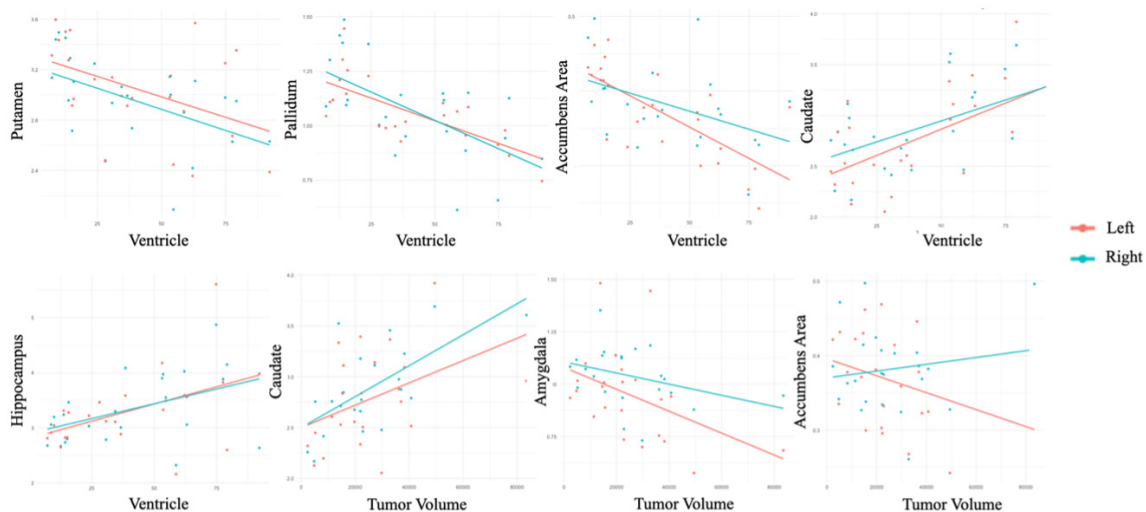


**Figure 4.** Scatterplot demonstrating the correlation between subcortical gray matter volumes and tumor volume, as well as the correlation between subcortical gray matter volumes and ventricular volume.

**Table 3.** The correlation relationship between tumor volume, ventricle volume, and subcortical gray matter structures

	Tumor volume		Total lateral ventricle volume	
	rho	P	rho	P
Left thalamus	0.32	0.128	0.33	0.120
Left caudate	0.51	0.011	0.46	0.028
Left putamen	-0.47	0.023	0.02	0.919
Left pallidum	-0.71	0.000	-0.12	0.579
Left hippocampus	0.52	0.011	0.31	0.152
Left amygdala	-0.27	0.199	-0.48	0.021
Left accumbens area	-0.72	0.000	-0.42	0.048
Right thalamus	0.16	0.466	0.19	0.384
Right caudate	0.48	0.020	0.63	0.002
Right putamen	-0.59	0.003	-0.14	0.510
Right pallidum	-0.55	0.006	-0.02	0.919
Right hippocampus	0.40	0.052	0.33	0.120
Right amygdala	-0.27	0.207	-0.41	0.054
Right accumbens area	-0.48	0.018	-0.05	0.834

years that encompasses changes in executive function and working memory, visual-spatial impairments, difficulties in language production, and personality alterations.<sup>12</sup> It has been suggested that defects in the circuits between the cerebellum and prefrontal cortex caused by cerebellar masses could be one of the causes of this syndrome.<sup>22</sup> Indeed, a widespread gyral reduction in the frontal region was detected in our study. However, longitudinal and advanced imaging studies are needed to establish the correlation between these findings.

In patients with cerebellar tumors, failure of surface reconstruction has limited the investigation of surface-based morphometric changes in adult patients with intracranial tumors. A study by Zhang et al.<sup>9</sup> found decreased gyrification in bilateral medial orbitofrontal gyrus and lingual gyrus in the contralateral hemisphere of patients with frontal LGGs. Similarly, our study revealed widespread decreased gyrification in the cerebral cortex. While gyrification is associated with neurodevelopment, studies have also shown that axonal damage can disrupt gyrification.<sup>23</sup> Medulloblastomas are embryonal tumors that come with genetic mutations, particularly in the pediatric population. Therefore, the question of whether this global gyrification reduction is due to widespread axonal damage or folding abnormalities caused by accompanying genetic abnormalities should be supported by future genetic and longitudinal studies.

Recent studies have demonstrated that the basal ganglia and cerebellum form a

connected network not only at the cortical level but also directly. Injection of rabies virus into the macaque putamen and globus pallidus externus significantly affected the cerebellum.<sup>24</sup> Our study demonstrated volume reduction in the putamen and pallidum in these patients, which may be associated with the involvement of this circuit. Recent functional MRI (fMRI) studies have identified a network involving the cerebellum, caudate nucleus, and prefrontal cortex, associated with executive functions, verbal fluency, and working memory. Abnormal activity in this network has been linked to diseases such as Alzheimer's disease.<sup>25</sup> Our study is the first to show a volume increase in the caudate nucleus and widespread cortical morphological changes in the frontal region in children with posterior fossa tumors, which may be associated with damage to the cerebello-ganglia-cortical network and subsequent impairment of executive functions. Future resting state fMRI studies in this population may support our findings.

The cerebellum is very important for functions such as balance and memory, as well as speech. It plays a crucial role in verbal fluency, grammar processing, and correcting language mistakes.<sup>26</sup> fMRI studies include the cerebellum in the language network along with the superior temporal lobe, pars triangularis, and precentral gyrus. These network clusters are predominantly in the left hemisphere, which is likely due to the language centers being primarily located in the left hemisphere in humans.<sup>27</sup> According to our findings, there is a reduction in volume asymmetrically in the left hemisphere in the

pars triangularis and supramarginal gyrus, which are associated with the speech center. This may explain the areas showing volume reduction in the asymmetric left hemisphere and the asymmetry in the findings in these patients.

Recent studies have demonstrated a strong relationship between the cerebellum and the hippocampus. An experiment conducted in mice showed that optogenetic stimulation of the cerebellum resulted in changes in hippocampal functional connectivity and altered cellular dynamics.<sup>28</sup> Furthermore, recent studies have shown that the cerebellum is involved in various functions associated with memory. One such study in patients with hippocampal glioma revealed a compensatory volume increase in the contralateral hippocampus.<sup>29</sup> Similarly, the bilateral hippocampal volume increase in our study may be associated with this compensation. In opioid-dependent patients, there is decreased functional connectivity between the nucleus accumbens, amygdala, and cerebellum.<sup>30</sup> The decreased volume of the accumbens and amygdala in patients with cerebellar tumors may be due to the involvement of this circuit.

Our study has several limitations. First, this study is retrospective and was conducted at a single center. Our sample size was limited, and we did not categorize or assess tumors according to their subtypes and locations. However, it is worth noting that tumors situated in the vermis may influence distinct pathways compared with those located in the cerebellar hemispheres. Moreover, tumors in the posterior fossa were not staged. Nevertheless, the implications could differ between rapidly progressing tumors and those with slower growth rates. On the other hand, the changes we identified, irrespective of tumor grade or developmental stage, highlight the necessity and interest in further investigation into this matter. Second, even though there is no statistically significant difference between the groups in terms of the use of 1.5 Tesla and 3 Tesla devices, those used in the patient and control groups are not exactly balanced. A covariate has been used to counteract this, but it may have partially affected the results. There were no neurocognitive data available for the patients, and therefore the widespread changes in the brain could not be supported by neurocognitive data. Only structural MRI was used in this study, and the findings could not be supported by advanced techniques, such as diffusion tensor imaging or fMRI. Prospective studies may support our findings.

In conclusion, posterior fossa tumors lead to widespread morphological changes in cortical structures, with the most dominant pattern being hypogyrification, accompanied by a decreased surface area and volume reduction. Although cortical thickening predominantly increases, there are also areas where cortical thickness decreases. Subcortical gray matter structures, except for the hippocampus and caudate nucleus, showed volume reduction. These findings are highly correlated with the lateral ventricle volume. Other authors have nothing to disclose.

### Conflict of interest disclosure

Meltem Necibe Ceyhan Bilgici, MD, is Section Editor in Diagnostic and Interventional Radiology. She had no involvement in the peer-review of this article and had no access to information regarding its peer-review.

## References

1. Ward E, DeSantis C, Robbins A, Kohler B, Jemal A. Childhood and adolescent cancer statistics, 2014. *CA Cancer J Clin*. 2014;64(2):83-103. [\[CrossRef\]](#)
2. Muzumdar D, Ventureyra EC. Treatment of posterior fossa tumors in children. *Expert Rev Neurother*. 2010;10(4):525-546. [\[CrossRef\]](#)
3. Marchi V, Guzzetta A, Cioni G. Cerebral Plasticity and functional reorganization in children with congenital brain lesions. Neonatology, Springer International Publishing, 2017:1-10. [\[CrossRef\]](#)
4. Klein D, Mok K, Chen JK, Watkins KE. Age of language learning shapes brain structure: a cortical thickness study of bilingual and monolingual individuals. *Brain Lang*. 2014;131:20-24. [\[CrossRef\]](#)
5. Barrett KC, Ashley R, Strait DL, Kraus N. Art and science: how musical training shapes the brain. *Front Psychol*. 2013;4:713. [\[CrossRef\]](#)
6. Bates E, Reilly J, Wulfeck B, et al. Differential effects of unilateral lesions on language production in children and adults. *Brain Lang*. 2001;79(2):223-265. [\[CrossRef\]](#)
7. Lv K, Cao X, Wang R, et al. Contralateral macrostructural plasticity in patients with frontal low-grade glioma: a voxel-based morphometry study. *Neuroradiology*. 2023;65(2):297-305. [\[CrossRef\]](#)
8. Mills KL, Tamnes CK. Methods and considerations for longitudinal structural brain imaging analysis across development. *Dev Cogn Neurosci*. 2014;9:172-190. [\[CrossRef\]](#)
9. Zhang S, Sun H, Yang X, et al. An MRI study combining virtual brain grafting and surface-based morphometry analysis to investigate contralateral alterations in cortical morphology in patients with diffuse low-grade glioma. *J Magn Reson Imaging*. 2023;58(3):741-749. [\[CrossRef\]](#)
10. Buckner RL. The cerebellum and cognitive function: 25 years of insight from anatomy and neuroimaging. *Neuron*. 2013;80(3):807-815. [\[CrossRef\]](#)
11. Petersen KJ, Reid JA, Chakravorti S, et al. Structural and functional connectivity of the nondecussating dentato-rubro-thalamic tract. *Neuroimage*. 2018;176:364-371. [\[CrossRef\]](#)
12. Schmahmann JD, Sherman JC. The cerebellar cognitive affective syndrome. *Brain*. 1998;121(Pt 4):561-579. [\[CrossRef\]](#)
13. Zhang Y, Zou P, Mulhern RK, Butler RW, Laningham FH, Ogg RJ. Brain structural abnormalities in survivors of pediatric posterior fossa brain tumors: a voxel-based morphometry study using free-form deformation. *Neuroimage*. 2008;42(1):218-229. [\[CrossRef\]](#)
14. Fuentes D, Contreras J, Yu J, et al. Morphometry-based measurements of the structural response to whole-brain radiation. *Int J Comput Assist Radiol Surg*. 2015;10(4):393-401. [\[CrossRef\]](#)
15. Dietrich RB, Bradley WG, Zaragoza EJ 4th, et al. MR evaluation of early myelination patterns in normal and developmentally delayed infants. *AJR Am J Roentgenol*. 1988;150:889-896. [\[CrossRef\]](#)
16. Reid LB, Cunnington R, Boyd RN, Rose SE. Surface-based fMRI-driven diffusion tractography in the presence of significant brain pathology: a study linking structure and function in cerebral palsy. *PLoS One*. 2016;11(8):e0159540. [\[CrossRef\]](#)
17. Radwan AM, Emsell L, Blommaert J, et al. Virtual brain grafting: enabling whole brain parcellation in the presence of large lesions. *Neuroimage* 2021;229:117731. [\[CrossRef\]](#)
18. Iglesias JE, Billot B, Balbastre Y, et al. SynthSR: a public AI tool to turn heterogeneous clinical brain scans into high-resolution T1-weighted images for 3D morphometry. *Sci Adv*. 2023;9(5):1-14. [\[CrossRef\]](#)
19. Cuschieri S. The STROBE guidelines. *Saudi J Anaesth*. 2019;12(Suppl 1):31-34. [\[CrossRef\]](#)
20. Greve DN, Fischl B. False positive rates in surface-based anatomical analysis. *Neuroimage*. 2018;171:6-14. [\[CrossRef\]](#)
21. Ailion AS, Roberts SR, Crosson B, King TZ. Neuroimaging of the component white matter connections and structures within the cerebellar-frontal pathway in posterior fossa tumor survivors. *Neuroimage Clin*. 2019;23:101894. [\[CrossRef\]](#)
22. Hoche F, Guell X, Vangel MG, Sherman JC, Schmahmann JD. The cerebellar cognitive affective/Schmahmann syndrome scale. *Brain*. 2018;141(1):248-270. [\[CrossRef\]](#)
23. Li M, Hua K, Li S, et al. Cortical morphology of chronic users of codeine-containing cough syrups: association with sulcal depth, gyrification, and cortical thickness. *Eur Radiol*. 2019;29(11):5901-5909. [\[CrossRef\]](#)
24. Milardi D, Quartarone A, Bramanti A, et al. The Cortico-basal ganglia-cerebellar network: past, present and future perspectives. *Front Syst Neurosci*. 2019;13:61. [\[CrossRef\]](#)
25. Qi Z, An Y, Zhang M, Li HJ, Lu J. Altered cerebro-cerebellar limbic network in AD spectrum: a resting-state fMRI study. *Front Neural Circuits*. 2019;13:72. [\[CrossRef\]](#)
26. Leiner HC, Leiner AL, Dow RS. Cognitive and language functions of the human cerebellum. *Trends Neurosci*. 1993;16(11):444-447. [\[CrossRef\]](#)
27. Lipkin B, Tuckute G, Affourtit J, et al. Probabilistic atlas for the language network based on precision fMRI data from >800 individuals. *Sci Data*. 2022;9:529. [\[CrossRef\]](#)
28. Krook-Magnuson E, Szabo GG, Armstrong C, Oijala M, Soltesz I. Cerebellar directed optogenetic intervention inhibits spontaneous hippocampal seizures in a mouse model of temporal lobe epilepsy. *eNeuro*. 2014;1(1):ENEURO.0005-14.2014. [\[CrossRef\]](#)
29. Liu D, Chen J, Ge H, et al. Structural plasticity of the contralesional hippocampus and its subfields in patients with glioma. *Eur Radiol*. 2023;33(9):6107-6115. [\[CrossRef\]](#)
30. Moulton EA, Elman I, Becerra LR, Goldstein RZ, Borsook D. The cerebellum and addiction: insights gained from neuroimaging research. *Addict Biol*. 2014;19(3):317-331. [\[CrossRef\]](#)